SCOUR OF THE SCREED LAYER UNDERNEATH A VERTICAL SEAWALL WITH A RUBBLE MOUND FOUNDATION

by

Christiaan Tomas Malan

Thesis presented in fulfilment of the requirements for the degree of

Master of Engineering in Ports & Coastal Engineering in the

Faculty of Engineering at Stellenbosch University.

Supervisor: Prof Koos Schoonees

December 2016

This page is intentionally left blank

Declaration

I, Christiaan Tomas Malan, hereby declare that all written, diagrammed or tabulated content contained within this research paper is of my own authentic work unless explicitly stated or referenced.

By submitting this thesis electronically, I declare that the entirety of the work contained therein is my own, original work, that I am the sole author thereof (save to the extent explicitly otherwise stated), that reproduction and publication thereof by Stellenbosch University will not infringe any third party rights and that I have not previously in its entirety or in part submitted it for obtaining any qualification.

_____ _____

CT Malan Date

Abstract

Scour is here defined as the removal of granular bed material by hydrodynamic forces in the vicinity of coastal structures. It is believed to be one of the most common causes of seawall failure.

This thesis studies the effect of scour of a rubble mound foundation underneath a vertical seawall. The effects and behaviours stated in this report may also be applied to vertical breakwaters constructed on a rubble mound foundation. Past studies on the scour process are discussed and several laboratory experiments performed to conclude what component of the rubble mound foundation is most susceptible to scour. Emphasis is placed on screed layer thickness, toe width, compaction and addition of sediment to the foundation during construction.

The hypothesis is thus put forward that a thicker screed layer will experience more damage compared to a thinner layer. The loosely packed 19mm stone layer is most susceptible to hydrodynamic forces as it is small stone easily exposed through the overlying armour layers. A shorter toe width of rock should produce less scour damage. A greater area of stone, not adhering to the filter rules, will wash out through the overlaying armour units. Compacting reduces the voids between the stone units and prevents the structure element from sinking into the screed layer under its own weight. Cohesive and non-cohesive soils added inadvertently during construction should wash out of the screed layer, leaving behind larger voids between the individual stones.

A physical model study was performed at the facilities of the CSIR in Stellenbosch. A fixed-bed, two-dimensional physical model in a glass flume has been set up to conduct an array of experiments to study the effects of the scour process on several foundation conditions and construction procedures. A method for measuring scour underneath a vertical structure was devised. Together with measured wave conditions of each test, an existing design criterion is proven and additional criteria are stated.

This thesis can conclude that the thickness of the screed layer should be designed meeting a minimum and maximum requirement to assure stability. Insight is provided on the importance and use of the filter rules governing the capability of rock being washed out. The significance of various construction methods and materials is stated, such as compaction of the foundation and the addition of sediments to the screed layer. It was concluded that these methods oppose the stability of the structure.

Recommendations concerning the execution of physical model tests regarding rubble mound foundations are stated in the thesis.

Opsomming

Uitskuring word hier gedefineer as die verwydering van korrelmateriaal in die omgewing van kusstrukture deur middel van hidrodinamiese kragte. Dit word beskou as een van die mees algemene oorsake van die swigting van seemure.

Hierdie tesis bestudeer die effek van uitskuring van 'n klipfondament onder 'n vertikale seemuur. Die effekte en gedrag wat in hierdie verslag gebruik en voorgelê word, kan ook toegepas word op vertikale golfbrekers gebou op ‘n klipfondament. Studies uit die verlede oor die uitskuringproses word bespreek en laboratoriumeksperimente word uitgevoer om tot gevolgtrekking te kom tot watter aspekte van die klipfondament die mees vatbaarste vir uitskuring is. Klem word geplaas op vlaklaagdikte, toonwydte, kompaksie en byvoeging van sediment tot die fondament tydens konstruksie.

Die hipotese word dus na vore gebring dat 'n dikker vlaklaag meer skade sal ervaar in vergelyking met 'n dunner laag. Die losweg verpakde 19mm kliplaag is meer vatbaar vir hidrodinamiese kragte, want hierdie klein klip word maklik uitgespoel deur die oorliggende beskermingslae. 'n Korter toon breedte van klip sal minder uitskuurskade veroorsaak. 'n Langer lengte van klip, wat nie die filterreëls gehoorsaam nie, sal uitspoel deur die oorliggende beskermingseenhede. Kompaktering verminder die ruimtes tussen die klipeenhede en verhoed dat die struktuurelement onder sy eie gewig in die vlaklaag insink. Aggregaat wat per ongeluk tydens konstruksie by die fondasiemateriaal bygevoeg word, sal uitspoel uit die vlaklaag, wat groter ruimtes tussen die individuele klippe agterlaat.

'n Fisiese model studie is uitgevoer by die fasiliteite van die WNNR in Stellenbosch. 'n Vaste-bed, twee-dimensionele fisiese model in ‘n glaskanaal is opgestel om verskeidenheid eksperimente uit te voer om die uitwerking van die uitskuringproses op verskillende fondament tipes en konstruksieprosedures te bestudeer. 'n Metode vir die meet van uitskuring onder ‘n vertikale struktuur is ontwikkel. Saam met gemete golftoestande van elke toets, is bestaande ontwerpkriteria bewys en addisionele kriteria vasgestel.

Hierdie tesis bevestig dat die dikte van die vlaklaag moet ontwerp word met 'n minimum-en maksimumvereiste om stabiliteit te verseker. Insig is gegee oor die belangrikheid en gebruik van die filterreëls, wat die vermoë om ‘n klip uit te spoel, bepaal. Die verskil van verskeie konstruksiemetodes en materiale word weergegee, soos verdigting van die vlaklaag en die toevoeging van sediment in die vlaklaag. Die verslag kom tot die gevolgtrekking dat hierdie metodes die stabiliteit van die struktuur

teenwerk. Aanbevelings met betrekking tot die uitvoering van ‘n fisiese model met klipfondamente word in die tesis gegee.

Acknowledgements

I hereby give thanks to those who made contributions to this thesis:

First and foremost, to my supervisor, Prof. Koos Schoonees for his help and guidance towards this thesis and inspiring me as a young engineer.

Secondly, I would like to thank Johan Kieviet and the model hall staff at the CSIR for their support, guidance and sharing of knowledge whilst conducting the physical model. Your physical model experience was vital to the success of my study.

To Victor Muller, a fellow student and close friend who conducted physical model experiments for his thesis “An appropriate size of toe rock for vertical seawalls” in partnership with me. Your help and support are greatly appreciated.

Mrs. C Rudman and Mr. R Briedenhann for providing me with geotechnical guidance and the necessary materials and equipment to conduct the experiments.

To my friend, Jano Theunissen, for help with the woodwork of the seawall model.

Lastly, to my family, for all the support they have given me throughout my years of studying.

TABLE OF CONTENTS

LIST OF TABLES

LIST OF FIGURES

1. Introduction

1.1 Background

Coastal erosion is a force that will always be of concern to man as it becomes a threat to areas where public or private structures are located. The main mechanism for coastal erosion is the relocation of soil. This is achieved by rising and falling water levels, currents, wave forces and wind. Many countries around the world experience coastal erosion and many utilise seawalls to prevent further erosion of their shorelines.

A seawall (Figure 1) is a structure separating land and sea, designed to prevent coastal erosion and further damage to the land such as flooding. Apart from providing coastal defence, a seawall provides protection to human habitation and recreational activities. Seawalls are massive structures built, usually parallel to the shoreline, to protect the shore against wave action, reflecting the energy back to the sea, whilst preventing movement of the soil at the back of the structure.

Figure 1: Vertical Seawall (Ian West, 2015)

The term “seawall” usually refers to a concrete wall constructed on a solid rock foundation. The subject of this study is a “composite seawall” which implies a concrete wall supported on a rubble mound foundation. A cross-section of a composite seawall indicating all the relative components of the foundation is illustrated in Figure 2.

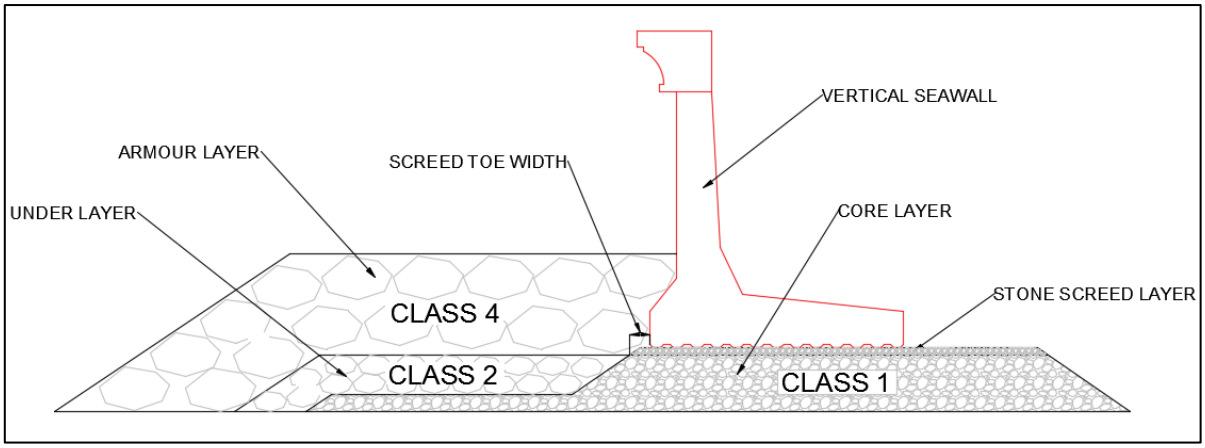

Figure 2: Composite vertical seawall with relevant components

Although the primary goal of seawalls is coastal protection, there are certain factors of constructing a seawall that can have some negative effects on the shoreline. Wave breaking and reflecting waves from the seawall create turbulence, capable of suspending sediments and displacing rubble mound stones (Bush et al., 2004) - thus making the structure susceptible to scour.

Scour is here defined as the removal by hydrodynamic forces of granular bed material in the vicinity of coastal structures. The term “scour” is used instead of the more general term “erosion” to distinguish the process caused by the presence of a structure (Burcharth & Hughes, 2006). Scour can be a result of a combination of many conditions such as reflected waves acting with incident waves, waves breaking on the structure, slope, and material of seabed etc. It is believed to be one of the most common causes of seawall and vertical breakwater failure.

With a vertical seawall or breakwater constructed on a rubble mound foundation, constant contact between the structure element and foundation is required by design. This provides sufficient friction between the two surfaces to ensure stability against the hydrodynamic forces which the structure must overcome. Scour undermines this surface contact by removing the rubble mound foundation underneath the structure and reducing support of the structure, promoting movement, settlement or failure of the structure. There are several failure modes that can occur as a result of scour damage (refer to Section 2.1.5).

Most scour damage would eventually reach a stable equilibrium condition if the hydrodynamic conditions remain unchanged over time, but if the scour is primarily induced by wave action it is more than likely to persist. It is difficult to determine if scour at a specific coastal project would reach such an equilibrium. The observed scour can be a result of energetic flow conditions that subsided before the full scour potential was realised. Infilling of sediment can occur prior to the measurement, or the observed scour is the partial development of an ongoing long-term process. Thus it is important to

study what effects different hydrodynamic conditions will have on a coastal structure. A sequence of the scour process is shown in Figure 3, with photographs taken at 500 wave intervals during conducted experiments.

Experience has shown that small alterations during construction of vertical seawalls or breakwaters can lead to great effects during the lifetime of the structure. This study focusses mainly on the layer of small stone on which the structure element rests, called the screed layer. This layer is most susceptible to scour as it consists of small stones easily washed out through the overlying layers, yet it supports the structure and provides friction between the base of the structure and its foundation.

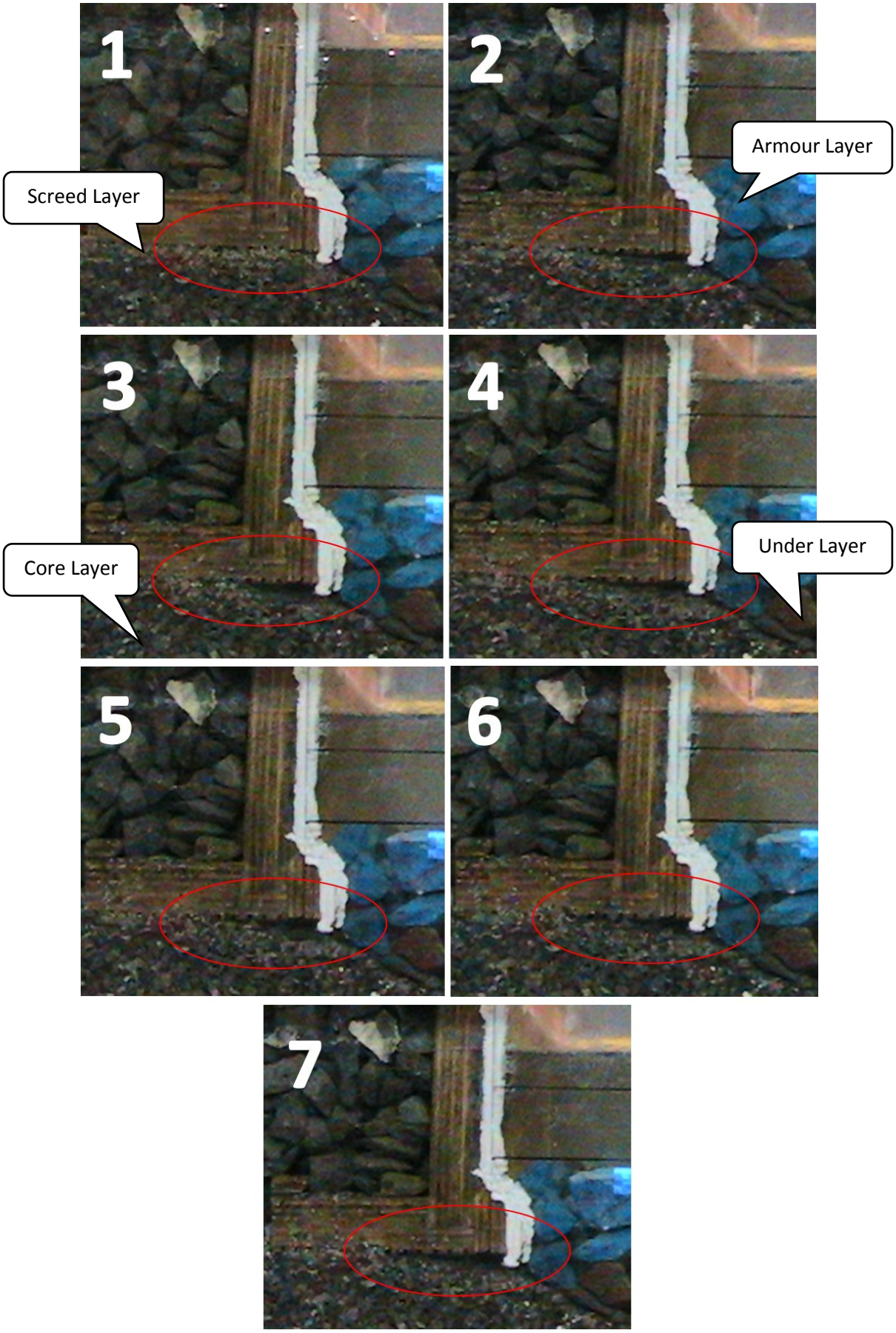

Figure 3: Scour process

1.2 Objective

The objective of this study is to review existing methods and to provide design guidance for scour protection at the foundation of vertical seawalls with emphasis on the stone layer directly underneath the structure, considering specifically the design and construction procedure of this screed layer.

1.3 Scope

The scope of this thesis encompasses the study of scour prediction by conducting several laboratory experiments to test the behaviour of scour underneath a vertical seawall by altering different parameters such as the thickness of the screed layer and the width of the screed toe (refer to Section 4.1 for a complete list of parameters considered). This thesis aims to provide the best practices to construct and maintain the supportive screed layer under a composite vertical seawall constructed with L-elements.

1.4 Strategy

The following strategy was proposed in order to meet the above-mentioned objective within the scope:

i. A literature review on the scour process focussing on the bed material of a rubble mound foundation, as well as a review of vertical seawalls in general.
ii. A physical model study was conducted to investigate the findings from the literature. Scaled model experiments were performed to measure the response of different foundation layouts to scour.
iii. The physical model test results are analysed and the principal driving forces of scour underneath a vertical seawall are identified.
iv. Based on the findings, conclusions are formulated as to how these forces can be countered.

1.5 Layout of Thesis

The thesis contains six chapters as described below:

1. *Introduction:* Briefly gives an overview on scour at a vertical seawall and states the intended outcomes of the thesis.
2. *Literature Study:* States current knowledge and substantive findings on the scour process, materials and physical modelling of scour.
3. *Problem Formulation:* Explains the issues to be addressed in this thesis.
4. *Experimental Design and Set-up for Physical Modelling:* States the scope of work done and hypothesised results.
5. *Results:* Discusses the results obtained from the physical model.
6. *Conclusions and Recommendations:* Gives a summary of all findings and recommendations for future work.

2. Literature Study

2.1 Structure

2.1.1 Design of a seawall

With the increase of construction of seawalls that have to meet higher safety standards, the following aspects should be considered in the design (Pilarczyk, 2003):

- Function of the structure
- Physical environment
- Construction method
- Operation and maintenance

Parameters have to be specified in order to design a structure. For the design of scour at hydraulic structures, loading (hydraulic conditions) and strength (morphological and geotechnical conditions) parameters are of main concern. The flow characteristics and turbulence intensities, determined by the geometry of the hydraulic structure, together with bed roughness will characterise the flow pattern in the vicinity of the structure.

2.1.2 Types of seawalls

The purpose of constructing a seawall is to prevent further landward retreat of the shoreline (i.e. loss of land due to wave action).

Seawalls can have a variety of different physical forms: vertical, curved and mound seawalls (Figure 4).

- a) Vertical seawalls are best suited for areas that have a lot of larger waves for long periods of time. Whilst providing coastal defence, vertical seawalls are subjected to a number of stresses from continuing beating waves and may need regular maintenance.
- b) Curved seawalls have a concave form facing the sea making it very effective at dispersing incident wave energy, reducing turbulence, to prevent water reaching the top of the structure and overtopping. Each curved seawall is unique to the shoreline and its coastal conditions and thus entails complex engineering and high construction costs.
- c) Mound seawalls are constructed from placing materials, such as sandbags, rocks, concrete blocks or gabions on top of each other. These structures are used in situations where wave energy is low and less demanding. Mound seawalls is a low-cost option and usually constructed in times of emergency.

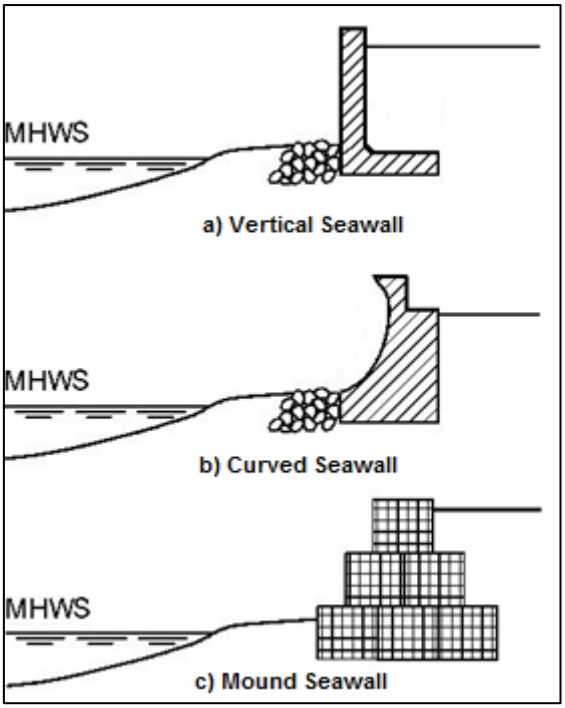

Figure 4: Types of seawalls

This study will focus on vertical seawalls, of which there are several types:

a) L-walls are gravity type structures, relying on the structure's own weight and the weight of earth used for the backfill for stability.

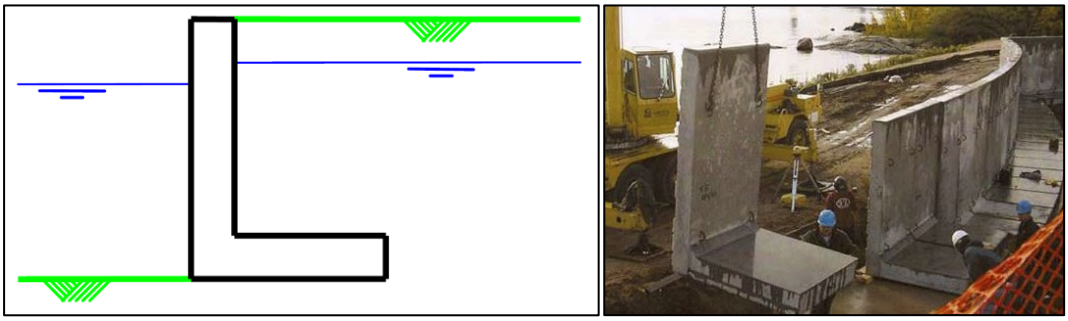

Figure 5:Example of L-wall (Meijer, E) (Vanhooseco,LLC)

b) Caisson walls are also gravity type structures relying on self-weight and the weight is the earth or water infill for stability.

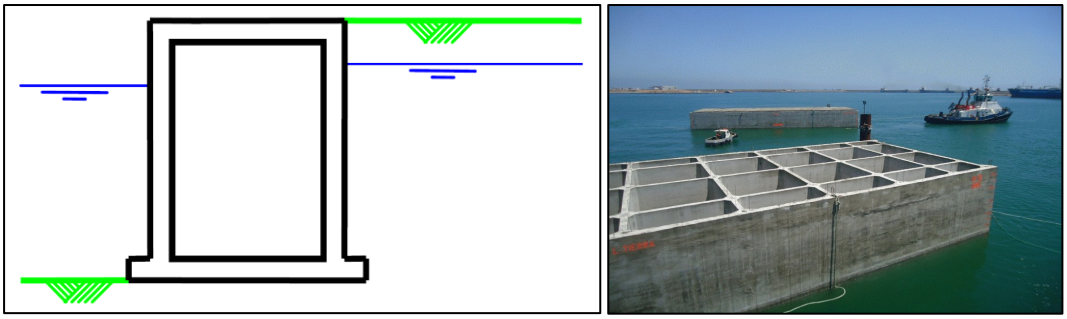

Figure 6: Example of Caisson wall (Meijer, E) (Cyes)

c) Sheetpile walls are constructed with piles driven or hammered into the earth, designed to resist horizontal loads by forming a continuous wall. Sheetpile structures are generally used where the bed material directly under the structure is not capable of supporting the load of the structure.

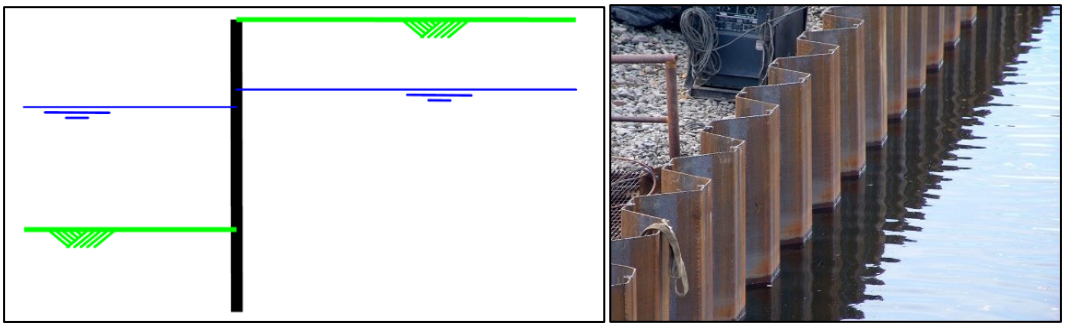

Figure 7: Example of Sheetpile wall (Meijer, E) (Gerdau)

d) Anchored walls are piled walls anchored to the earth with one or more rods. The rods are usually connected to an anchor block, compacted into the earth behind the seawall.

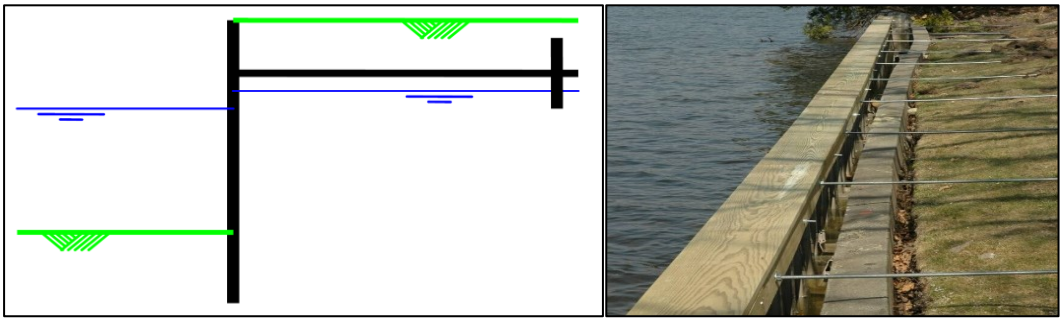

Figure 8: Example of Anchored wall (Meijer, E) (WaterWorks Marine)

This report examines the scour process underneath vertical seawalls with the emphasis on seawalls constructed with L-elements.

2.1.3 L – elements

Although it being a relatively new construction method, a number of seawalls around the world are composed of reinforced concrete L-elements. A simple L-element is composed of a bottom slab with a vertical wall rigidly cast to it as shown in Figure 9. Limited concrete is used compared to caissons or similar structures.

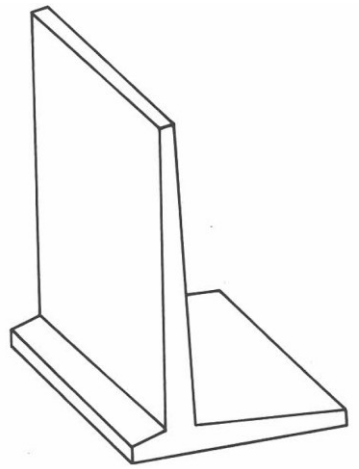

Figure 9: L-element (Pitkala, 1986)

As with caissons, the elements are precast onshore, but transferred and installed by crane in dry (under the shelter of a cofferdam) or wet conditions (directly into the sea). By casting the concrete on the dry ground, a more controlled environment allows for the concrete to reach its desirable strength and durability quantities. The seawall is constructed by installing these elements side by side, and sealing the joints between the elements according to the requirements set forth by the backfilling material. Generally, in-situ cast concrete, plaster or geotextiles are used to seal these joints. Figure 10 explains the sequence of constructing a seawall using L-elements.

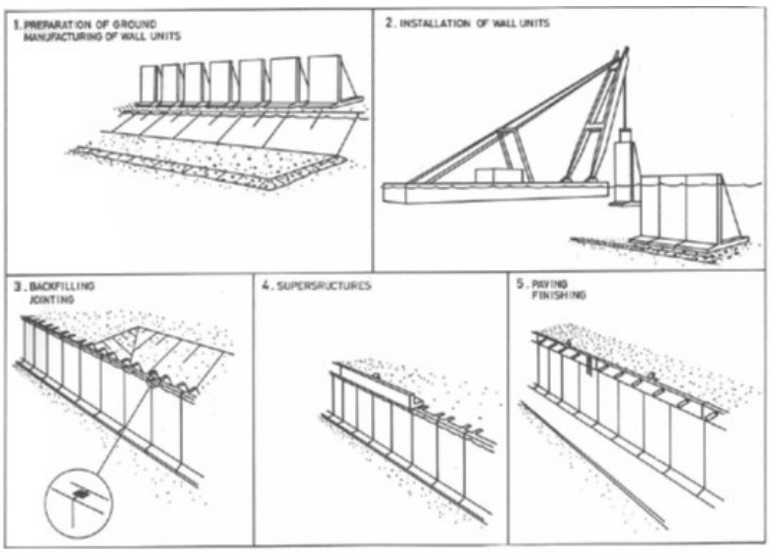

Figure 10: Sequence of construction of L-elements (Pitkala, 1986)

A general precondition for L-element seawalls, as for any other gravitational structure, is a bearing base at a suitable depth. Construction is done on levelled rock but for many sites mass exchange is done where poorly bearing clays and silts are removed and replaced by gravel or mainly, quarry fillings. These filled foundations are also constructed in either dry or wet conditions.

2.1.4 Foundation

The foundation of a vertical seawall constructed with precast concrete elements is composed of layers of different grading stone. Normally it is composed of a bedding layer and a core of quarry-run stone covered by one or more layers of larger grading stone acting as underlayers. Lastly, an armour layer is placed over underlayers to protect all the layers from wave attack. Before the concrete elements are lowered into position, a screed layer, consisting of fine rock (19mm), is laid over the foundation to level the surface. This screed layer allows the structure element to sink into the layer under its self-weight, assuring level placement of the structure. The main objective of the design of a foundation is to assure safety against failure in the soils under the structure, allowing for limited (acceptable) deformations in these soils. The geotechnical failure modes of the structure related to granular material failure are discussed in section 2.4.4.

2.1.5 Structural Failure Modes

When structures are constructed in marine environments, the stability of these structures must be duly safeguarded. If a structure is damaged in such a way that the performance and functionality are below the minimum anticipated by design, the structure is considered a failed structure (Burcharth & Hughes, 2006). The stability of a structure's foundation requires particular attention due to the action of scour or partial liquefaction, especially if the structure is constructed on porous or non-cohesive soils.

When shear stress is exerted on loosely packed soil, the sediment particles tend to adopt a denser packing as illustrated in Figure 11. Over-pressure occurs in the pore water as the pores are filled with water, diminishing the effective stresses and thus reducing the frictional resistance of the soil. The increase in over-pressure may reach a stage that there is no contact between the individual sediment particles. In such a case, all the frictional resistance is lost and the soil acts as a heavy liquid (Figure 11).

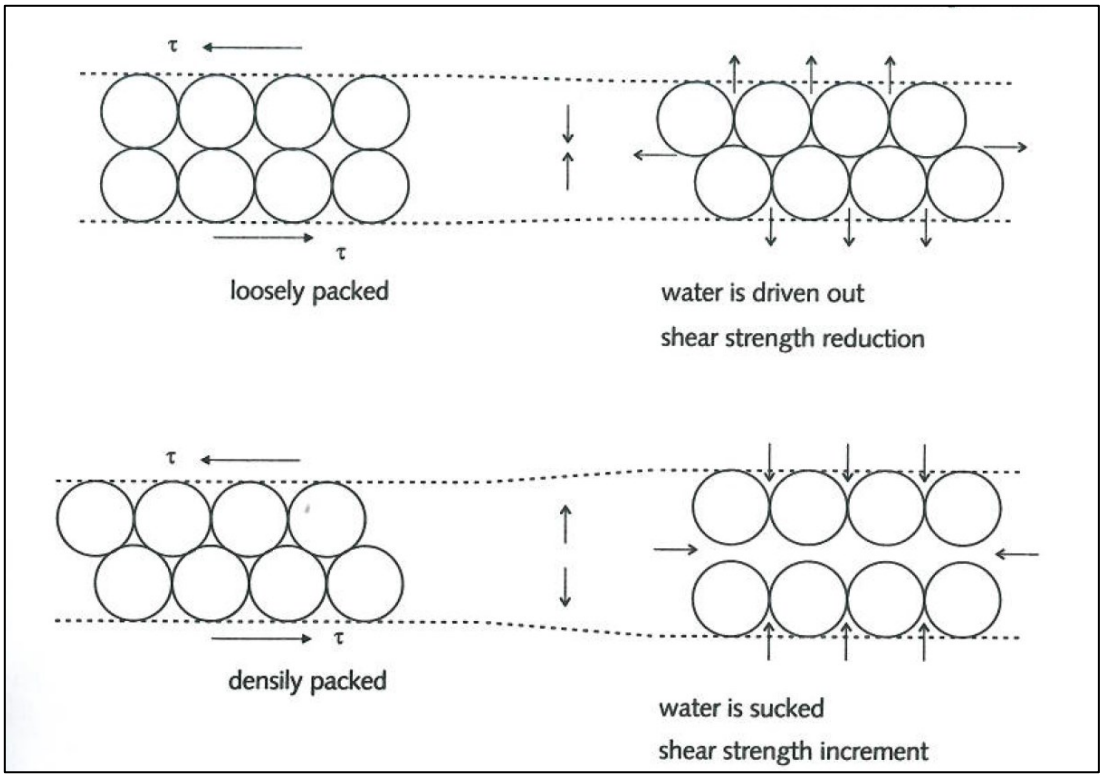

Figure 11:Effect of shear on loose and dense sand (Hoffmans, G.J. & Verheij, H. 1997)

This creates flow slides where large quantities of the foundation can liquefy and flow out under the structure. These flow slides can undermine the structure by a progressive failure under the bed protection, leading to major structural failure. The consequences of flow slides, compared to shear failure, are usually more serious for hydraulic structures (Hoffmans & Verheij, 1997).

Different types of failure modes exist namely:

- Sliding failure
- Overturning failure (seaward or landward)
- Settlement failure
- Slip failure

Each type is a result of certain forces acting on the structure. By identifying the failure mode, the reason for failure can by concluded. Typical failure modes of gravity-type seawalls are presented in Table 1.

Table 1:Failure Modes (Burcharth & Hughes, 2006)

Sliding failure:	
The structure slides seaward when the resulting pressure on the rear of the wall exceeds the sum of the frictional resistance over the base of the wall and the passive resistance at the toe. This is the result of the active soil pressure and groundwater acting on the rear of the structure.	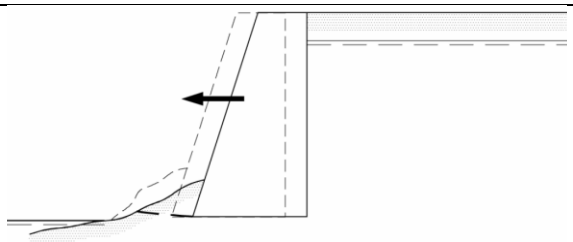
Overturning failure:	
The Seaward overturning of a seawall is a result of scour in front of the structure. It reduces both the passive resistance and the bearing capacity of the foundation allowing the resulting load from the active backfill pressure, the high groundwater table and the weight of the structure itself to overturn the structure seaward.	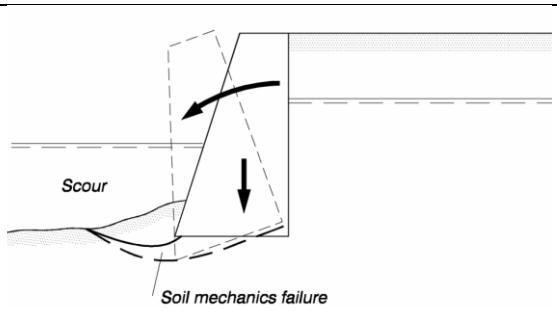
Landward overturning is due to scouring of the landward side of the structure caused by overtopping. This results in the loss of passive resistance from the backfill allowing wave loads, acting on the seaward side of the structure, to tilt the structure landward.	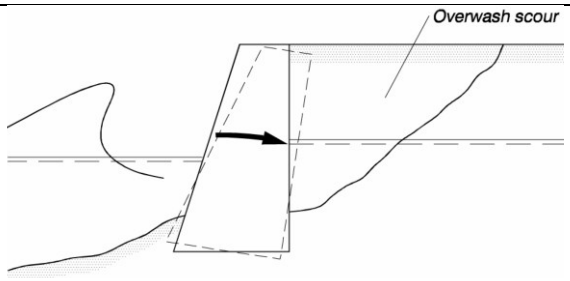
Settlement failure:	
Consolidation of the foundation soil or soil mechanics failure leads to settlement. The self-weight of the structure exceeds the bearing capacity of the soil in the foundation allowing the structure to sink into the bed.	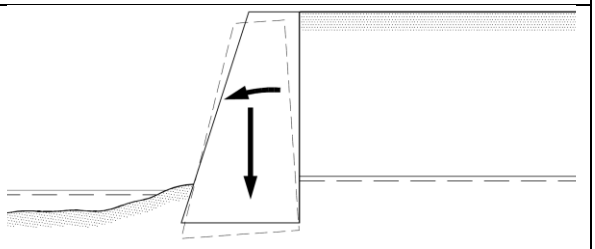
Slip failure:	
Rotational slip failure occurs when the driving moment, caused by the weight of the soil, groundwater and surface loads exceeds the restoring moment given by the soil strength.	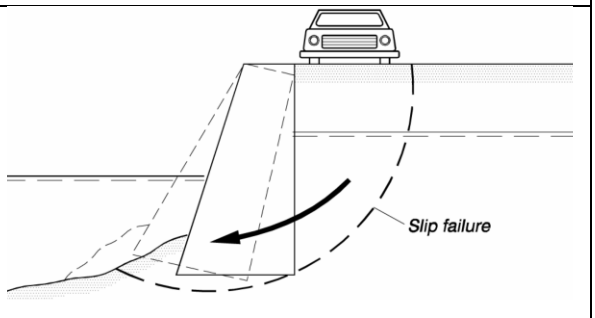

Scour undermines the frictional forces between the base of the structure element and its foundation that commonly result in sliding or slip failure. With stones being washed out of the screed layer underneath the structure due to scour, settlement failure also occurs regularly.

2.2 Soils and Rock

Soils and rocks are all geological materials. The only difference is their position in the transformation cycle of the earth's crust. Soils are loose particulate material that becomes denser as time progresses. On the opposite end, rocks are continuous stiff materials that are progressively fractured, eroded and dissolved to be transformed into soils.

Particle sizes of soils can range from over 100mm to less than 0.001mm. Figure 12describes the size ranges of soil. The terms 'silt', 'clay', 'gravel' etc. are used to describe only the particle sizes between specified limits.

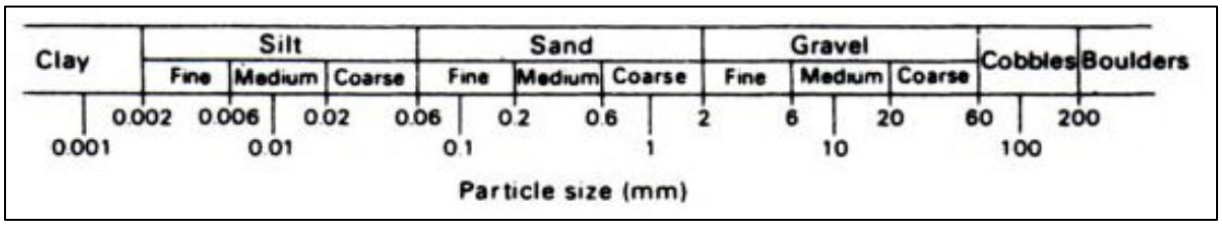

Figure 12: Soil particle size ranges (Craig, 2012)

Fine soils have smaller particles with smaller voids, but vary large variations of the total volume of voids between the loosest and the densest states whereas course soils have larger particles with larger voids but smaller variations of the total volume of voids between the loosest and densest particles. The behaviour of soils depends on its nature. Clay have viscous contacts and cohesive forces that interact with pore water. Coarser particles are less sensitive to water and can evolve in different ways, depending on their mineralogy.

The particle size as well as the nature of the soil determines the behaviour of flow through the soil. The addition of soil to the foundation may change the flow regime through the supportive screed layer, leading to a change in the scour process.

2.3 Scour of Sediment

2.3.1 General

As soon as a structure is placed in a marine environment the presence of the structure will cause flow patterns in its vicinity to change. These changes in flow characteristics cause the average bed shear stress to increase close to the structure, as well as increasing the degree of turbulence. As a result, the sediment transport capacity changes and a local disequilibrium between actual sediment, transport and the capacity of flow to transport sediment exists. As scour proceeds, a new equilibrium may be reached as the hydraulic conditions are adjusted.

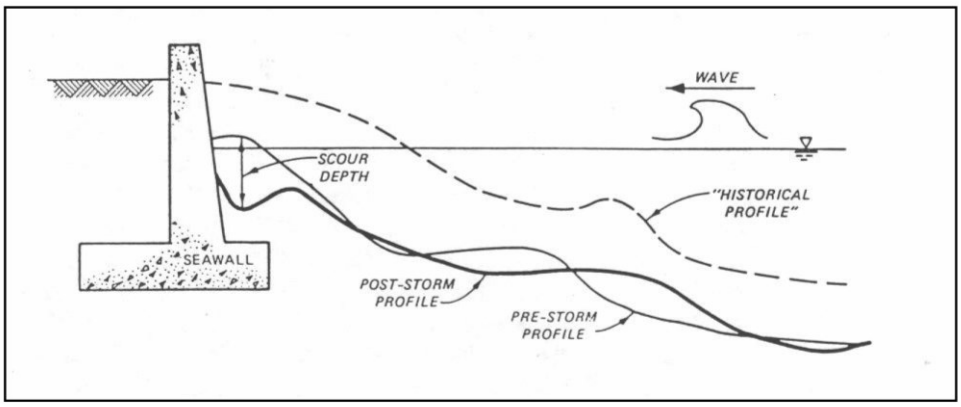

Figure 13: Scour due to breaking waves at a vertical seawall (Kraus 1988)

Two types of scour occur at a structure - general scour and local scour. Both possible processes have different length and time scales. Scour caused by each of these two processes can, as a first approximation, be added together linearly to obtain resulting scour.

General scour typically has a longer time-scale than local scour, as it is the scour that occurs due to the natural flow of the water without the presence of a structure. Bed-level changes due to general scour include slope changes, because of local currents and tides. Local scour is a direct result of the influence of a structure on the flow.

2.3.2 Scour development

Scour can be classified into two categories, clear-water scour and live-bed scour. When the bed material in the natural flow upstream of the scour hole is at rest, clear-water scour occurs. If flow that is not supporting sediment causes scour, the depth of the scour hole will reach its limit asymptotically. Live-bed scour is scour with sediment transport over the upstream undistributed bed. The equilibrium scour depth of live-bed scour is smaller than that of clear-water scour, because sediment particles that are continuously transported by the flow, enters the scour hole. Although the equilibrium scour depth is smaller in the case of live-bed scour, the scour increases rapidly with time and then fluctuates about a mean value as illustrated in Figure 14.

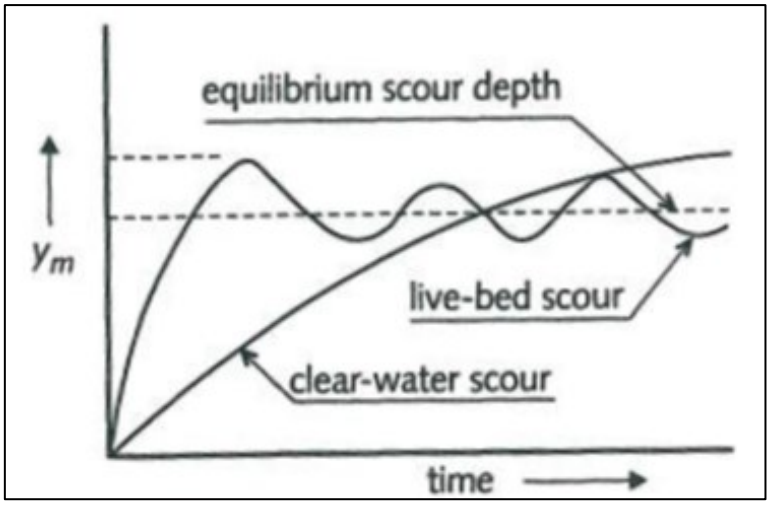

Figure 14: Scour depth as a function of time (Hoffmans, G.J. & Verheij, H. 1997)

Four phases in the evolution of scour were distinguished using scale model experiments, based on clear-water scour with small Froude numbers (Zanke, 1978). Figure 15 schematizes the four phases: initiation, development, stabilization and equilibrium.

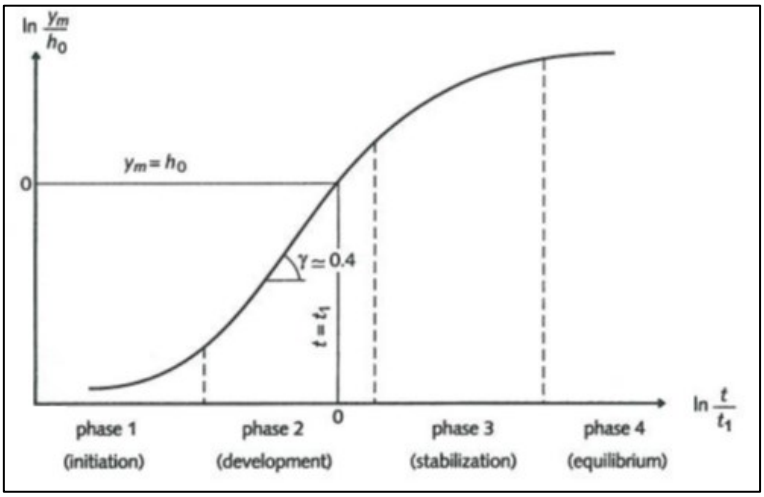

Figure 15: Development of the scour process (Hoffmans, G.J. & Verheij, H. 1997)

The initiation phase indicates that the flow in the scour hole is nearly uniform in the longitudinal direction. Scour capacity is most severe during this phase. During the development phase the shape of the scour hole do not change, but the scour depth increases considerably. Hoffmans and Verheij (1990) showed that the upper part of the scour hole is in equilibrium whereas the lower part is still developing during the development phase. Compared to the initiation phase, the suspended load close to the bed has decreased significantly. In the stabilization phase, the development of maximum scour depth decreases. Because of the lower erosion forces in the scour hole, the dimensions of the scour hole increases more in the longitudinal direction than in the vertical direction. The equilibrium phase is defined when the dimensions of the scour hole no longer change.

2.3.3 Time Scale

For a substantial amount of scour to occur, a certain amount of time must elapse. This elapsed time is called the time scale or duration of the scour event. About 50 flume experiments were conducted by Xie (1981) using different sand diameters (106 < d_{50} < 780µm). The wave height (*H*), wave period (*T*) and flow depth (*h*) were varied during these experiments with ranges of 0.05 < *H* < 0.11m, 1.17 < *T* < 3.52s, 0.2 < *h* < 0.5m. The flume experiments indicated that the development of a scour hole is a function of the number of waves it is exposed to. During the first 1 000-2 000 waves scour depth increased rapidly, reaching half of the equilibrium value. Equilibrium was reached with about 7 000 waves for steep waves (*H/λ* > 0.02) and 10 000 waves for flat waves (*H/λ* < 0.02), were *λ* is the wave length.

Based on research by Breusers, Xie (1981) the development of scour at a vertical seawall is described by:

$$y_m = y_{m,e} \left({}^{t}/_{t_m} \right)^{\gamma} \quad for \quad t < t_m \tag{1}$$

where: t = time (s)

t_m = time at which $y_m \approx y_{m,e}$ (s)

y_m = maximum scour depth (m)

$y_{m,e}$ = equilibrium scour depth (m)

γ = 0.3-0.4 (fine sediment γ = 0.3)

2.3.4 Prediction of scour depth

Based primarily on 2D laboratory experiments and limited field observations, a rule of thumb that is used as a general guide states, “the maximum depth of a scour at a vertical wall (*Sm*) is approximately less than or equal to the nonbreaking wave height (*H*) that can be supported by the water depth (*h*) at the toe of the structure” (Burcharth & Hughes, 2006).

Sm = H or Sm ≈ h (2)

However, in some cases this general rule produces an underestimated scour depth.

Fowler (1992) conducted a series of flume experiments to study methods to predict maximum scour depth at a vertical seawall. Fowler did 18 irregular waves tests and 4 tests with regular waves, placing

the seawall at different locations. Waves broke well seaward of the seawall, or immediately in front of the seawall during all his tests. A planar beach was used with a slope of 1:15.

It was found that the maximum scour depth occurs directly in front of the seawall. Fowler's findings are shown in Figure 16.

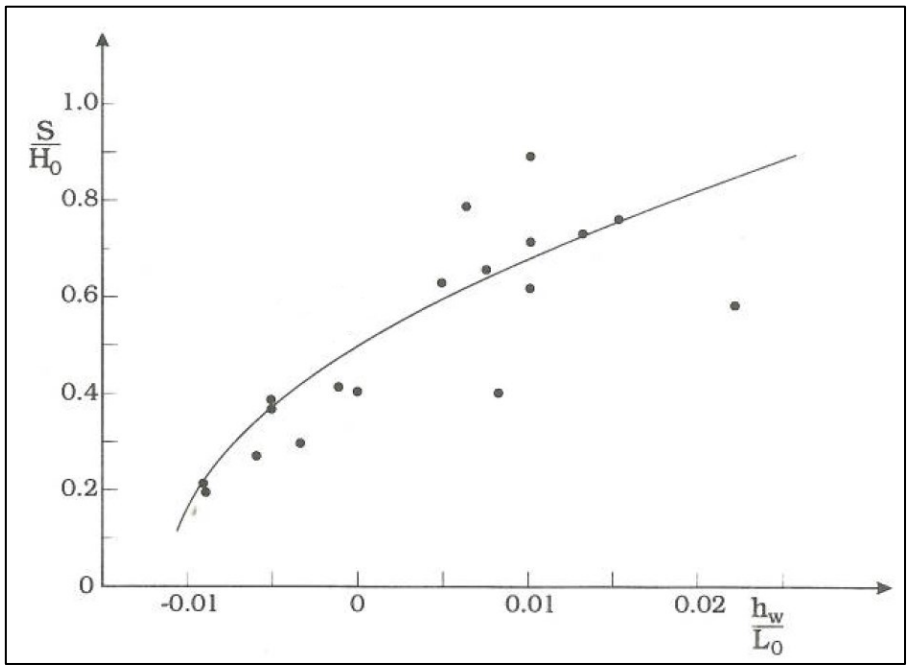

Figure 16: Relative scour depth versus relative depth at seawall (Fowler, 1992)

Although the scatter is quite large, these results show a reasonable correlation between *S/H* and *h/L*. It is clear that the scour depth increases with increasing *h/L.* This is because as the seawall is moved seaward, the breaking of the waves takes place closer to the seawall, therefore the scour depth will increase.

Based on a mathematical analysis of his irregular wave data, Fowler proposed the following equation to predict for maximum scour in front of a vertical seawall:

$$y_{m,e} = H_s\sqrt{22.75h/\mathrm{L} + 0.25} \tag{3}$$

where: h = flow depth at structure (m)

H_s = significant wave height (m)

$y_{m,e}$ = equilibrium scour depth (m)

L = wavelength

This equation is valid for coastal situations where -0.011 < *h/L* < 0.025 and 0.015 < H_s/L < 0.04.

2.3.5 Scour by normally incident breaking waves

At present, the mechanisms responsible for scour due to breaking waves are not well understood, yet we know the downward flows created by breaking waves scours the bed in front of a vertical seawall (Burcharth & Hughes, 2006). A plunging breaker, breaking in front of a vertical seawall, will penetrate down to the bed mobilizing the sediment at the toe. Similarly, a plunging breaker breaking directly onto the seawall directs water downward on the toe, in the form of a jet, mobilizing the sediment. These processes lead to scour at the toe of the seawall (Burcharth & Hughes, 2006).

Figure 17 shows the typical bottom profile sequence in front of a vertical seawall. These values were obtained by Folwer (1992) with laboratory experiments using breaking waves.

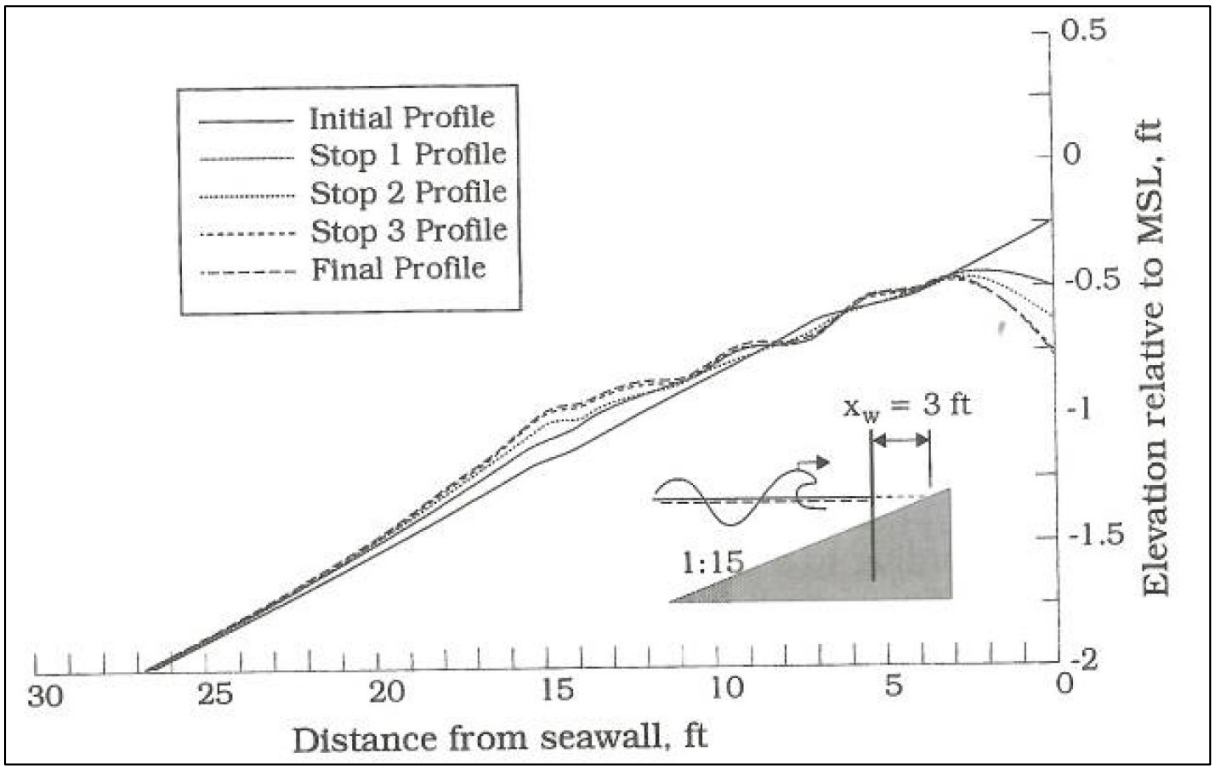

Figure 17: Typical bottom profile sequence (Fowler, 1992)

2.3.6 Scour by normally incident non-breaking waves

When there are no breaking waves, almost all the energy from the waves reaching the structure is reflected. The incident waves and reflected waves create a standing wave field with amplified horizontal particle velocities below the surface of the water. The sediment on the seabed responds to the fluid velocities by eroding the sediment where the bottom shear stresses are high and depositing it where the shear stresses are low (Burcharth & Hughes, 2006).

There are two modes of sediment transport, namely suspension-mode and no-suspension-mode. Xie (1981) introduced the following equations: Suspension-mode sediment transport occurs when

$$\frac{U_m - U_{cr}}{w} \geq 16.5 \tag{4}$$

and in contrast, no-suspension-mode sediment transport occurs when

$$\frac{U_m - U_{cr}}{w} \leq 16.5 \tag{5}$$

where: U_m = maximum orbital velocity at bed (m/s)

U_{cr} = critical velocity corresponding to the incipient sediment transport (m/s)

w = fall velocity of sediment grains (m/s)

Xie (1981) termed the type of sand for suspended mode as fine sand and for the no-suspended-mode, as coarse sand.

Based on the results of 12 movable-bed model experiments, Xie (1981) states the following empirical expression for the maximum scour depth for normally incident, non-breaking, regular waves for fine sand scour (suspended mode).

$$\frac{S}{H} = \frac{0.4}{\left[\sinh\left(\frac{2\pi h}{L}\right)\right]^{1.35}} \tag{6}$$

and for the case of coarse sand (non-suspended-mode)

$$\frac{S}{H} = \frac{0.3}{\left[\sinh\left(\frac{2\pi h}{L}\right)\right]^{1.35}} \tag{7}$$

where: S_m = maximum scour depth (m)

H = incident regular wave height (m)

h = water depth (m)

L = incident regular wavelength (m)

A similar laboratory-based empirical expression for a more appropriate case of normally incident, non-breaking irregular waves was given by Hughes and Fowler (1991)

$$\frac{S_m}{(U_{rms})_m T_p} = \frac{0.05}{[\sinh(k_p h)]^{0.35}} \tag{8}$$

where: T_p = wave period of the spectral peak (s)

k_p = wave number associated with the spectral peak by linear wave theory

$(U_{rms})_m$ = root-mean-square of the horizontal bottom velocity, which is given by Hughes (1992) as

$$\frac{(U_{rms})_m}{g k_p T_p H_{m0}} = \frac{\sqrt{2}}{4\pi \cosh(k_p h)}\left[0.54 \cosh\left(\frac{1.5 - k_p h}{2.8}\right)\right] \tag{9}$$

where: H_{m0} = zeroth-moment wave height (m)

g = gravitational acceleration (m/s²)

This is empirically based and should not be applied outside the range $0.05 < k_p h < 3.0$.

Figure 18 compares Xie's regular wave results with the results of Hughes and Fowler's irregular-wave experiments. It can be seen that the scour depth for irregular waves is considerably less than for regular waves. In many cases the predicted maximum scour due to irregular waves does not represent a threat to the structure.

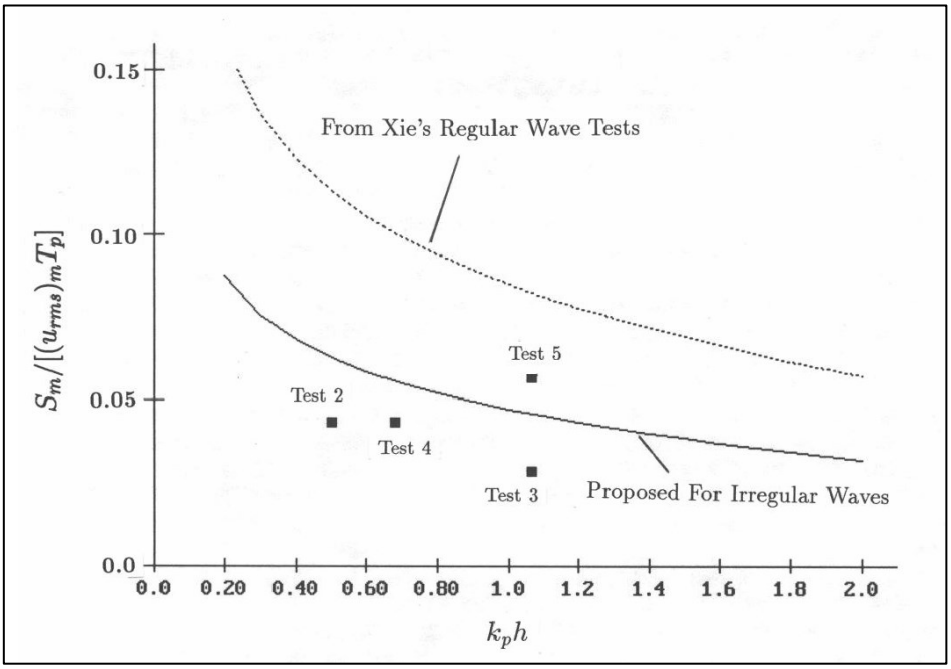

Figure 18: Scour prediction for nonbreaking waves at vertical seawall (Hughes and Fowler, 1991)

2.4 Scour of Granular Material

2.4.1 General

This study focuses on the stability of the granulated filter layer. The armour layer is directly exposed to wave and current attack creating drag, lift and abrasion forces, but some of the most critical conditions occur at the interface of the underlayer (base layer) and the base layer. The base layer protects the underlying base material from scour by waves and currents without excessive build-up of pore pressure in the underlying material. Granular filters are commonly used as a bedding layer on which a coastal structure rests. Advantages of using a granular filter are: (Burcharth & Hughes, 2006).

- Materials used in a granular filter layer (stone or gravel) are usually very durable.
- A good contact surface between the filter layer and the base material is provided by granular filter layers.
- Granular filter layers provide a more uniform construction base as it levels out bottom irregularities.
- The porosity of granular filters helps damp wave energy.
- Self-weight of the filter layer contributes to its stability, especially during construction.
- The loose nature of a granular filter allows larger stones or the structure to sink into it contributing to stability. This also allows for impacts by stones that shift during the lifespan of the structure.
- Granular filter layers are easy to repair and in some cases, it can be self-healing.
- Filter materials are widely available and inexpensive.

Granulated material such as gravel or small stone are used to construct geometrically closed filter layers so that one or more of the following filter layer functions are achieved:

- Preventing the migration of underlying sand or soil particles through the voids within the filter layer into the overlaying layers. Turbulent flow within the foundation or excessive pore pressures can cause fine particles of the base material to be washed out. Without a filter layer material in the foundation or underlayer would be lost causing differential settlement of the structure. Figure 19 illustrates the grading comparison between the base and filter layers.
- Distribution of structure weight over the underlying base material to provide more uniform settlement.
- Reduction of hydrodynamic loads on the structure's outer layers by dissipating the flow energy.

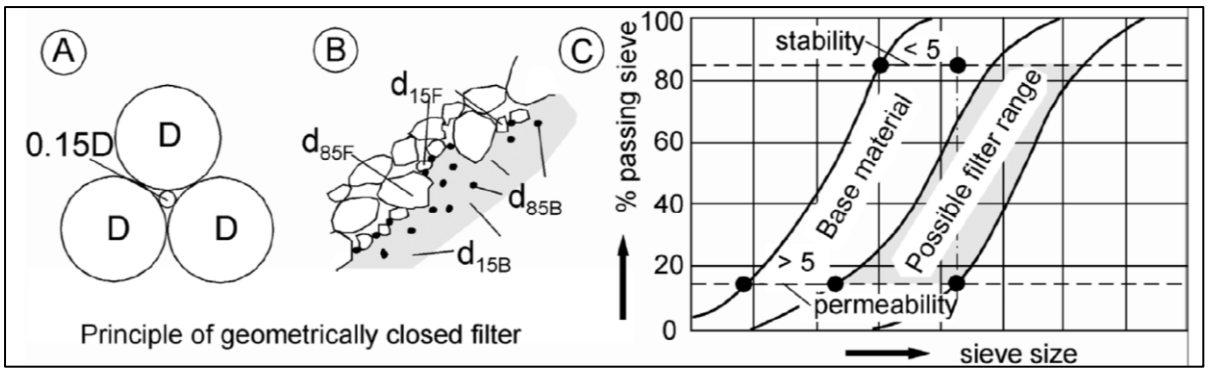

Figure 19: Interface stability of granular materials (CIRIA, C. Cetmef 2007)

2.4.2 Geometrically Closed and Open Filters

The purpose of a granular filter is to prevent scour of fine grains through the overlaying rock layer. Two design criteria can be applied: (CIRIA,C. Cetmef 2007).

Geometrically closed filter layers implies that the voids of the overlaying rock layer are too small for the finer grains to pass through. This is the traditional design approach as it is relatively simple to design. It is in some cases, however, an uneconomical design approach when a large number of filter layers are required. A flexible approach should be adopted, taking into account limitations of the local supply of quarry run.

Geometrically open filter layers, where the overlaying layer is packed less tight, have been developed to produce more economical designs. The criteria are based on the principle that the hydraulic load is too small to initiate scour of the base layer and requires detailed knowledge of hydraulic loads caused by water movement inside and along the filter layers.

Thus the purpose of each of the design approach is to prevent the transport of fine materials through the filter layer but allow for water transport.

2.4.3 Design criterion of Granular Filter Layers

Originally the design criteria for granular filter layers were based on the geometry of the voids between packed, uniform spheres. Allowances have been made for grain-size distributions which led to the following established geometric filter design criteria (Burcharth & Hughes, 2006).

2.4.3.1 Internal Stability Criterion

The criterion for a geometrically closed filter layer has been formulated by Kenney and Lau (1985):

$$[F_{4D}/F_D - 1]_{min} > 1.3 \tag{10}$$

F_{4D} and F_D are two dependant cumulative mass percentages of the grain size distribution curve defined in Figure 20. The values of $[F_{4D}/F_D - 1]$ varies moving along the curve. The minimum value is found at the flattest part of the curve.

A similar acceptability criterion for geometrically closed filter was formulated by Pilarczyk (1998). Equation 11 limits the grading width coefficient of uniformity of the filter layer. A filter layer with a wide range of gradation may lose finer particles causing instability.

$$\frac{D_{60}}{D_{10}} < 10 \tag{11}$$

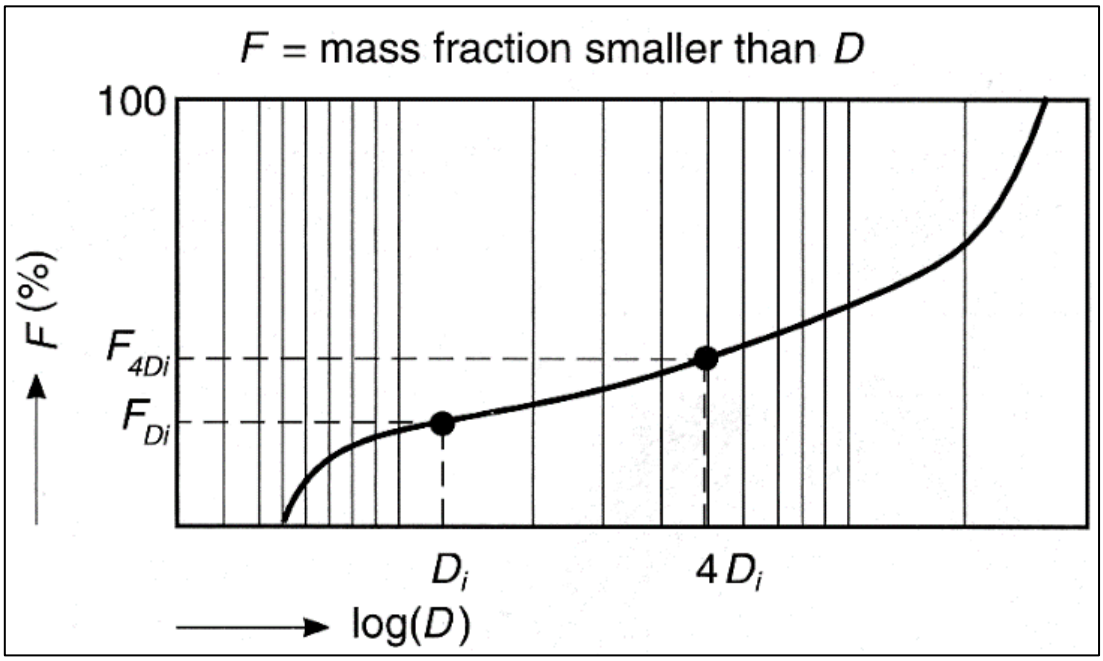

Figure 20: Particle size distribution characteristics relevant to internal stability (CIRIA,C. Cetmef 2007)

For geometrically open granular filters, Equation 12 was formulated (den Adel et al., 1988). It defines the critical hydraulic gradient. This should be compared to the actual hydraulic gradient, i. Stability is guaranteed if $i < i_{cr}$.

$$i_{cr} = \frac{1}{2}[F_{4D}/F_D - 1]_{min} \tag{12}$$

2.4.3.2 Retention Criterion

Also known as the interface stability, the retention criteria for a geometrically closed filter layer is given in Equation 13. (Burcharth & Hughes, 2006).

$$\frac{D_{15(filter)}}{D_{85(foundation)}} < 5 \tag{13}$$

The grain-size diameter exceeded by 85percent of the filter material should be less than approximately five times the grain-size diameter exceeded by the coarsest 15 percent of the underlying (foundation) material to prevent the loss of foundation or base material. A barrier is formed as the coarser particles from the underlying layer are trapped in the voids of the filter layer, not allowing the finer particles of the underlying layer to be washed out.

For geometrically open filter layers, a design relationship was developed by Bakker et al. (1994) based on the assumption that the highest hydraulic load is linked to the overlaying layer and that there is no reason for designing the filter layer stronger than the overlaying layer. The simplified relationship is given in Equation 14.

$$\frac{D_{15(filter)}}{D_{50\,(foundation)}} = \frac{15.3R}{C_0 D_{50t}} \tag{14}$$

where R is the hydraulic radius in meters, C_0 is a coefficient accounting for between the average hydraulic gradient in the foundation layer and the hydraulic gradient at the filter interface. A conservative value is $C_0 = 30$. The median sieve size stone diameter of the overlaying layer is represented by D_{50t} in meters. D_{50t} represents the hydraulic load through a Shields-type relationship. The higher the current velocity, the larger the value of D_{50t} and the smaller the value of $D_{15(filter)}$ needs to be in order to protect the foundation material for a given $D_{50\,(foundation)}$ value.

2.3.4.3 Permeability criterion

The permeability requirements for geometrically closed or open filter layers is to assure that flow resistance is small enough to prevent pore pressures contributing to the instability of the structure. To reduce the hydraulic gradient across the layer, adequate permeability of the filter layer is needed. The simplified expression is given in Equation 15 (De Groot et al., 1993).

$$\frac{D_{15(filter)}}{D_{15(foundation)}} > (4\ to\ 5) \tag{15}$$

2.3.4.4 Layer thickness

Filter layers constructed with coarse gravel or larger material, such as stone, should have a minimum thickness of at least two to three times the diameter of the larger stones in the grain-size distribution (Pilarczyk, 1990). The filter layer should never be less than 30cm thick to ensure that the irregularities in the bottom surface are completely covered. Thicker filter layers should be considered for shallow depths, exposure during construction, construction method and strong hydrodynamic forces, but no general rules can be stated.

2.4.4 Granular Filter Layer Failure Modes

A granular filter layer fails when the following situations occur: (Burcharth & Hughes, 2006).

- The base layer has eroded through the filter layer. Erosion can occur by wave and current-induced external flows parallel to the interface or by outgoing flow washing out particles perpendicular to the interface between the base and filter layer.
- The granular filter layer becomes internally unstable. Filter layers having a very wide range of gradation allows the finer fraction of the grain-size distribution to flush out between the coarser material resulting in instability. This could cause differential settlement of the overlayers, compaction of the filter layer and an increase in the layer's permeability.
- The contact surface of the filter layer and the base material or overlayer becomes unstable, and lateral shearing motion occurs between layers constructed on a slope.

2.5 Scour at Other Coastal Structures

The following structures mentioned in this section lies outside the scope of this thesis. To accurately predict scour damage at these structures detailed site-specific hydrodynamic conditions are needed.

Scour occurs at all coastal structures and is influenced by the effects of waves, wind, tides, currents and storm surge on both the structure itself and the foundation of which the structure rests. Where the structure is exposed to oscillatory flow the Keulegan-Carpenter (KC) number acts as a design parameter. The KC number is a dimensionless quantity describing the relative importance of the drag forces over inertia forces for objects in oscillatory fluid flow (Dean & Dalrymple, 1991) defined as:

$$KC = \frac{U_m T_w}{D} \tag{16}$$

where: U_m = maximum undisturbed orbital velocity of water particles at bed of structure

T_w = period of the oscillatory flow

D = diameter of structure

For the sinusoidal case, the KC number will be identical to

$$KC = \frac{2\pi a}{D} \tag{17}$$

with a equal to the amplitude of the motion.

Small KC numbers indicate that the orbital motion of the water particles is small relative to the total width of the structure. In such cases, separation behind the structure may not even occur. On the other hand, a large KC number denote water particles traveling large distances relative to the width of the structure, resulting in separation and probably vortex shedding (Sumer & Fredsøe, 2006). For a larger value of KC, it is expected that equilibrium scour depth will reach a constant value, considering the finite lifetime of the large-scale vortices in the lee-wake zone.

Sumer and Fredsøe conducted a series of physical model tests over a few years, studying the experimental verification of the KC number with different coastal structures. Their conclusions are discussed in the following sections.

2.5.1 Scour at the head of a vertical-wall breakwater

Three kinds of flow regimes were identified during the tests for flow around circular head of a vertical-wall breakwater:

- For KC < 1, unseparated flow regime.
- For 1 < KC < 12, separated flow regime with no horse-shoe-vortex formation in front of the breakwater.
- For KC > 12, separated flow regime with horse-shoe-vortex in front of the breakwater.

When KC < 1 the maximum scour depth is found to be practically nil, however, a slight disposition pattern, induced by the steady streaming around the head of the breakwater may exist. For KC numbers larger than 1, the normalized scour depth S/B increases with increasing the KC number.

Another important parameter is the effect of the presence of a co-directional current flow. With a given KC number and a slight current, the scour depth increases considerably.

Equation 18 shows scour depth versus KC number which can be used to predict scour damage at the round-head of a vertical breakwater. The equation is described in Figure 21.

$$\frac{S}{B} = 0.5C[1 - \exp\{-0.175\ (KC - 1)\}] \tag{18}$$

In which C is an uncertainty factor with a mean value of 1 and standard deviation of $\sigma_C = 0.6$.

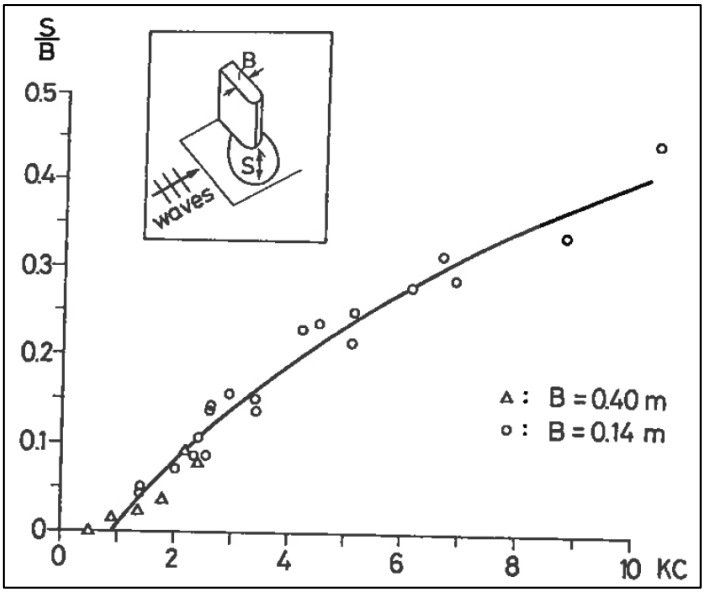

Figure 21: Normalized equilibrium scour depth as a function of KC, at the head of the breakwater with no protection layer; Live-Bed (ϑ> ϑcr) (Sumer & Fredsœe, 1997a)

2.5.2 Scour at the round head of a rubble-mound breakwater

Two mechanisms cause scour around the round head of a rubble-mound breakwater:

- Steady streaming, which occurs above the bed, around the head of the breakwater.
- Plunging breakers, which occurs at the head of the breakwater.

Regarding steady streaming, the scour hole is formed in front of the breakwater head and adjacent to it and is governed by the KC number. As the KC number is increased, so will the scour damage.

For plunging breakers, the scour damage is governed by a parameter involving wave period, wave height, water depth and acceleration due to gravity. The parameter is described by Equation 19. The larger the value of this parameter the larger the scour hole.

$$T_p/\sqrt{gH_s}\Big/_h \tag{19}$$

Scour due to steady streaming can be predicted with Equation 20 described in Figure 22.

$$S/B = 0.04C_1[1 - \exp\{-4(KC - 0.05)\}] \tag{20}$$

Where C_1 is an uncertainty factor with a mean value of 1 and standard deviation of $\sigma_{C1} = 0.2$.

For the prediction of scour by plunging breakers Equation 21 can be used described in Figure 23.

$$S/H_s = 0.01C_2\left(T_p\sqrt{gH_s}/h\right)^{1.5} \tag{21}$$

Where C_2 is an uncertainty factor with a mean value of 1 and standard deviation of $\sigma_{C1} = 0.34$.

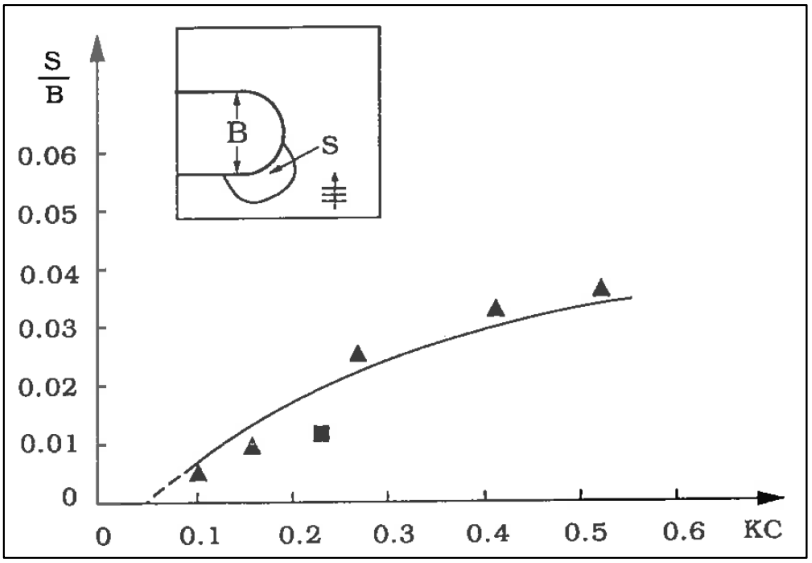

Figure 22:Maximum depth of scour hole in front of the breakwater. Scour induced by steady streaming (Sumer & Fredsøe, 1997b)

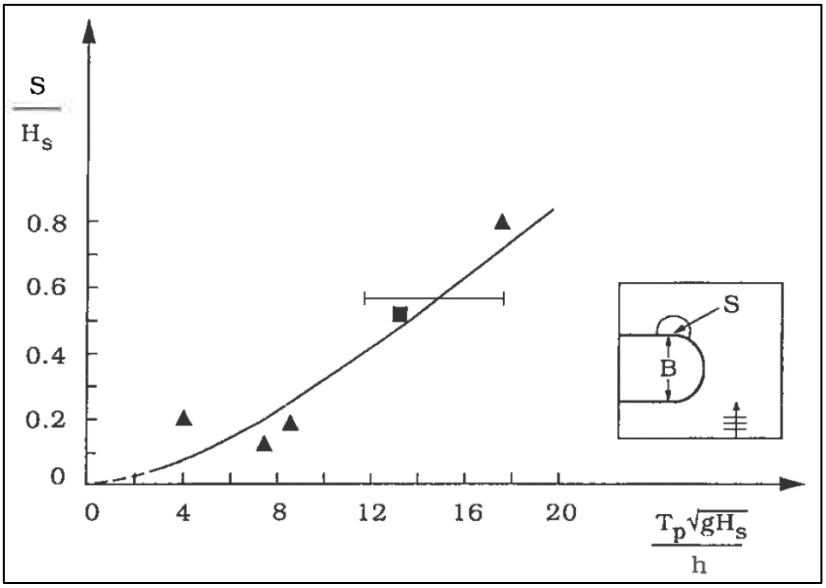

Figure 23:Maximum depth of scour hole at the lee-side of the breakwater. Scour induced by the plunging breaker. (Sumer & Fredsøe, 1997b)

2.5.3 Scour below pipelines in waves

The scour below a pipeline in waves is governed by the action of the lee-wake of the pipe. The relationship between equilibrium scour depth and the KC number can be expressed by the following equation for a pipe in contact with the seabed: (Sumer and Fredsøe, 1990)

$$S/D = 0.1\sqrt{KC} \tag{22}$$

Another important parameter to be taken into account is the position of the pipe with respect to the seabed. With an increased KC number, the scour can occur at distances of several pipe diameters from the seabed. Figure 24 illustrates the prediction of scour depth versus the KC number.

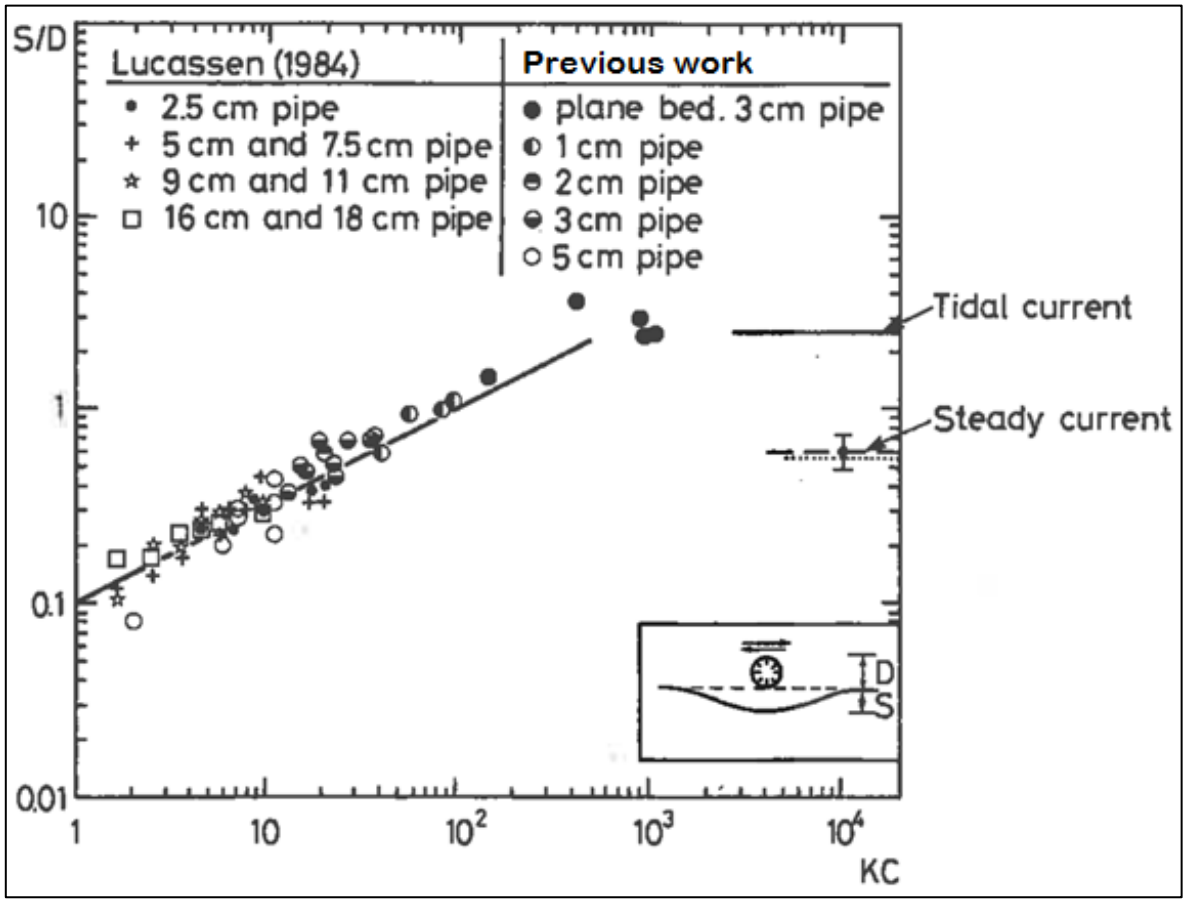

Figure 24:Equilibrium scour depth versus Keulegan-Carpenter number; Live-Bed (ϑ> ϑ_cr) (Sumer & Fredsøe, 1990)

2.5.4 Scour around a vertical circular cylinder

When a vertical cylinder is exposed to a progressive wave, near-bed 3D steady streaming occurs. This steady stream can reach values as high as 20-25% of the maximum value of the undisturbed near-bed orbital velocity. Combined with the phase-resolved component of the flow, this streaming will induce scour around the vertical cylinder. The scour damage generally increases with increasing the KC number and D/L, the diffraction parameter.

The equation for predicting scour around a vertical circular cylinder is expressed with Equation 23 and shown in Figure 25. (Sumer and Fredsøe,2001)

$$\frac{S}{D} = 1.3[1 - \exp\{-0.03(KC - 6)\}] \tag{23}$$

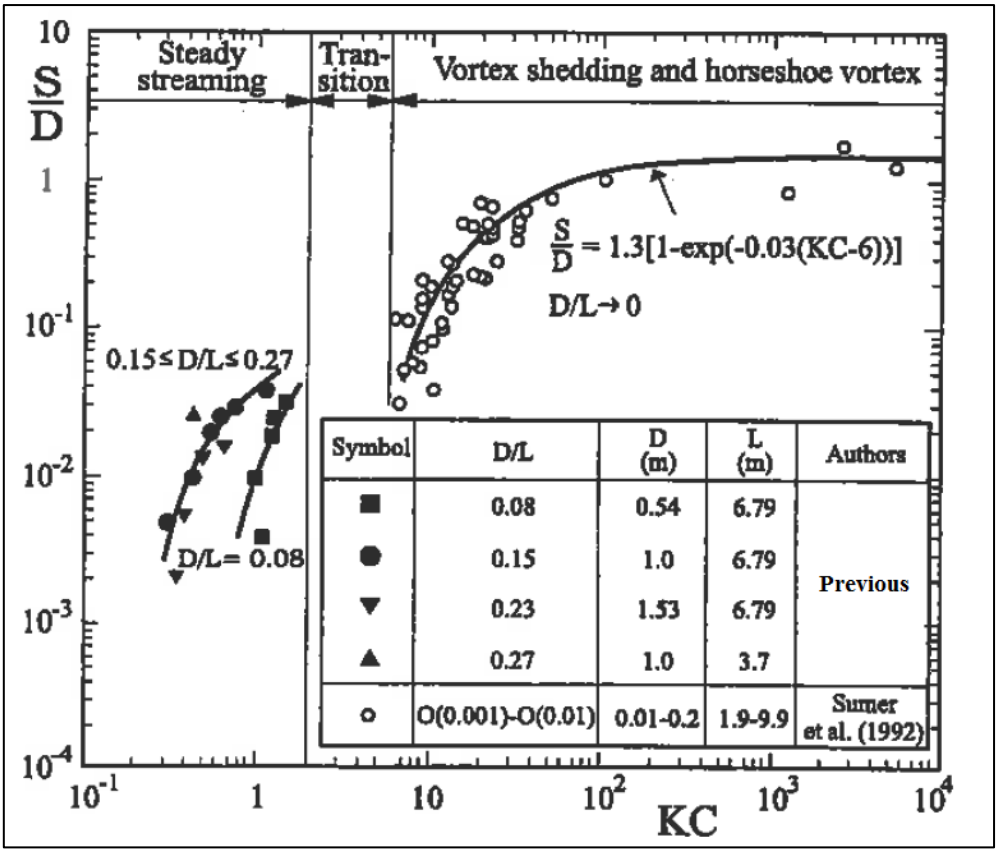

Figure 25:Maximum scour depth at the periphery of a cylinder base. Live-Bed (ϑ> ϑ_cr) (Sumer & Fredsøe, 2001a)

2.6 Grading Curves

A sample of quarry run will display a range of rock masses or sizes. For the assessment of rock mass or sizes, the percentage of total mass or size lighter or smaller than a given mass or size is presented as a cumulative curve. The mass or dimension is expressed as M_x or D_x respectively, where x per cent of the total sample is lighter or smaller that M or D.

The steepness of the curve indicates the uniformity in mass or dimension, termed the grading width or gradation of a sample. A well-graded sample implies no significant gaps in material mass or size over the total width of the grading.

For granular material, it is important to determine the grading for the following reasons: (CIRIA, C. Cetmef, 2007)

- The packing and void porosity of bulk-placed materials is highly dependent on the slope of the grading curve.
- Filtering through the sample, especially across transitions between different granular materials, is governed by rules based on gradation.
- During bulk handling and stockpiling wide graded material will tend to segregate.

2.7 Governing Parameters

The scour process at a vertical seawall may be governed by the following effects:

- Breaker type
- Presence of the seawall
- Sediment properties
- Granular material properties
- Wave boundary layer over the seabed

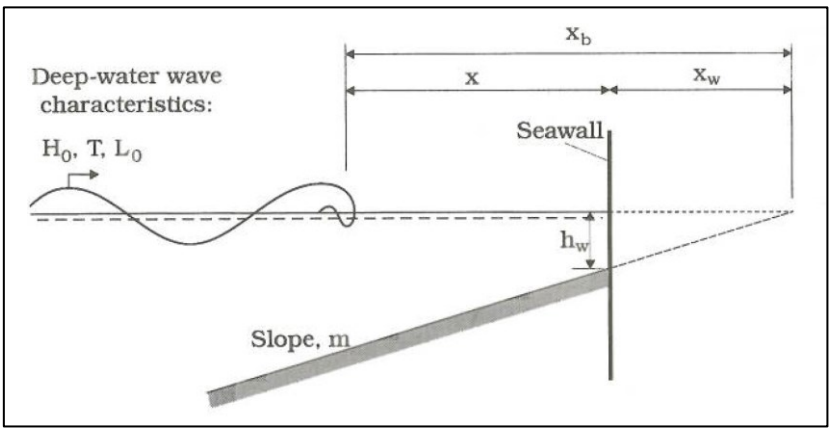

Figure 26: Definition sketch

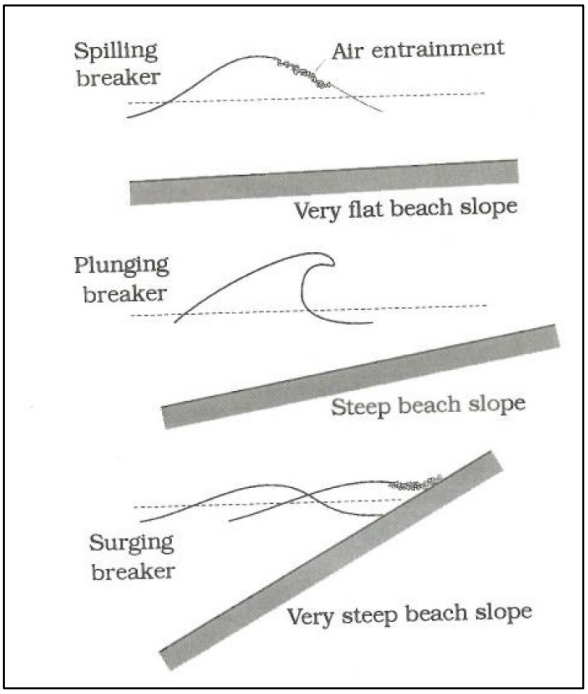

Figure 27: Breaker Types (Hughes and Fowler 1991)

2.7.1 Breaker Type:

There are three types of breaking waves as shown in Figure 27: spilling breakers, plunging breakers and surging breakers (Fredsøe and Deigaard, 1992). The breaker type is an essential factor in determining maximum scour. Thus the parameters governing breaker types will govern the scour:

$$\frac{H_0}{L_0}, m \tag{24}$$

2.7.2 Presence of the seawall:

The presence of a structure will influence the scour process. The value of h_w, the water depth at the toe of the seawall, is a significant parameter. Scour is also dependant on the distance of the breaking point of the wave from the seawall, x. These two parameters are normalized to produce the non-dimensional parameters $\frac{h_w}{L_0}$ (or alternatively $\frac{h_w}{H_0}$) and $\frac{x}{L_0}$. An additional parameter, characterizing the penetration of the breaking wave down to the bed mobilizing the sediment $\frac{T_w\sqrt{gH_0}}{h_w}$, must be taken into account. Thus the following three parameters are responsible for scour regarding the presence of the seawall:

$$\frac{h_w}{L_0}, \frac{x}{L_0}, \frac{T_w\sqrt{gH_0}}{h_w} \tag{25}$$

2.7.3 Sediment properties:

The conventional Shields parameter and the fall-velocity-to-friction-velocity ratio govern the scour process with regard to the properties of the sediment at the toe of a vertical seawall.

$$\theta, \frac{w}{U_{fm}} \tag{26}$$

Where θ is defined by $\theta = \frac{U_{fm}^2}{g(s-10)d}$ and U_{fm} is the maximum value of a characteristic friction velocity. Under live-bed conditions ($\theta > \theta_{cr}$) θ may be seen as insignificant because its influence on scour is weak.

2.7.4 Granular material properties:

The disposition of a granular particle is dependent on the mass of the particle and the space in which the particle can move. The voids in the foundation layers is a product of the grading of the material. The governing parameters with respect to the granular materials are:

$$M, D \tag{27}$$

2.7.5 Wave boundary layer:

The flow in the boundary layer is influenced by the bed category of the boundary-layer flow. Thus the governing parameters are

$$\frac{L_0}{d}\left(or\ alternatively \frac{H_0}{d}\right), RE \tag{28}$$

where RE is the boundary-layer Reynolds Number. Because the bed acts, in most engineering problems, as a rough boundary layer under storm conditions RE may be seen as insignificant.

2.7.6 All Governing Parameters

Thus, the following ten parameters govern the scour process underneath a vertical seawall if the initial bed is assumed to be planar: (Dean, 1991)

$$\frac{H_0}{L_0}, m, \frac{h_w}{L_0}, \frac{x}{L_0}, \frac{T_w\sqrt{gH_0}}{h_w}, \frac{w}{U_{fm}}, \frac{L_0}{d}, M, D \tag{29}$$

If the seawall is placed on a developed coastal profile, then the initial profile of the seabed will also be a parameter.

To ensure a constant scour process throughout all experiments for the purpose of this study, all these governing parameters should be kept constant.

2.8 Physical Modelling

The description of physical processes, related to structures constructed with rocks and sediment, with formulae, physical modelling or by engineering judgement, is always an approximation of reality. The value of physical modelling is to enable the optimisation of a design or a particular element of the structure by a more accurate approximation. A physical model integrates the appropriate equations governing the processes without simplifying assumptions.

Modelling a hydraulic process should meet the following requirements: (CIRIA,C. Cetmef, 2007)

- The model should be properly defined, such as the limits of the model, boundary conditions for all unknown values, interface conditions between different materials and general equations have to be solved.
- Define the mechanical and hydraulic models for all materials involved.
- Define the analytical or numerical methods used for solving the equations derived from principles of continuum mechanics.

2.8.1 Model Scale

2.8.1.1 Froude law of scaling

The Froude Number is a parameter that expresses the relative influence of inertial and gravity forces in hydraulic flow.

$$\sqrt{\frac{inertial\ force}{gravity\ force}} = \sqrt{\frac{\rho L^2 V^2}{\rho L^3 g}} = \frac{V}{\sqrt{gL}} \tag{30}$$

A physical interpretation of this parameter is that it gives relative importance of inertial forces acting on a fluid particle to the weight of the particle (Munson, et al. 1990). For similarity, the Froude Number must be the same in the model as in prototype. This criterion assures model flows in which inertial forces are balanced primarily by gravitational forces. This is the case for flows with a free surface. The Froude law of scaling is the most important scaling criterion to be considered when conducting hydraulic model experiments.

2.8.1.2 Scaling law to simulate wave transmission

When the hydraulic flow is dominated by viscous forces, the ratio of inertial to viscous forces is an important parameter.

$$\frac{inertial\ force}{viscous\ force} = \frac{\rho LV}{\mu} \tag{31}$$

This is known as the Reynolds Number and to achieve similitude, this number should be the same in the model as in prototype.

In the case of a rubble-mound structure, being modelled according to the Froude law of scaling, with stone sizes geometrically reduced from prototype values, relatively less wave transmission will be experienced through the structure. This is due to the frictional losses that are greater in the model as in prototype. By increasing the model stone size by the following relationship, this scale effect is countered (Hughes, 1993).

$$\frac{L_p}{L_m} = K\frac{D_p}{D_m} \quad or \quad N_L = KN_D \tag{32}$$

where: L = geometrically undistorted model characteristic length

D = stone size linear dimension

K = factor greater than unity

Two methods have been proposed in literature, one by Le Méhauté (1965) and one by Keulegen (1973) for sizing the core material of a rubble mound structure to give correct wave transmission. Hudson, et. al (1979) recommended that both methods be used to calculate the K factor, and an average taken to use in Equation 32. (Hughes, 1993)

Le Méhauté method:

Le Méhauté developed a nomogram using analytical considerations and available data for the calculation of the K factor. Le Méhauté's nomogram is given in Figure 28.

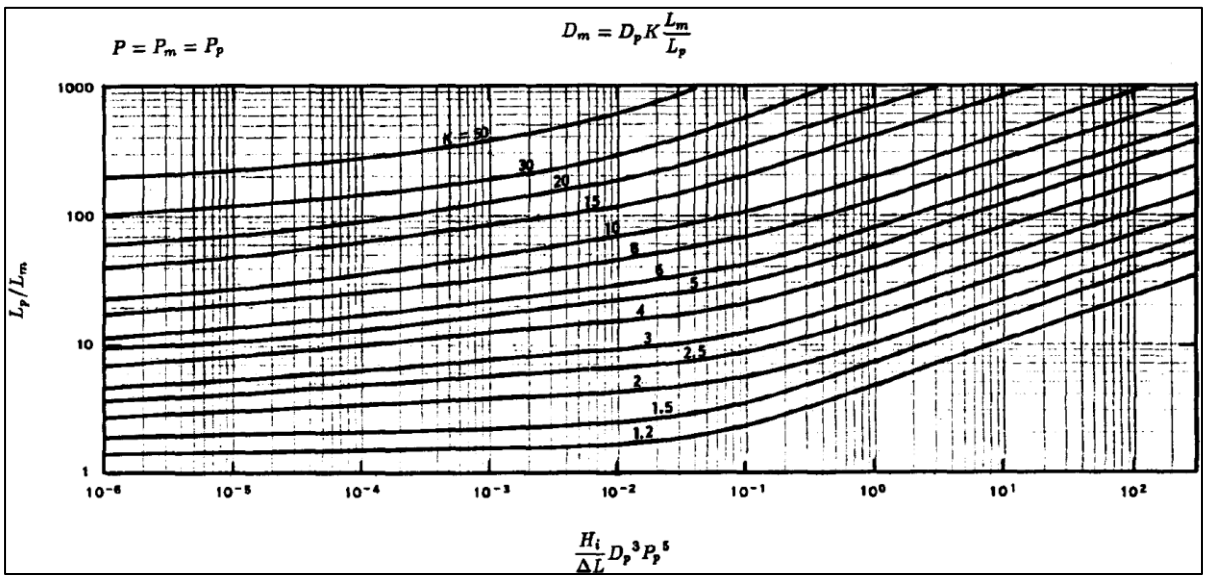

Figure 28: Nomogram for sizing model rubble-mound structures for the simulation of wave transmission in undistorted physical models (Hudson, et al. 1979)

The solid lines in Figure 28 are constant values of the factor K. The geometric length scale is represented by the y-axis and the x-axis and shows a dimensional factor that combines several parameters of the rubble-mound structure:

$$\frac{H_i}{\Delta L}\, D_p^3\, P_p^5 \tag{33}$$

where: H_i = height of the incident wave

ΔL = average width of the core material section

D_p = effective quarrystone diameter of the prototype core material in centimeters

P = porosity of the core material (0 < P < 1)

It is important to note that D_p must be a prototype stone diameter in centimeters. Parameters H_i and ΔL form a ratio that should be reserved in a geometrically undistorted model and can thus be presented as either model or prototype values.

Keulegan method:

Keulegan developed empirical equations based on experiments he conducted. Two equations were presented, one that renders wave transmission in prototype when the structure Reynolds number is greater than 2 000 and the energy losses are assumed to be a product of wave dissipation, and another that renders wave transmission in the model when the Reynolds number falls between 20 and 2000, and viscous dissipation occurs within the structure. The equations are:

For R_n > 2000

$$\left(\frac{H_i}{H_t}\right)_p = 1 + \gamma_p \left(\frac{H_i}{2h}\right)_p \left(\frac{\Delta L}{L}\right)_p \tag{34}$$

where

$$\gamma_p = \frac{P_p^{-4}}{10.6} \left(\frac{L}{D}\right)_p \left(gh\frac{T^2}{L^2}\right)_p^{4/3} \tag{35}$$

For 20 < R_n < 2000

$$\left(\frac{H_i}{H_t}\right)_m^{2/3} = 1 + \gamma_m \left(\frac{H_i}{2h}\right)_m^{2/3} \left(\frac{\Delta L}{L}\right)_m \tag{36}$$

where

$$\gamma_m = \frac{P_m^{-4}}{1.52}\left(\frac{vT}{DL}\right)_m^{1/3}\left(\frac{L}{D}\right)_m\left(gh\frac{T^2}{L^2}\right)_m^{4/3} \tag{37}$$

For the above equations, the structure Reynolds number is calculated with

$$R_n = \frac{PH_iLD}{2vhT} \tag{38}$$

and the variables are defined as:

H_i = incident wave height

H_t = transmitted wave height

L = incident wavelength

h = water depth

T = wave period

v = kinematic velocity

D = characteristic dimension (10% smaller) of quarrystone core material

ΔL = average width of core material section

g = gravitational acceleration

P = porosity of core material

The velocity, that represents the maximum seepage velocity at the entrance of the structure, used to calculate the Reynolds number is given by:

$$V_{seepage} = \frac{PH_iL}{2hT} \tag{39}$$

Keulegan (1973) derived this velocity for a uniform shallow water wave whose amplitude decreases exponentially through the porous foundation structure.

Equations 34 and 38 are used with prototype parameters to determine the prototype-scale wave transmission given by Equation 40.

$$\left(\frac{H_i}{H_t}\right)_p = \left(\frac{H_i}{H_t}\right)_m \tag{40}$$

Similarity of wave transmission requires that the same wave transmission ratio is used in the model equations (36 and 37), along with model parameters to determine the value for D_m. The values of D_m and D_p can be used in Equation 32 to find the value of factor K.

As previously mentioned, an average should be taken of Le Méhauté (1965) and Keulegen (1973) methods to determine the K factor to be used in Equation 32.

For the physical model used in this study, all rock sizes except the screed layer can be modelled following the Froude law of scaling as the flow between the larger rocks are not dominated by viscous forces. The Reynolds number of these rocks, calculated with Equation 33, are usually greater than 2000. The Reynolds number of the screed layer is usually smaller than 2000 indicating that relatively less wave transmission will be experienced through the structure. By increasing the model stone size, according to Le Méhauté and Keulegan (as discussed in this section), the scale effect is countered. The calculations of the increase in grain size for the screed layer is shown in Appendix E.

2.8.2 Laboratory and Scale Effects

There are always differences between a model and prototype responses that arise from the limitations of laboratory facilities. Laboratory effects can influence an experiment to the extent where no suitable approximation to the prototype is possible. Common laboratory effects are wave generation techniques and solid model boundaries.

Scale effects arise when a model is reduced in size compared to prototype. It is not possible to simulate all relevant forces in the model at the proper scale dictated by the similitude criteria. A common scale effect of hydraulic models is the viscous forces that are relatively larger in a model than in prototype.

2.9 Summary of Literature Study

From the literature study, it can be stated that the methods used to construct a vertical seawall has a significant effect on the performance of the structure. Each structure is designed to overcome certain forces due to its purpose and location, and the slightest deviation from the design specifications during construction can compromise the stability of the structure. Scour is often responsible for the failure of seawalls. It diminishes the effective stresses between the particles in the foundation reducing the frictional resistance between the foundation and the structure element, which can result in various failure modes.

Although extensive research has been done on scour in front of vertical seawalls constructed on a sandy seabed, very little can be applied to the scour process underneath a vertical seawall constructed on a rubble mound foundation i.e. a composite type structure. For a rubble mound foundation, great

care should be given to the filter rules of granular material in order to prevent the transport of fine materials through the overlaying rock layers but still allow for water transport through the foundation.

Previous research done on scour at other coastal structures use the Keulegan-Carpenter number as one of the governing parameters. To calculate this parameter, the maximum undisturbed orbital velocity of water particles at the bed of the structure is used. It is not possible to measure nor calculate this velocity between rocks underneath the structure, thus the KC number cannot be used as a governing parameter in this thesis. All the parameters governing the scour process underneath a vertical seawall are stated in Equation 29.

When conducting a physical model, it is important to ensure all scaling and laboratory effects are correctly accounted for.

3. Problem Formulation

3.1 Problem Statement

From previous studies the scour process of a sandy seabed in front of a vertical structure is well understood. Prediction methods have been formulated by many such as Fowler (1992) and Xie (1981) and are used as a rule-of-thumb in the industry.

The purpose of this thesis is to study the effects of scouring underneath a vertical seawall constructed on a rubble mound foundation. It is evident from site surveys that the construction method of the rubble mound foundation, with emphasis on the screed layer, is the main reason for scour problems to occur. This thesis focusses on different foundation layouts and construction procedures of vertical seawalls.

A series of physical model tests were conducted by the author to study the scour process and degree of scour for several foundations conditions and construction procedures. These laboratory experiments were conducted at the Council of Scientific and Industrial Research (CSIR), situated in Stellenbosch.

3.2 Constraints

This study was limited by the following constraints:

3.2.1 Available Equipment

The wave flume at the Department of Civil Engineering of Stellenbosch University was in use at the time the author had to conduct experiments. It was decided to book time at the CSIR in order to use their glass wave flume. All the necessary equipment at this facility were available to the author in order to complete the tests.

3.2.2 Time

The author had limited time to conduct the physical model tests due to the availability of the laboratory. Three weeks were booked at the CSIR's facilities. It was evident from the start of the research that a strict schedule had to be maintained to complete various phases of the experiments. These phases include grading of rock, building of the bed slope, construction of the cross section, setting up the instruments and conducting of an array of tests.

3.3 Design Approach

The design of the cross-section of the proposed vertical seawall was previously studied. The previous model focused on the stability of the armour units and overtopping by subjecting the model to a range of wave conditions. The cross-section was modelled with the core layer as impermeable, constructing the core layer as part of the vertical wall. The proposed research serves as an extension to previous experiments, studying the effect of scour underneath a vertical seawall constructed on a permeable rubble foundation in the Middle East.

3.3.1 Cross-Section

The proposed cross-section is illustrated in Figure 29. The structure is built on medium to dense sand dredged between 1m and 2m deep to provide a stable construction surface. The L-element is fitted with a recurved top to minimise overtopping. The core of the foundation is comprised of Class 1 rock. Overlaying the core is a Class 2 under layer and an armour layer of Class 4 rock. The gradings of the different class rock is shown in Table 2. The screed layer of 19mm stone located directly underneath the structure element is the layer of interest for this study.

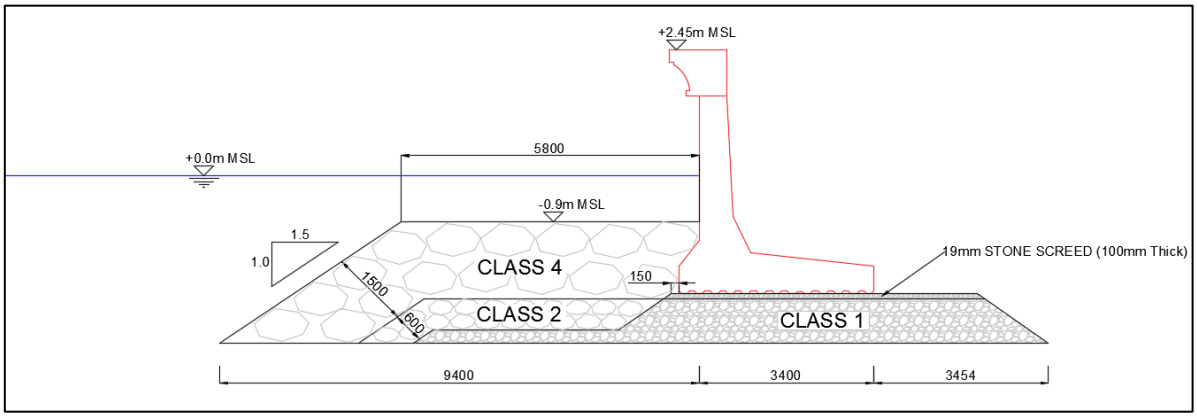

Figure 29: Original cross-section design

The design shown in Figure 29, will serve as the basis design for the testing procedure. Alterations will be made to study specific aspects of the foundations such as the effect of a thicker screed layer, longer toe width or compaction of the foundation.

A thicker screed layer exposes a greater area of small stone susceptible to scour. During construction, the thickness of the screed layer must be checked and assured that it has been distributed evenly so that the weight of the structure element is distributed evenly over the screed layer. The width of the rock toe on the seaward side of the structure, described in Figure 30, not adhering to the filter rules will cause the layer to wash out through the overlaying layers. This small width of rock can easily be constructed shorter or longer and thus it is important to check the dimension of this parameter during construction. The rock toe should always adhere to the filter rules.

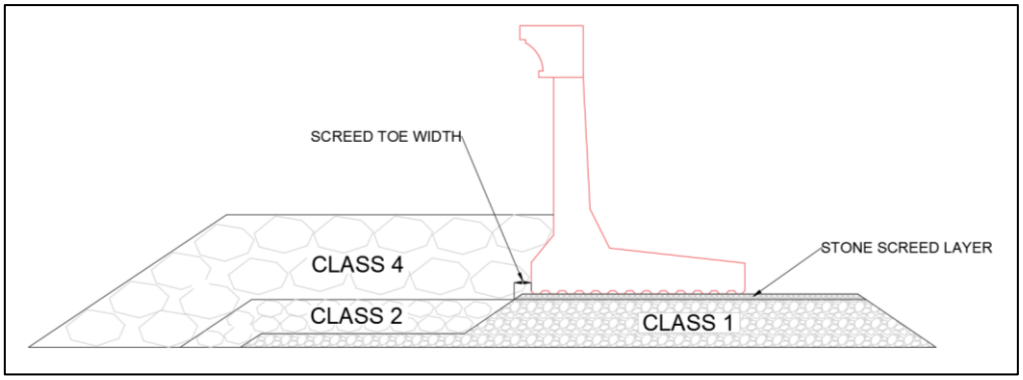

Figure 30: Definition sketch

Negligence during the construction phase can lead to an unstable structure. Compacting the foundation or adding sediment can simply be done by construction equipment resting on the foundation or wind blowing sediment particles over the foundation. Such factors need to be managed during the construction phase of the structure.

An alternative design is also proposed to serve as a solution to minimise the effect of scouring. This design is illustrated in Figure 31. The solution design strives to adhere to the filter rules as the under layer (Class 2 rock) completely covers the core layer at the toe of the structure. The screed layer is also protected as it is completely overlaid by the core layer (Class 1 rock). Two Class 5 armour stones are placed at the toe of the seawall to increase the stability and protect the underlying layers.

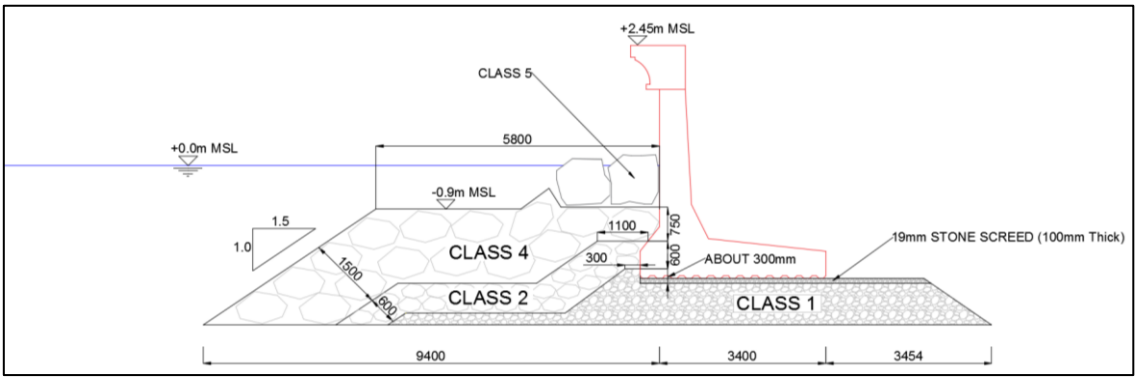

Figure 31: Solution cross-section design

Table 2: Rock grading

Name	Rock Class	Grading	Median mass (M_{50})
Core	1	50mm – 150mm	100mm
Under layer	2	1kg – 500kg	60kg
Armour layer	4	500kg – 1000kg	700kg
Roundhead Armour	5	1t – 4t	2.5t

3.3.2 Prototype Wave conditions

It is proposed to simulate a 1 in 100-year storm condition in the Persian Gulf. The same wave conditions were used throughout all the tests to study the effects of scour. The proposed wave condition is tabulated in Table 3.

Table 3: Prototype Wave condition

Condition	Water Level (MSL) [m]	Hm0 [m]	Tp [s]
1 in 100	0.4	1.5	8

4. Experimental Design and Set-up for Physical Modelling

4.1 Scope of work

As indicated by the literature, a physical model is necessary to validate certain aspects of the proposed designs. The effect of the hydrodynamic forces on the stability and performance of the screed layer, directly underneath the vertical structure, were identified as the critical aspect to investigate. The extent of damage due to scour was measured with each test. A fixed bed, two-dimensional physical model was proposed to investigate this phenomenon with the following parameters chosen as constant and variable:

4.1.1 Constant Parameters

- Wave conditions
- Bathymetry
- Grading of quarry run rock for the armour, under, core and screed layer
- Position of the vertical structure

4.1.2 Variable Parameters

- Screed layer thickness
- Width of the screed toe
- Construction procedure (different degrees of compaction of the foundation)
- Addition of sediment to the screed layer (to simulate a contaminated screed layer)

4.2 Hypothesis

From site surveys, it is expected that scour will occur and that material from the screed layer will be removed. Various aspects of the foundation, such as the thickness of the screed layer, the width of the screed toe and the construction procedure will be tested independently from each other. The values of thickness and length of the foundation chosen for the tests are not based on specific design criteria, but rather to see what effect the scour will have on the specific aspect of the foundation being tested.

It is hypothesised that a thicker screed layer will experience more damage compared to a thinner layer. The loosely packed 19mm stone layer is most susceptible to hydrodynamic forces as it is small stone easily exposed through the overlying armour layers. A thicker screed layer exposes a greater area of small stone, unable to overcome the damaging effects of scour.

Concerning the effect of the narrow screed toe width immediately in front of the vertical seawall, it is predicted that a narrower width of rock will result in less scour damage. A greater area of stone, not adhering to the filter rules, will result in the layer being washed out through the overlaying armour units.

Compacting the layer of screed reduces the voids between the stone units making the stability of each individual stone more dependent on its neighbouring stone. This also implies that the structure element is not allowed to sink into the screed layer under its own weight. It is therefore hypothesised that while the compacted screed layer is exposed to wave action, a stone removed from the screed layer will cause the layer to lose stability, causing more scour damage. Added sediments are hypothesized to increase scour damage. Cohesive and non-cohesive soils are expected to wash out of the screed layer leaving larger voids between the individual stones contributing to instability.

4.3 Model Scale

In a physical model, all physical processes should be scaled appropriately. Some processes are however not possible to scale down for practical reasons and in most occasions, it is not necessary. Model scales are typically chosen to be as large as possible to diminish scale effects. Because not all physical processes can be scaled down, some scale effects are expected in a hydraulic model. These scale effects are a product of the properties of water, such as density, surface tension, and viscosity.

For small waves, surface tension of the water-air surface can play a role in wave celerity. Hughes (1995) explained that for depths over 2 centimetres and wave periods larger than 0.035 seconds surface tension is negligible.

Viscosity does not play a significant role in the rotational free gravity surface waves. For the small distance the waves have to travel, energy dissipation from friction with the bottom surface is not significant. However, this report focusses on the screed layer underneath the vertical structure. There will be relatively less wave transmission through this layer as these stone sizes are geometrically reduced from prototype scale, creating greater frictional losses. By increasing the size of the modelled stones, this scale effect is countered. Calculations of screed layer stone sizes are given in Appendix E. Reynolds scaling is explained in section 2.7.1.2 of the literature.

The dominating forces that drive the waves in this model are inertia and gravity. Therefore, the set-up for this model was chosen to ensure similitude with the Froude law of scaling, explained in section 2.7.1.1.

A scale of 1:20 is chosen for the proposed experiments. This model scale was chosen so that crucial characteristics of the structure as well as a sufficient area of the seaward topography was included in

the model. A summary of all given scale factors is given in Table 4. The principle magnitudes, from which the scaling for the other magnitudes is derived, are listed as the first three.

Table 4: Principle scale factors

Variable	***Unit***	***2D Scale***
Length	m	$n = 20$
Time	s	$n^{1/2} = 4.472$
Mass	kg	$n^3 = 8000$
Volume	m³	$n^3 = 8000$
Force	N	$n^3 = 8000$
Discharge	m²/s	$n^{3/2} = 89.44$

4.4 Equipment

This research was conducted at the Council of Scientific and Industrial Research (CSIR). This facility is equipped with state-of-the-art facilities which was made available to the author.

4.4.1 Flume

The 2D glass wave flume used during the experiments is shown in Figure 32. It is 0.75 m wide, 30m long and has a depth of 1 m.

4.4.2 Wavemaker

The flume is equipped with a custom built, single paddle wavemaker developed by HG Wallingford. The wavemaker uses a rack-and-pinion, piston-type wave paddle with an integrated Dynamic Wave Absorption System that enables testing of high reflecting structures by compensating for waves reflected back off the structure.

The wavemaker can produce both regular and irregular waves with a maximum wave height of approximately 40cm in a water depth of 60cm between frequencies of 0.4 and 0.6 Hz. Waves are generated using digitally filtered white noise and summation of sine wave both in real time and using an offline playback method. The wavemaker is capable of producing irregular waves that conform to two standard spectral shapes, JONSWAP and Pierson-Moskowitz. The JONSWAP wave spectrum will be used in the proposed tests. For long crested waves, the software modifies the motion of the piston in real time to ensure that set down propagates realistically without interference by unwanted second order effects.

Figure 32: Wavemaker and glass wave flume

4.4.3 Probes

In order to record the incident and reflected waves, capacitance probes are used. These probes are custom built by the CSIR and are much less influenced by variations in water temperature than resistance probes. The voltage reading captured from the probes varies as the water level around the probe varies. The voltage readings are coupled to the corresponding water level by means of calibration. The data is simultaneously captured in a binary voltage format and amplified in order to convert the data to a time-series of the variation in surface elevation, from which wave parameters can be calculated. An example of probe output is given in Appendix G.

4.4.4 Camera equipment

Digital cameras were mounted on tripods facing perpendicular to the glass flume. Photographs of the foundation was taken on each side of the flume before and after each test to be used for comparison. Video footage of each test was also taken to study the process of scour. The cameras were mounted on fixed locations to ensure the images were taken from the same positions.

Figure 33: Probes and camera equipment

4.5 Model Construction

4.5.1 Bathymetry

The fixed-bed foreshore to deep-water bathymetry consisted of a 1:55 slope directly in front of the structure, 1.2 meters long, connected to a 1:20 slope stretching to deep-water for 8.6 meters. To accommodate for proper wave transformation, the bathymetry will be constructed 8.4 meters from the wave maker. The cross-section will be constructed on a horizontal surface. A description of the proposed bathymetry is given in Figure 34.

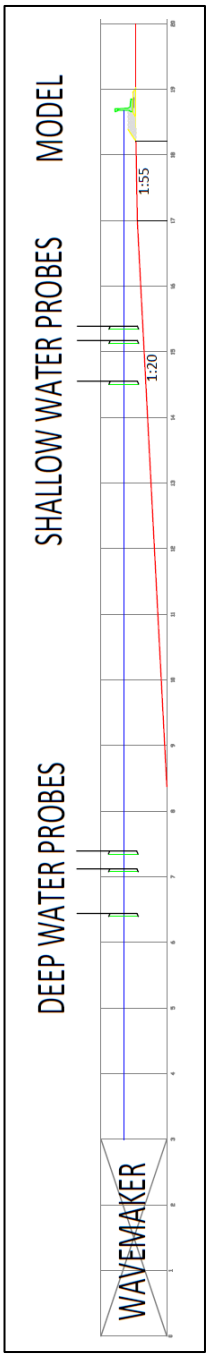

Figure 34: Long-section of flume

The foreshore slope was constructed by the model hall team of the CSIR. The fixed bed boundary of the model, simulating the prototype seabed, was modelled using light cement and finished using a smooth steel float. The construction method assures a uniform bottom roughness over the whole bathymetry. The construction process of the bathymetry is shown in Figure 35.

Figure 35: Construction of bathymetry

4.5.2 Rock Grading

A rock grading was performed on the material of each layer. A number of 100 samples were randomly taken from each of the available rock piles of uniformly graded rock and weighed. For the grading of the Class 1 rock, 100 samples were measured with a Vernier calliper. Different rock sizes were mixed in relationship to acquire the desired rock grading for each layer. This relationship was calculated using the theoretical grading curve for each layer. Grading curves are described in Section 2.5 of the literature. The grading curve for each rock class is shown in Appendix A:

The screed layer followed the scaling equations of Le Méhauté (1965) and Keulegen (1973), as the frictional losses experienced in this layer will be greater if the stones are geometrically reduced to model scale, resulting in less wave transmission. The new scaled dimension of screed stone is calculated as 1.55mm to represent the 19mm prototype screed layer stone. Calculations are shown in Appendix E. Small rock was sieved and the particles acquired between the 2mm sieve and 1.18mm sieves were used to compile the screed layer.

Figure 36: Material of scaled screed layer

4.5.3 Sediment Samples

Two sediment samples were prepared to study the effect of cohesion on the screed layer. It was decided to compile a mix with predominately sand particles and another with clay. Fine particles of rock, sand and clay were sieved through a number of sieves. The fines captured between the 0.425mm and 0.3mm sieves as well as the fines between 0.25mm and 0.15mm were chosen to compile the sediment samples. The mixture design for each sediment sample is shown in Table 5.

Table 5: Sediment mixes (model values)

	SAND mixture		**CLAY mixture**	
	Sieve Size		Sieve Size	
	0.425mm - 0.3mm	0.25mm - 0.15mm	0.425mm - 0.3mm	0.25mm - 0.15mm
Rock fines	600g	600g	600g	600g
Sand fines	600g	300g	300g	150g
Clay fines	300g	150g	600g	300g

Both mixture designs use the same relationship in terms of particle weight. The only difference between the sediment samples is that the amount of sand and clay were interchanged. The clay material acquired by the author was full of clumps and had to be crushed, hence the two different grading of clay.

The mixture designs of the sediment samples were chosen to simulate material which could be easily mixed in with the screed layer during construction process by accident. Both sediment samples were evenly mixed in with the screed layer with a ratio of 30% to 70% respectively.

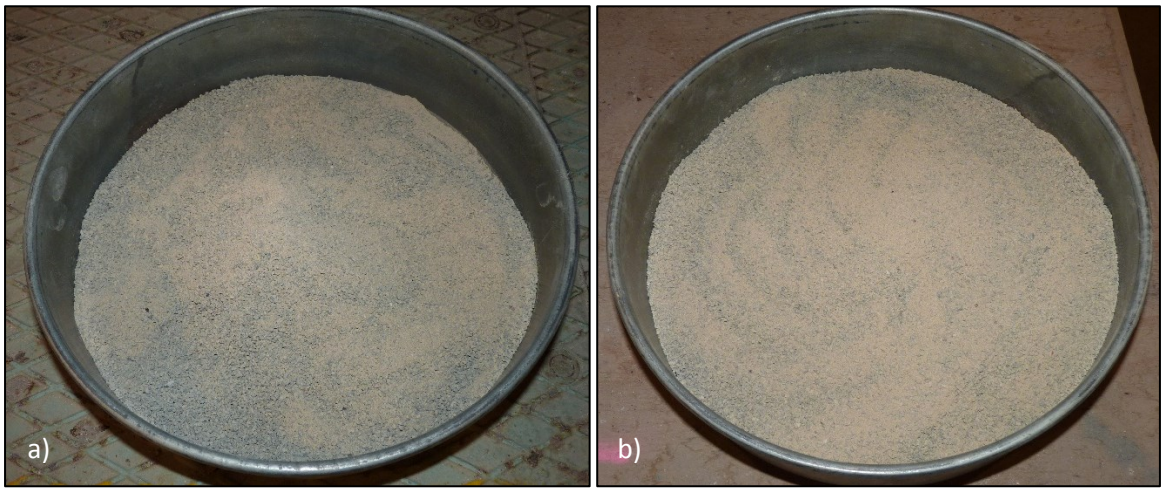

Figure 37: Screed layer material mixed with a) sand b) clay

4.5.4 Positioning of Probes

Six single probes were used in the 2D flume to record the wave conditions in the model. Three probes were used to measure wave heights in deep water and the other three was positioned in shallow water. The probes were spaced according to the minimum amount required by the reflection analysis software used. The probe spacing was calculated according to the relating wave periods used, which was transformed to wavelengths that provided the minimum and maximum distances between the probes. The deep and shallow water probe spacing are given in Table 6.

Table 6: Probe positions

Deep water			**Shallow water**		
X_{12}	X_{23}	X_{13}	X_{12}	X_{23}	X_{12}
68cm	27cm	95cm	62cm	22cm	84cm

4.5.5 Cross-Section Construction

The vertical seawall model was constructed out of marine plywood, which is a rigid impermeable material, resembling the vertical face of a concrete wall. The base of the wooden model was serrated to scale with a table saw to represent the roughness of the base of the prototype structure.

Figure 38: Vertical seawall model

A scaled down template of the cross-section was printed out and placed in appropriate locations on both sides of the flume, along the reference line. The section was traced onto the side of the flume in order to reconstruct the cross-section multiple times. Each stone layer of the foundation was placed as it would be constructed in prototype allowing each stone to be placed under its own weight. Great care was taken to ensure each layer was placed level before the next layer was constructed. After the wooden model was lowered into position the sides of the seawall were sealed with marine putty. Sealing the gap between the model and the glass flume restricts flow passing the structure and minimises boundary effects. To ensure a stable position of the wooden model, a backfill of stone and sections of train track were placed behind the seawall.

Images of the construction of the cross-section are given in Appendix C.

4.6 Data Acquisition

The required output for this research, described in the scope of work, includes validation of wave conditions, visual inspection, and assessment of scour damage.

4.6.1 Wave measurement

The wave parameters were captured by the capacitance probes positioned in the flume. These probes operate in tandem with the GEDAP software system (Generalized Experiment control and Data Acquisition Package), a general purpose software system designed to analyse and manage laboratory data including real-time experimental control and data acquisition functions. This software package was designed with an emphasis on random wave generation and analysis in hydraulic laboratory basins (Miles & Fluke, 2013). The software produced a time series of water elevation measurements as well as a calculated wave spectrum displaying significant and maximum wave heights together with peak and mean wave periods in prototype values (see Appendix G). All analysis was done by computers shown in Figure 39.

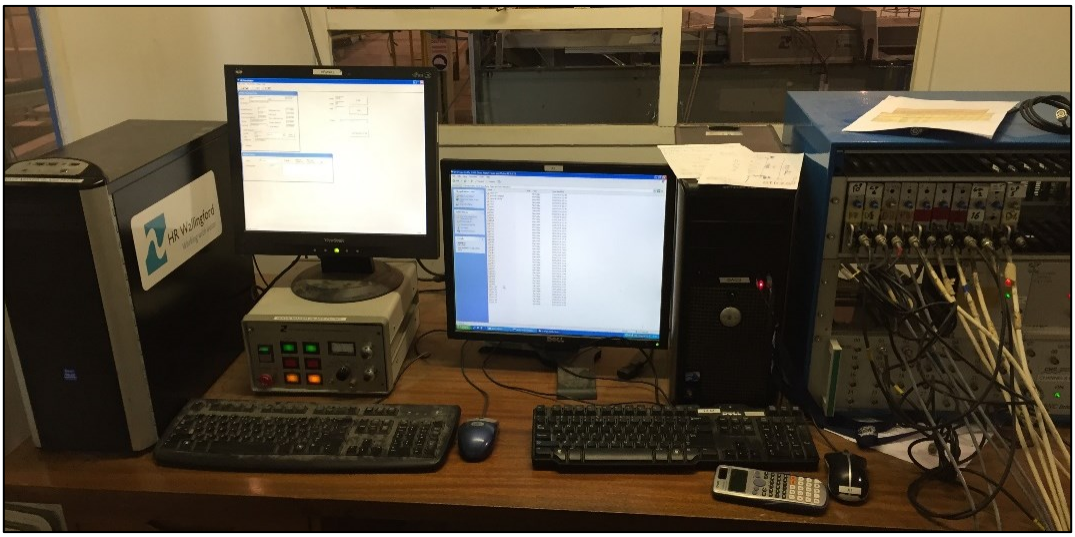

Figure 39: Control room for glass flume at the CSIR hydraulics laboratory

4.6.2 Scour Damage assessment

Scour damage assessment was done by visual inspection. Digital cameras on either side of the flume recorded damage to the foundation experienced during each test. 'Before' and 'after' photographs were analysed comparatively to inspect the damage to the foundation. Video footage of each test was also observed to study the process of scour.

No standard method exists to measure scour damage underneath a structure. Wooden dowels were used to probe underneath the base of the structure and the length which it penetrated was measured. Two different sizes of dowels were used, one with a diameter of 5mm (100mm prototype), named “Small”, and another with a diameter of 10mm (200mm prototype), named “Large”.

Figure 40: Measuring equipment

The staffs were shoved under the base of the structure one after the other at 5cm intervals across the model providing consistency through all the tests. The apparatus and testing procedure are shown in Figures 40 and 41.

Figure 41: Damage assessment

4.7 Testing Conditions

Twelve tests were proposed to be conducted prior to the start of the experiments. The conducted test series are presented in Tables 7.

Table 7: Conducted tests (Prototype values)

Test		Screed Layer Thickness [mm]	Screed Toe Width [mm]	Compaction	Addition of Sediment	Added Plastic Backside	Duration [waves]	Exposed Wave Height (Hs) [m]	Exposed Wave Period (T) [s]
A1		100	150	No	None	No	2000	1.46	8.101
A3		200	150	No	None	No	2000	1.522	7.863
B1		100	250	No	None	No	2000	1.364	8.069
B2		100	450	No	None	No	2000	1.505	7.829
C1		100	150	Sunken: -50 mm	None	No	2000	1.685	7.806
C2		100	150	Yes	None	No	2000	1.703	7.806
D1		100	150	Yes	SAND mixture	Yes	2000	1.524	7.831
D2		100	150	Yes	CLAY mixture	Yes	2000	1.413	7.821
E1		100	150	No	None	Yes	2000	1.636	7.831
F1		100	Alternative design	No	None	Yes	2000	1.43	7.831
Rpt1	1	100	150	No	None	No	1000	2.031	7.968
	2	100	150	No	None	No	2000	2.009	7.968
	3	100	150	No	None	No	3000	1.996	7.753
Rpt2	1	100	150	No	None	No	1000	1.491	7.976
	2	100	150	No	None	No	2000	1.469	7.976
	3	100	150	No	None	No	3000	1.482	7.976

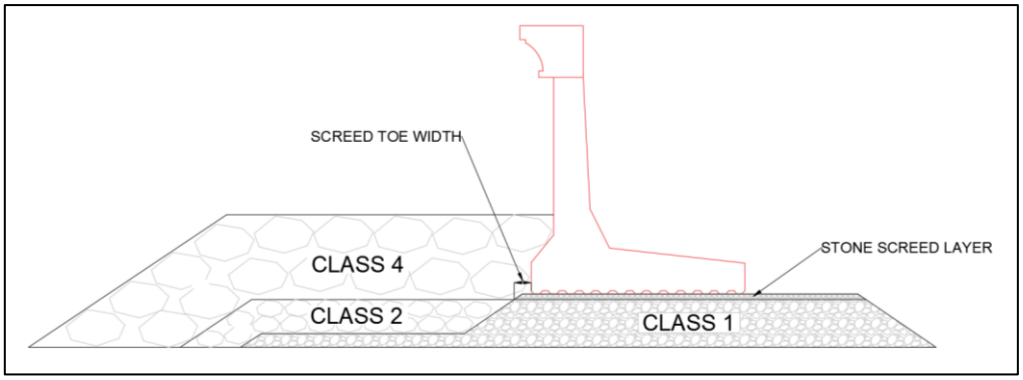

Figure 42: Definition Sketch

The definition sketch, Figure 42, indicates the dimensions of the screed layer and the screed toe width directly in front of the structure.

Compaction was done with a hand tamper (Figure 43) ensuring that the surface of the screed layer remained level. The screed layers of tests C2, D1 and D2 were compacted in the dry, gently under the self-weight of the tamper until no more deformation was visible. No stones were crushed during the process.

Figure 43: Compaction tamper

For test C1, the wooden model was sunken into the screed layer by applying external downward force onto the model during construction, simulating the structure sinking deeper into the screed layer under its own weight.

While performing the test series, concern was raised regarding the backfill of the model. Constructed from graded rock, the backfill was believed to be too porous, compared to a soil backfill in prototype. It was decided to line the back of the structure element and foundation with plastic for test E1, to counter this effect. For the construction of the plastic lining see Figure C6 in Appendix C.

Test case A1 was repeated twice (Rpt1 and Rpt2) to establish the degree of variation of the results. These tests were exposed to 3 000 waves, measuring the scour after each set of 1000 waves to observe the progress of scour damage with time.

To ensure meaningful comparison of the results of each test case, the same procedure was followed for each test. The following steps describes the principle aspects of the procedure:

1) Water level check. The flume is filled or drained to achieve the design water level.
2) The probes are calibrated and "rezero-ed" at the design water level.
3) Photographs are taken by all cameras.
4) Program wavemaker with design wave parameters and to generate 3.9 JONSWAP cycles.
5) 30 seconds from activating the wavemaker, the probes are triggered to start measuring.
6) Video footage is recorded.
7) Wavemaker and probes stop after 3.9 JONSWAP cycles are completed.
8) When water level has stilled, photographs are taken by all cameras.
9) Collect scour data from the test.
10) Wave data is analysed and checked.

4.8 Accuracy and Limitations

4.8.1 Constraints experienced during testing

The temperature of the water in the flume lowered considerably over the 2 weeks when the tests were conducted. The low temperatures influenced the wavemaker's resistance probes causing the Dynamic Wave Absorption System to produce slightly larger waves than anticipated. This was compensated for by adjusting the input wave height according to the voltage measured by the resistance probes of the wavemaker. The target wave height was 1.5m. The waves heights recorded ranged between 1.36m and 2.03m. The wave periods recorded varied between 7.75s and 8.1s with a target wave period of 8s.

The glass flume leaked during all tests. The rate of leakage was monitored regularly as the leakage rate was not constant every day. This effect was countered by calibrating the water inlet before each test. This constraint caused inaccurate measurements in test B2.

4.8.2 Methods to maximise accuracy

Probes were calibrated daily to ensure tests were conducted with updated calibration values as the water level is lowered after each test for the construction of a new cross-section. Before the study commenced, the wavemaker was well calibrated with no structure in place.

The voltage readings from the resistance probes of the wavemaker were regularly monitored to ensure the Dynamic Wave Absorption System functioned properly and the desired input wave height was calculated correctly.

5. Results

5.1 Data processing

5.1.1 Raw data

Results of each test have been acquired using the procedure explained in Section 4.6.2. The raw data from each test was plotted as seen in Figure 44. The raw data graphs can be seen as a top view of the structure element's foundation. Scour damage is presented as the horizontal distance (measured from the seaward face of the seawall) that the 100mm ("Small") and 200mm ("Large") prototype diameter probes could penetrate. The raw data of each test is given in Appendix B.

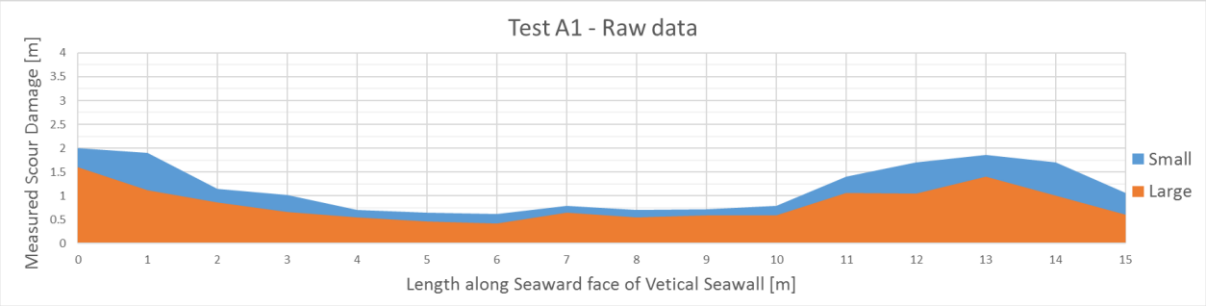

Figure 44: Raw data from test A1

By inspection of the scour damage of all the tests, it was decided that 15cm (3m prototype) on each side of the 75cm (15m prototype) wide model will be neglected. This is a conservative assumption primarily based on the raw data from test F1, which produced the most constant data over the length of the model. It can clearly be seen that the boundary conditions have a definite influence on the obtained data. Figure 45 illustrates the raw data from test F1 with the boundary conditions included.

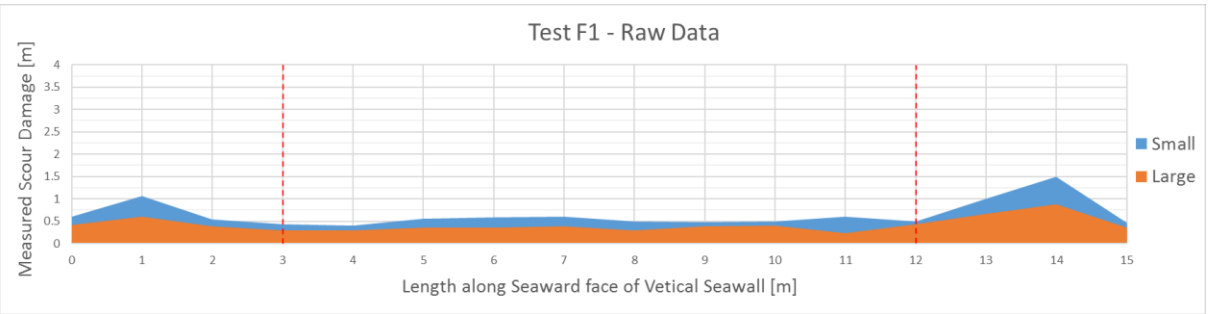

Figure 45: Raw data from test F1 with boundary conditions shown

In order to compare the scour damage of a test to another, the average between the small and large measurements was taken. Then the average of over the length of the structure was taken. This average value represents the measured scour damage of a test. This value is just an approximation of the scour damage as it may vary within a certain confidence interval.

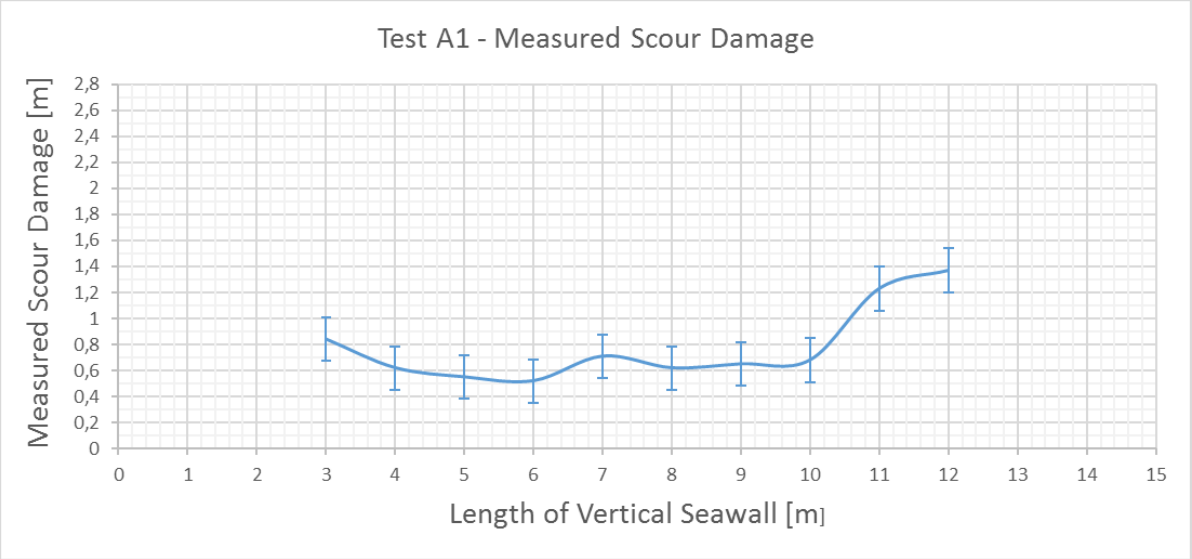

Figure 46: Measured scour damage across length of seawall with confidence intervals as a function of the foundation condition

5.1.2 Confidence Intervals

By analysing the repeated tests together with test A1, it was seen that the measured scour damage is a function of the foundation condition being tested (test A1, A3, B1 etc.) and the wave-height it is exposed to. Section 4.8.1 explains the variation in exposed wave-height. Because these two functions (foundation type and exposed wave height) have a simultaneous effect on the measured scour damage it was decided to calculate their effects separately and adding their distinctive confidence intervals together.

For the function of the foundation condition, the confidence interval was calculated with the measurements taken over the length of the structure. It was decided that a 90% confidence interval on the average obtained, will be satisfactory. The basis of the statistical analysis is given in Appendix F. As an example, the confidence interval of the scour damage, as a function of the condition, of test A1 is shown in Figure 47.

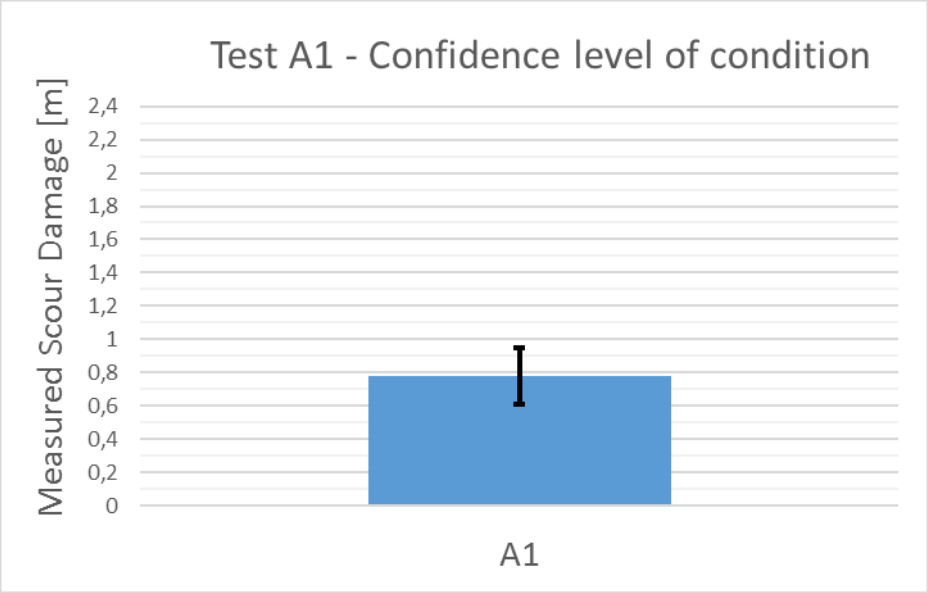

Figure 47: Confidence interval of mean measured scour, as a function of the foundation condition, test A1

Calculating the confidence interval as a function of the exposed wave height, required the results of tests Rpt1 and Rpt2. The measured scour damage from test Rpt1 and Rpt2 after it has been exposed to 2000 waves together with the measured scour damage from test A1, was plotted against their exposed wave height, Figure 48. All three tests were performed with the same foundation condition.

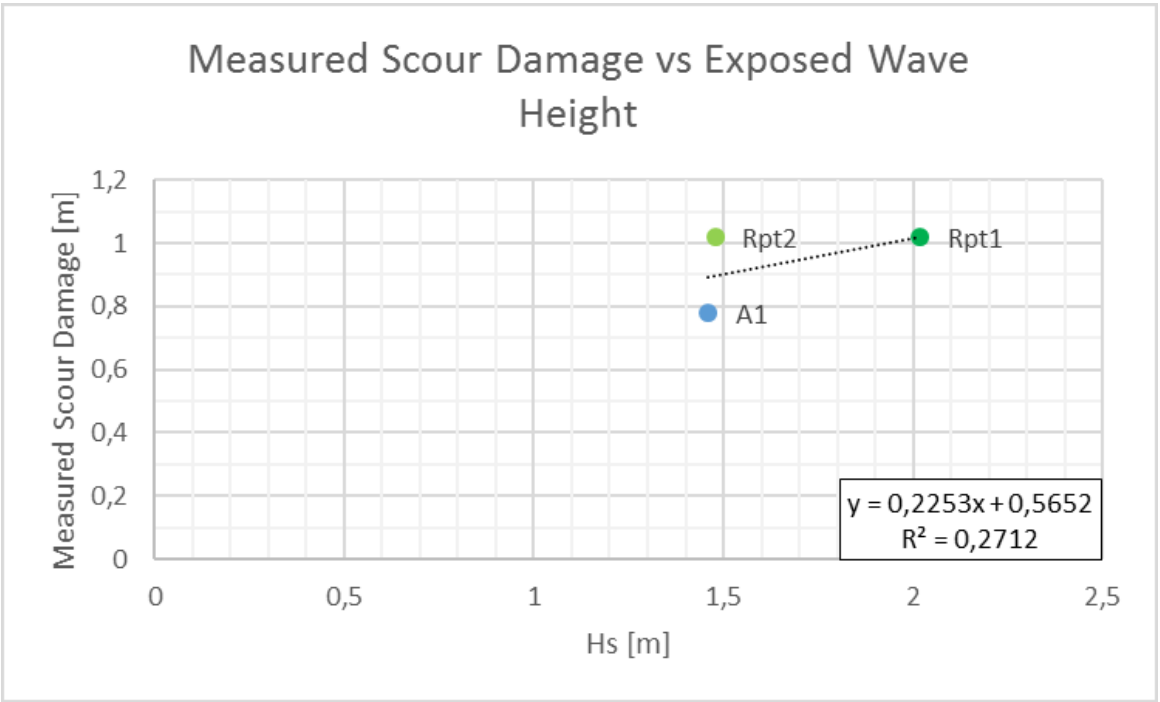

Figure 48: Measured scour damage vs exposed wave height

A trend line was plotted in order to obtain an equation to predict the scour damage with a given exposed wave height. This trend line is just an approximation and accounts for only 27% of the data as the plotted data varies seemingly. These relationships between the predicted and measured scour damage are illustrated in Equation 41 and in Figure 48.

The equation of the trend line was used to predict a value for scour damage for Test A1.

$$S = 0.2253Hs + 0.5652 \tag{41}$$

$$S = 0.2253(1.46) + 0.5652 \ = 0.894m$$

The predicted scour damage was compared to the measured scour damage for Test A1 and a difference of 15% was calculated.

$$\frac{predicted\ S}{measured\ S} - 1 = \frac{0.894}{0.779} - 1 = 15\%$$

Thus, the measured scour damage of each test may vary by 15% as a result of the variance in exposed wave height.

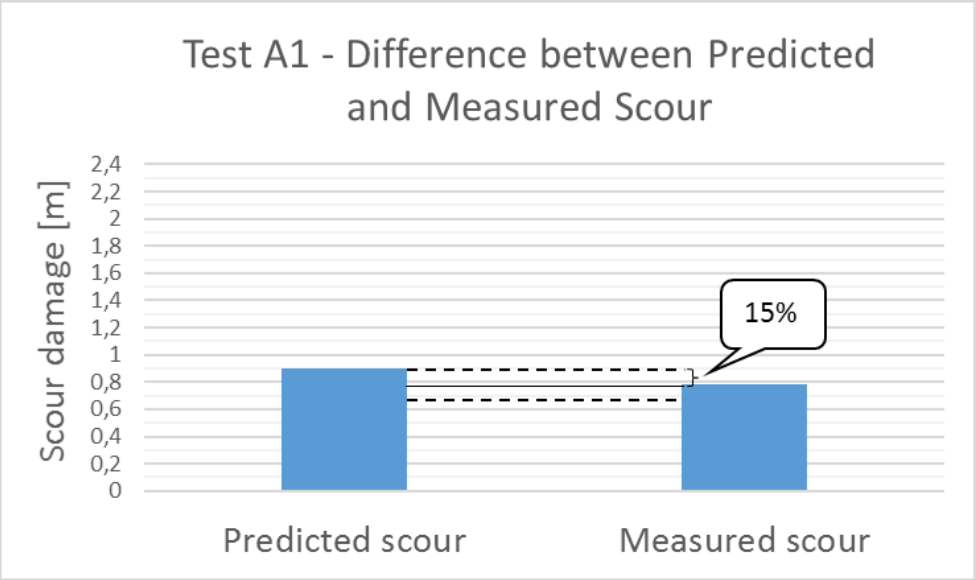

Figure 49: 15% difference between predicted and measured scour damage, from test A1

By adding the confidence intervals from the function of foundation condition and exposed wave height of each test, an interval of possible scour damage is created for a single test. Note the scour damage is given as prototype values.

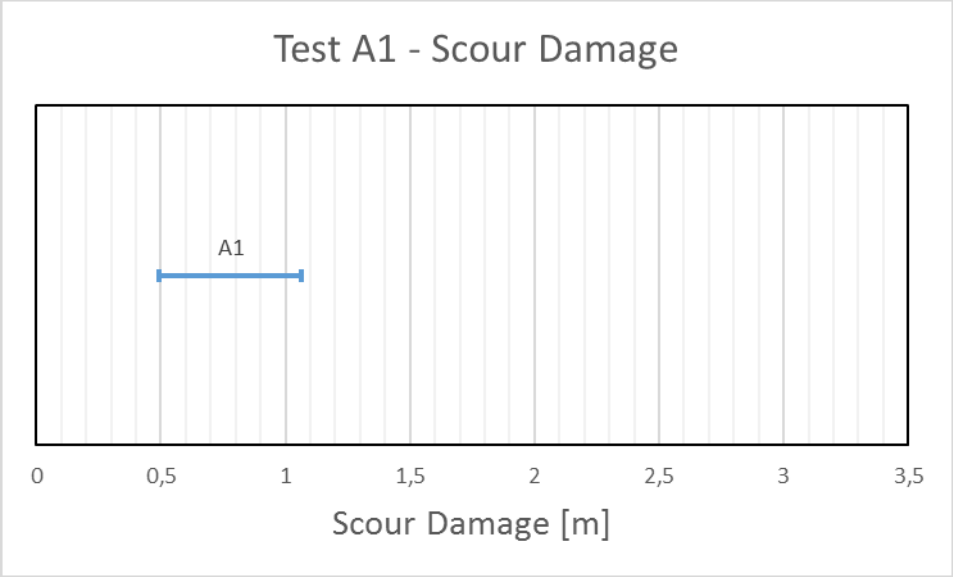

Figure 50: Possible scour damage for a given condition

Now all the possible outcomes of each test can be calculated and compared to each other.

5.1.3 Comparison of tests

Now that the range of possible outcomes of each test is calculated, these outcomes must be compared with each other to see if the results are significantly different from one another. This comparison was done by calculating the correlation between two tests.

The correlation was calculated as a percentage of how much the ranges of two tests overlap. As shown in Figure 51, the percentage was taken over the total range of two tests (S_1/S_2). A correlation of more than 50% implies that no significant difference can be stated.

$$\text{i.e. } S_1/S_2 < 50\% \rightarrow significant\ difference$$

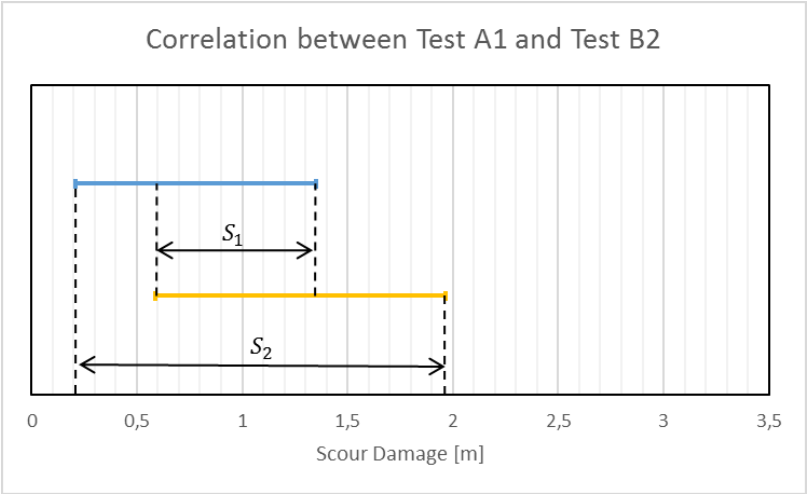

Figure 51: Parameters for correlation between two tests

5.2 Time Scale

Figure 52 shows the measured scour damage as a function of the number of waves the foundation condition is exposed to. The results of Rpt1 and Rpt2 are shown with no confidence levels as the foundation conditions were the same in each test. The variation of exposed wave height is also neglected as the same wave height was experienced throughout a test series. Thus, this figure illustrates the variation in time of the scour process.

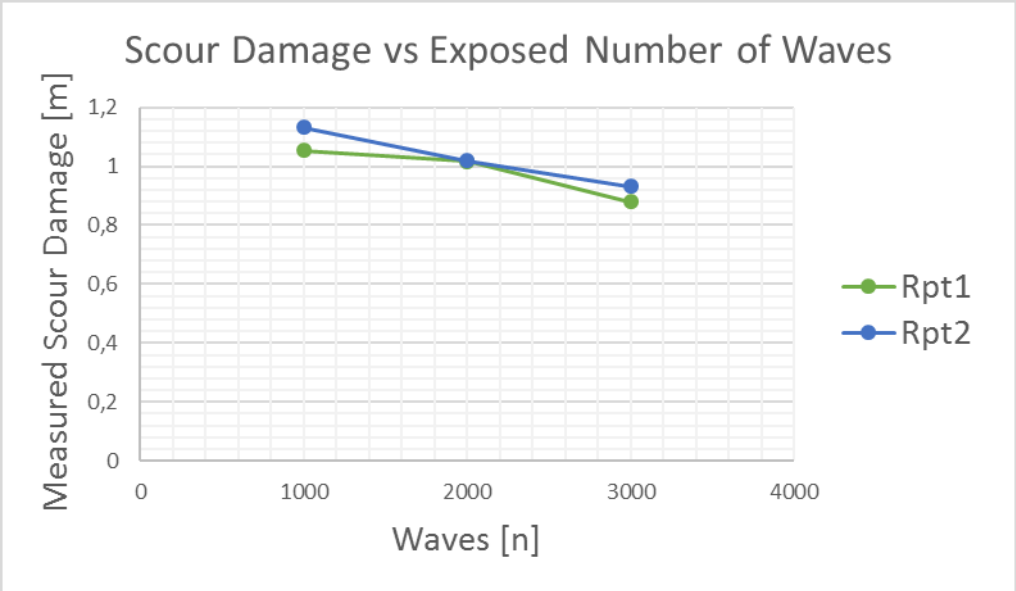

Figure 52: Scour damage as a function of time

Figure 52 shows a decrease is scour damage over time. This is because equilibrium scour damage has already been reached before the structure have been exposed to 1000 waves. For the next 2000 waves, a small amount of infilling occurs. This is a result of the fluctuation of the scour process about the mean damage value, explained in Section 2.3.2. It is speculated that the measured scour depth will increase a small amount when exposed to more than 3000 waves and then decrease again, fluctuating about the mean.

From these results, it was conservatively decided that all tests should be exposed to 2000 waves.

5.3 A Series – Thickness of Screed Layer

Table 8: Parameters and results of series A

	A1	A3
Screed Thickness	100mm	200mm
Toe Width	150mm	150mm
Compacted Foundation	No	No
Sediment Addition	None	None
Exposed Wave height (Hs)	1.46m	1.52m
Scour damage	0.78m	1.44m
Confidence Interval	0.49 – 1.06m	0.89 – 1.99m

With a correlation value of 11.7%, the two results of the A series are significantly different. Thus, it can be stated that a thicker screed layer is more susceptible to scour. However, the results do not imply that the screed layer should be as thin as possible. The screed layer plays a crucial role in the stability of the structure. Pilarczyk (1990) stated that the thickness of such a layer should be at least two to three times the diameter of the larger stones in the grain-size distribution.

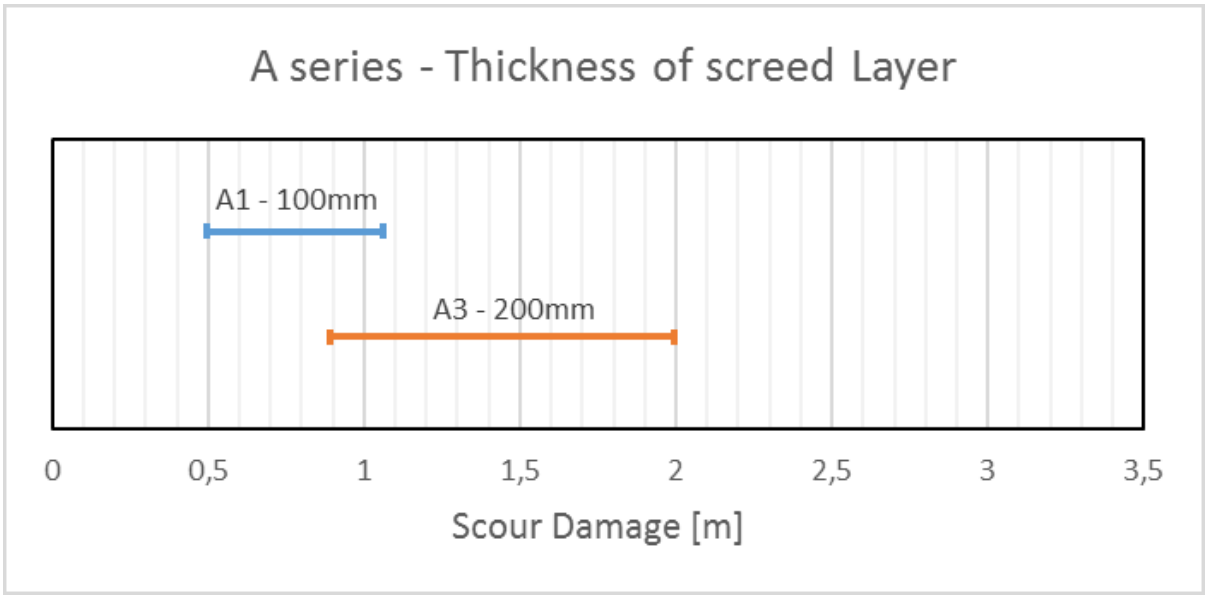

Figure 53: Scour damage of series A

Table 9: Correlation between tests in series A

Comparison	A1 = A3
Correlate	11.7%
Significantly Different	Yes

The results obtained support Pilarczyk's design criterion with the addition that the screed layer should not be thicker than five times $(100/19 = 5.26)$ the diameters of the larger stones in the grain distribution.

5.4 B Series – Screed Toe Width

Although all three tests in the B series are significantly different from each other, the series produced unexpected results. The 250mm toe width test showed more scour damage than both the 150mm and 450mm toe width tests. The case that the 250mm toe width experienced more scour damage than the 150mm toe width is expected as this means a bigger toe area, not adhering to the filter rules, is exposed. As mentioned in Section 4.8.1 the glass flume experienced a leak and an error was made by the author during the 450mm toe width test when the water level rose by 20cm (prototype value). This explains the low scour damage for the 450mm toe width test. The hydraulic forces on the screed layer were less in the deeper water. Thus the results of 450mm toe width test can be dismissed. Refer to Figures D1 and D2 in Appendix D for photographs of risen water level.

Table 10:Parameters and results of series B

	A1	B1	B2
Screed Thickness	100mm	100mm	100mm
Toe Width	150mm	250mm	450mm
Compacted Foundation	No	No	No
Sediment Addition	None	None	None
Exposed Wave height (Hs)	1.46m	1.36m	1.51m
Scour damage	0.78m	2.081m	1.276m
Confidence Interval	0.49 – 1.06m	1.65 – 2.52m	0.93 – 1.62m

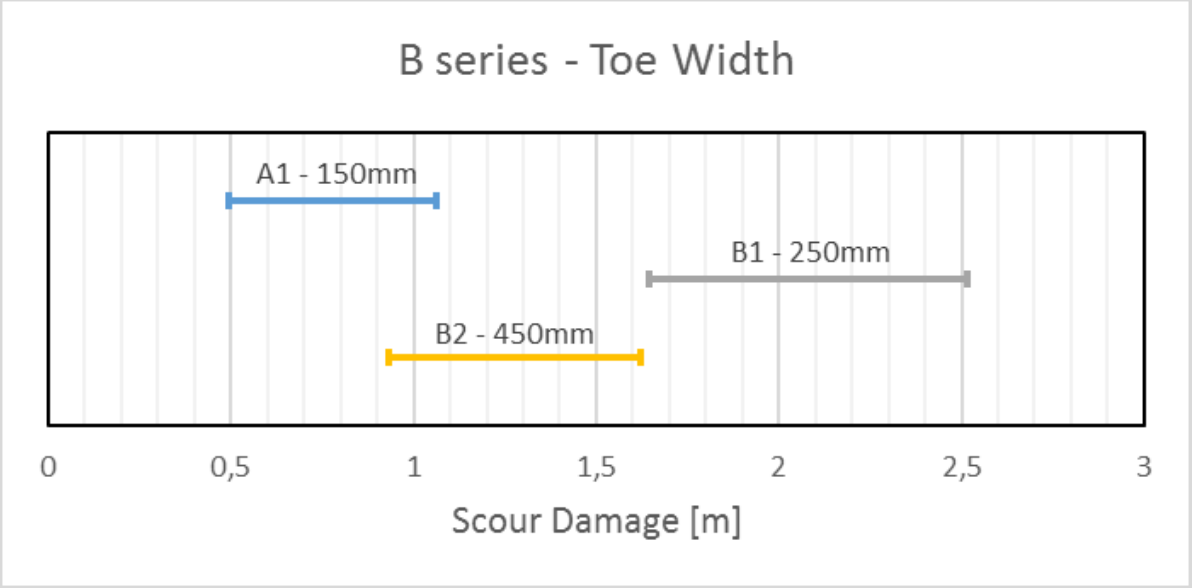

Figure 54: Scour damage of series B

Table 11: Correlation between tests in series B

Comparison	A1 = B1	A1 = B2	B2 = B1
Correlate	0%	11.73%	0%
Significantly Different	Yes	Yes	Yes

From the results of the 150mm and 250mm tests, it can be stated that the screed toe width, not adhering to the filter rules, contribute significantly to the scour process under a vertical seawall. It is recommended that the toe of the screed layer be as small as possible, always adhering to the filter rules.

5.5 C Series – Compacting the foundation

No significant difference was determined between the tests where the wall was placed on or sunken into the screed layer. This indicates that the weight of the backfill is heavy enough to sink the seawall into the screed layer until the maximum capacity for both cases.

If the foundation is compacted before the seawall is placed, noticeably more scour damage occurred. A compacted foundation causes the seawall not sinking into the screed layer, leaving the serrated base standing upon the screed layer. The serrated base can create unwanted flow patterns underneath the seawall if it is not filled with stones, increasing scour forces. Another possible cause is that an individual stone relies more on its neighbouring stone for stability if the layer is compacted. Removing one stone creates instability of another stone, inducing an accelerated chain reaction of scour damage.

Table 12:Parameters and results of series C

	A1	C1	C2
Screed Thickness	100mm	100mm	100mm
Toe Width	150mm	150mm	150mm
Compacted Foundation	No	Sunken	Yes
Sediment Addition	None	None	None
Exposed Wave height (Hs)	1.46m	1.69m	1.7m
Scour damage	0.78m	0.881m	1.33m
Confidence Interval	0.49 – 1.06m	0.58 – 1.18m	0.98 – 1.68m

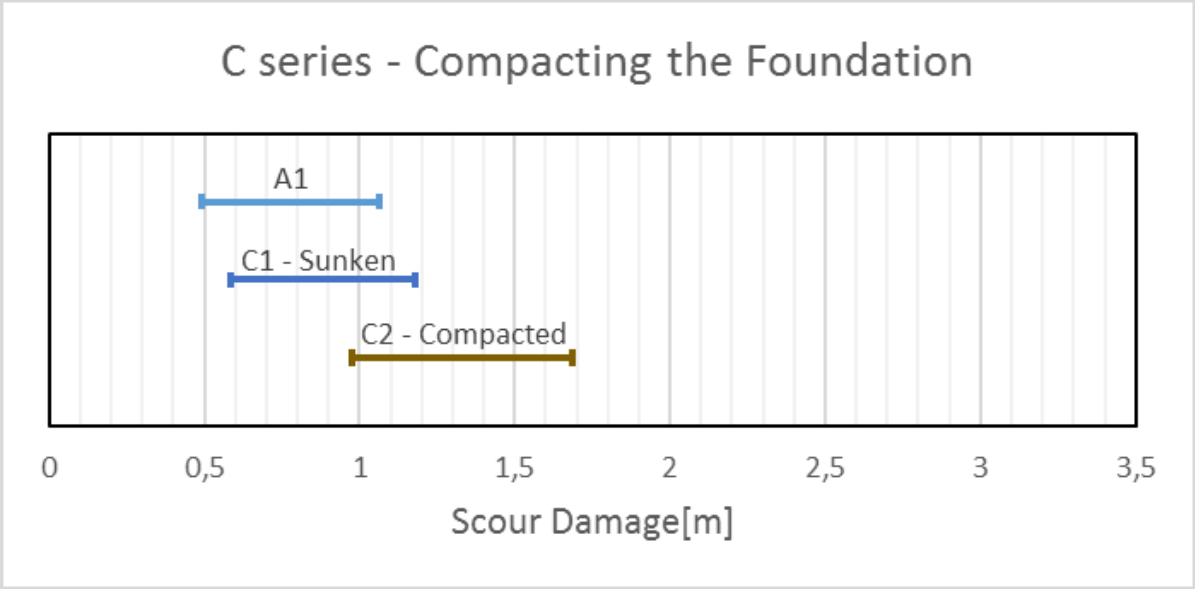

Figure 55: Scour damage of series C

Table 13: Correlation between tests in series C

Comparison	A1 = C1	A1 = C2	C1 = C2
Correlate	70.18%	7.45%	18.41%
Significantly Different	No	Yes	Yes

Thus, it can be stated that the appropriate construction method should consist of spreading the screed layer evenly, allowing the stones to position itself under its own weight so that the seawall can sink into the screed layer under its own weight and the weight of the backfill.

5.6 D Series – Addition of Sediment

All tests in the D series shows significant difference to each other. The test with the sand mixture shows less damage than the test with no added sediments. The test with the clay mixture experienced the least amount of scour damage. This was not expected as it was hypothesized that the sediment particles will wash out of the screed layer easily, leaving behind large voids. In both tests, the foundation was compacted in the dry. It is believed that the clay acted as a cohesive agent as it wetted, contributing to the strength of the screed layer.

In retrospect, the tests should have been conducted with the sediment not mixed into the screed layer evenly before construction. Instead, the sediment should be added to the screed layer during the construction process in order to simulate a prototype condition more accurately. This is more likely to create concentrated sediment clusters underneath the seawall more susceptible to scour. Refer to Figures D4 and D5 in Appendix D for photographs of sediment mixture during construction.

Table 14: Parameters and results of series D

	C2	D1	D2
Screed Thickness	100mm	100mm	100mm
Toe Width	150mm	150mm	150mm
Compacted Foundation	Yes	Yes	Yes
Sediment Addition	None	Sand mixture	Clay mixture
Exposed Wave height (Hs)	1.7m	1.52m	1.41m
Scour damage	1.33m	1.05m	0.81m
Confidence Interval	0.98 – 1.68m	0.73 – 1.37m	0.56 – 1.06m

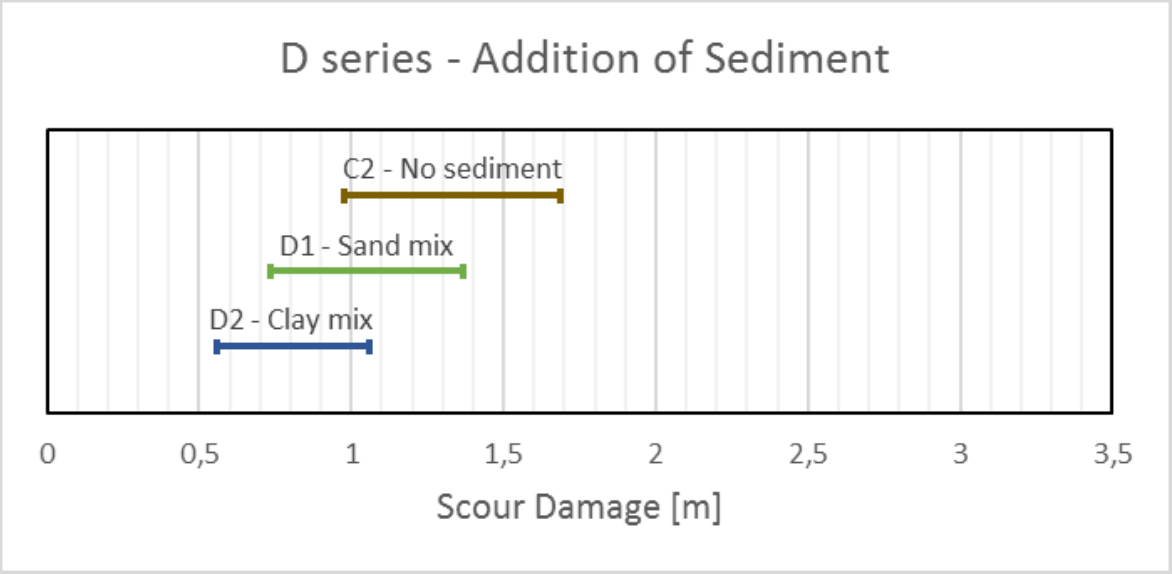

Figure 56: Scour damage of series D

Table 15: Correlation between tests in series D

Comparison	C2 = D1	C2 = D2	D2 = D1
Correlate	41.34%	7.37%	40.08%
Significantly Different	Yes	Yes	Yes

Although the tests indicate that the addition of a cohesive sediment increased the defence of the structure against scour, it is not recommended. More comprehensive tests should be conducted before a general recommendation on this aspect can be stated.

5.7 E Series – Addition of plastic backside

The two results from the E series shows 100% correlation. This validates the scale model, that no unwanted flow through the foundation was apparent. Refer to Figure C6 in Appendix C for photographs of the construction of the plastic lining.

Table 16: Parameters and results of series E

	A1	E1
Screed Thickness	100mm	100mm
Toe Width	150mm	150mm
Compacted Foundation	No	No
Sediment Addition	None	None
		Plastic
Exposed Wave height (Hs)	1.46m	1.64m
Scour damage	0.78m	0.836m
Confidence Interval	0.49 – 1.06m	0.63 – 1.04m

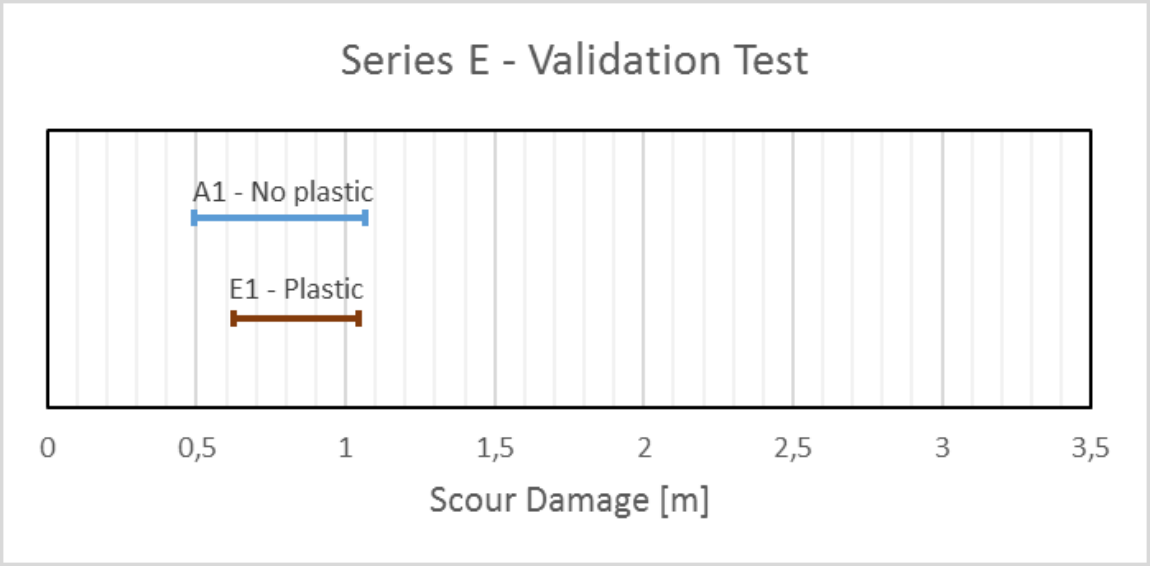

Figure 57: Scour damage of series E

Table 17: Correlation between tests in series E

Comparison	A1 = E1
Correlate	73.65%
Significantly Different	No

It is recommended that caution always be taken when conducting a physical model and that all physical processes be accounted for.

5.8 F Series – Solution

This design strives to adhere to the filter rules as the under layer (Class 2 rock) completely covers the core layer at the toe of the structure. The screed layer is also protected as it is completely overlaid by the core layer (Class 1 rock). Two Class 5 armour stones are placed at the toe of the seawall to increase the stability and protect the underlying layers.

The tested solution showed significantly less damage than the original design although some scour damage did occur. With visual inspection after the test very little scour damage can be seen at the toe of the structure (Figure 59). The scour that was experienced can be a result of the 100mm core layer, overlaying the screed layer at the toe of the structure, not being thick enough. It is stated in Section 2.3.4.4 of the literature that a filter layer should be at least two to three times the thickness of the larger stones in the grain-size distribution. In this case of the tested solution, the overlaying layer was as thick as one stone diameter. Although it is apparent that the solution performed better against the original design, it still does not adhere to the filter rules making it susceptible to scour. Figure 60 shows the cross-section of the solution constructed in the flume.

Table 18: Parameters and results of series F

	A1	F1
Screed Thickness	100mm	200mm
Toe Width	150mm	Solution
Compacted Foundation	No	No
Sediment Addition	None	None
Exposed Wave height (Hs)	1.46m	1.43m
Scour damage	0.78m	0.431m
Confidence Interval	0.49 – 1.06m	0.34 – 0.52m

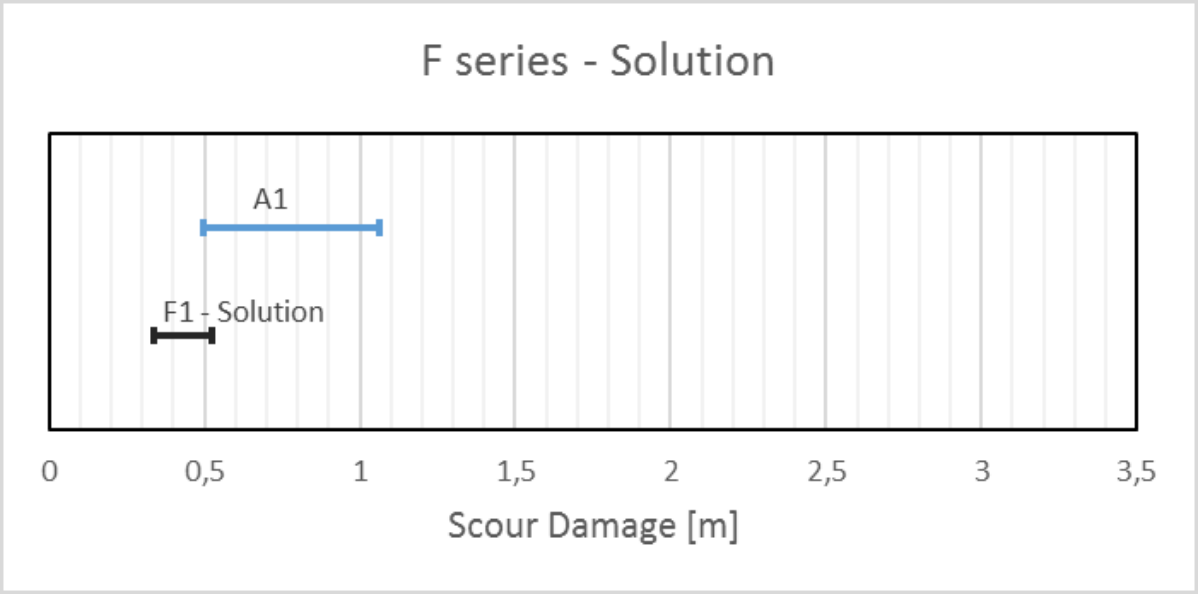

Figure 58: Scour damage of series F

Table 19: Correlation between tests in series F

Comparison	A1 = F1
Correlate	3.92%
Significantly Different	No

It is recommended that great care is taken when designing filter layers for protection against scour, making sure all filter rules are satisfied.

Figure 59: Toe of structure after test F1 (Armour layer manually removed for scour measurement)

Figure 60: Test F1 before test

6. Conclusions and Recommendations

6.1 General

The inadequate design and construction of defensive coastal structures can translate into considerable cost in the future. A great influence of the stability of such structures lies in the foundation on which it is constructed, therefore attention should be paid to the design of the rubble mound foundation and ensuring that all design criteria are met and appropriate construction methods are used.

A number of previous studies were conducted allowing us to have a proficient understanding of the scour process in the vicinity of most coastal structures. However, some aspects of the scour process within a rubble mound foundation are not fully understood. This report provides findings and conclusions on the behaviour on a rubble mound foundation underneath a vertical seawall exposed to scour. These conclusions may also be applied to the rubble mound foundation of a vertical breakwater.

6.2 Conclusions from Literature Study

Based on the literature study the following conclusions can be drawn:

- The method used to construct a vertical seawall has a significant effect on the performance of the structure. Each structure is designed to overcome certain forces due to its purpose and location, and the slightest alteration during construction can compromise the stability of the structure. Scour is often responsible for the failure of seawalls. It diminishes the effective stresses between the particles in the foundation reducing the frictional resistance between the foundation and the structure element, which can result in various failure modes.
- Although extensive research has been done on scour in front of vertical seawalls constructed on a sandy seabed, very little of this can be applied to the scour process underneath a vertical seawall constructed on a rubble mound foundation. For a rubble mound foundation, great care should be given to the filter rules of granular material in order to prevent the transport of fine materials through the overlaying rock layers, but still allow for water transport through the foundation.
- Previous research done on scour at other coastal structures uses the Keulegan-Carpenter number as a design parameter. This parameter is a product of the maximum undisturbed orbital velocity of water particles at the bed of the structure. It is not possible to measure nor calculate this velocity between rocks underneath the model structure, thus the KC number cannot be used as a governing parameter in such designs. All the parameters governing the

scour process underneath a vertical seawall are given by the breaker type, the presence of the seawall, the sediment properties, the granular material properties and the wave boundary layer over the seabed:

$$\frac{H_0}{L_0}, m, \frac{h_w}{L_0}, \frac{x}{L_0}, \frac{T_w\sqrt{gH_0}}{h_w}, \frac{w}{U_{fm}}, \frac{L_0}{d}, M, D$$

All these governing parameters are kept constant throughout the conducted experiments to ensure a constant scour process for all foundation conditions tested.

- When conducting a physical model, it is important to ensure all scaling and laboratory effects are correctly accounted for.

6.3 Conclusions from Physical Model Tests

This study investigated what effect different aspects of a rubble mound foundation underneath a vertical seawall/breakwater will have on scour damage. The objective was to review existing designs and various parameters and provide design guidance for scour protection at the foundation of vertical seawalls or breakwaters. Physical model tests were conducted altering the foundation layout and the following conclusions can be drawn:

- A thicker screed layer is more susceptible to scour damage although a minimum layer thickness of at least two to three times the diameter of the larger stones in the grain-size distribution is required with a maximum layer thickness of five times the diameter of the larger stones in the grain-size distribution. The thickness of the screed layer should allow for sufficient space for the structure element to settle into it, providing level stability whilst experiencing sufficient interlocking and friction forces between the individual stones, overcoming the scour forces.
- The screed toe width directly in front of a vertical seawall should be as narrow as possible, overlaid with at least one filter layer with adequate thickness. Care should be taken when designing filter layers and a good understanding of the grain-size distributions is needed to ensure all filter rules are met.
- The screed layer should not be compacted in any way during construction. A structure element not allowed to settle into the screed layer can cause unwanted flows underneath the structure, especially if it has a serrated base. If this is the case, less friction and support is created underneath the structure element that will contribute to the instability of the structure.

- No sediment (sand, silt or clay) should be added to the foundation screed layer, whether for design purposes or due to poor quality control during construction.
- Although a design of such a structure may meet all the design criteria, great emphasis should be placed on the construction method. With the repeated tests, it was concluded that the stability of the structure relies heavily on the quality and procedure of the construction process. Small design alterations during the construction phase of the structure can have significant effects on the stability of the structure and thus sufficient control and monitoring during the construction phase is important.

6.4 Recommendations for Further Work

In order to improve and expand the knowledge obtained in this study, the following recommendations should serve as a guide:

- In order to decrease the confidence intervals of measured scour damage, more tests should be repeated. Limited time forced the author to run most tests only once. In cases where experimental errors were undergone, such as the case with Test series B, tests should be repeated to ensure accurate results.
- Although great care was given to the construction process of each model simulation, some inconsistencies were experienced during the repeatability tests. The contrast between two identical foundation layouts exposed to the same wave conditions shows that more attention should be paid during the model construction phase. It is recommended that the weight of model screed layer to be placed, be measured beforehand to ensure that the exact amount is added between two identical tests, rather than to measure the thickness of the layer whilst constructing the foundation.

7. References

3 Types of Sea Walls: Which Is Best for Your Waters? | Renegar Construction, Lake Norman NC. 2016. *3 Types of Sea Walls: Which Is Best for Your Waters? | Renegar Construction, Lake Norman NC*. [ONLINE] Available at: http://renegarconstruction.com/dock-dock-seawall-sytems-construction-blog/3-types-sea-walls-waters/. [Accessed 11 March 2016].

Bakker, K. J., Verheij, H. J., and de Groot, M. B. 1994. "Design Relationship for Filters in Bed Protection," *Journal of Hydraulic Engineering*, American Society of Civil Engineers, Vol 120, No. 9, pp 1082-1088.

Burcharth, H. & Hughes, S. 2006. *Coastal Engineering Manual: Fundamentals of Design, Chapter 5, Part VI.* USA

Bush, D.M., Neal, W.J., Longo, N.J., Lindeman, K.C., Pilkey, D.F., Esteves, L.S., Congleton, J.D. and Pilkey, O.H. 2004 Living with Florida's Atlantic Beaches: Coastal Hazards from Amelia Island to Key West. USA: Duke University Press.

Chadwick, A. 2004. *Hydraulics in Civil and Environmental Engineering, Fourth Edition*. 4 Edition. CRC Press.

CIRIA, C. Cetmef (2007). *The Rock Manual.The use of rock in hydraulic engineering C,* 683

Craig, R.F, 2012. *Craig's Soil Mechanics*. 8th ed. Abingdon, Oxon: Spon Press.

Cyes. 2011. *Cyes - News*. [ONLINE] Available at: http://www.cyes.es/es/acercaprensanoticias_amplia.php?id=102#prettyPhoto. [Accessed 22 July 2016].

Dean, R.G. 1991. *WATER WAVE MECHANICS FOR ENGINEERS AND SCIENTISTS (Advanced Series on Ocean Engineering) (v. 2)*. Edition. World Scientific Publishing Company.

De Groot, M B, Bakker, K J and Verheij, H J (1993). "Design of geometrically open filters in hydraulic structures". In: J Brauns, M Heibaum and U Schuler (eds), *Filters in geotechnical and hydraulic engineering. Proc 1st int conf Geo-Filters, Karlsruhe, 20-22 Oct 1992.* AA Balkema, Rotterdam, pp 143-154

Fowler, J.E. 1992. *Scour problems and methods for prediction of maximum scour at vertical seawalls.* USA

Fredsøe, J. & Deigaard, R. 1992. *Mechanics of coastal sediment transport.* World scientific

Gerdau. 2015. *Z-Profile, Steel Sheel Piling*. [ONLINE] Available at: http://sheet-piling.com/pzc-z-profile/. [Accessed 21 July 2016].

Hoffmans, G.J. & Verheij, H. 1997. *Scour manual.* CRC Press. Delft

Hudson, R.Y., Herrman, F. A., Sager, R. A., Whalin, R. W., Keulegan, G. H., Chatham C. E., and Hales, L. Z. 1979. "Coastal Hydraulic Models," Special Report No. 5, US Army Engineer Waterways Experiment Station, Vicksburg, Mississippi.

Hughes S.A, 1993. *Physical Models and Laboratory Technique (World Scientific Series on Nonlinear Science. Series A, Mono)*. Edition. World Scientific Publishing Company.

Keulegan, G.H. 1973. "Wave Transmission Through Rock Structures," Research Report H-73-1, US Army Engineer Waterways Experiment Station, Vicksburg, Mississippi.

Le Méhauté, B. 1965. "Wave Absorbers in Harbors," Contract Report No. 2-122, US Army Engineer Waterways Experiment Station, Vicksburg, Mississippi.

Montgomery, D.C. 2010. *Applied Statistics and Probability for Engineers*. 5th International student edition Edition. John Wiley & Sons Ltd.

Meijer, E, 2010. Comparative analysis of design recommendations for quay walls. *Graduation project*, 1, 9.

Miles, M. D., & Funke, E. R. (2013, November). *The GEDAP Software Package for Hydraulics Laboratory Data Analysis.* Ottawa: National Research Council.

Pilarczyk, K.W. 2003. Hydraulic and Coastal Structures in International Perspective. The Netherlands

Pilarczyk, K.W. 1990. *Coastal protection.* AA Balkema Rotterdam

Pitkala, L. 1986. Retaining Wall made of L-Elements as a Quay Structure. *Bulletin of the Permanent International Association of Navigation Congresses,* (54). :11-18.

Sumer, B.M. & Fredsøe, J. 1900. Scour below pipelines in waves. Journal of Waterway, Port, Coastal, and Ocean Engineering, 116, 307-323.

Sumer, B.M. & Fredsøe, J. 1997. Scour at the head of a vertical-wall breakwater. *Coastal Engineering*, 29, 201-230.

Sumer, B.M. & Fredsøe, J. 1997. Scour at the round head of a rubble-mound breakwater. *Coastal Engineering*, 29, 231-262

Sumer, B.M. & Fredsøe, J. 2001. Wave scour around a large vertical circular cylinder. *Journal of Waterway, Port, Coastal, and Ocean Engineering*, 127, 125-134

Sumer, B.M. & Fredsøe, J. 2002. *The mechanics of scour in the marine environment.* World Scientific. Technical University of Denmark

Sumer, B.M. 2006. *HYDRODYNAMICS AROUND CYLINDRICAL STRUCTURES (REVISED EDITION) (Advanced Series on Ocean Engineering (Hardcover))*. Revised ed. Edition. World Scientific Publishing Company. Technical University of Denmark

Vanhooseco,LLC. 2014. *Precast*. [ONLINE] Available at: http://www.vanhoosecoprecast.com/products/panels-l-wall/. [Accessed 22 July 2016].

WaterWorks Marine. 2016. *Vinyl Seawalls*. [ONLINE] Available at: http://www.waterworksmarine.com/Seawalls.html. [Accessed 21 July 2016].

West, I. (2015), *The sinuous concrete of the new seawall on the East side of Lyme Regis* [ONLINE]. Available at: http://www.southampton.ac.uk/~imw/Lyme-Regis-to-Charmouth.htm [Accessed 3 July 2016]

Xie, S. 1981. *Scouring patterns in front of vertical breakwaters and their influences on the stability of the foundation of the breakwaters,*

Zanke, U. 1978. *Zusammenhänge zwischen strömung und sedimenttransport. teil 1: Berechnung des sedimenttransportes-allgemeiner fall.* EV

Appendix A: Grading Curves

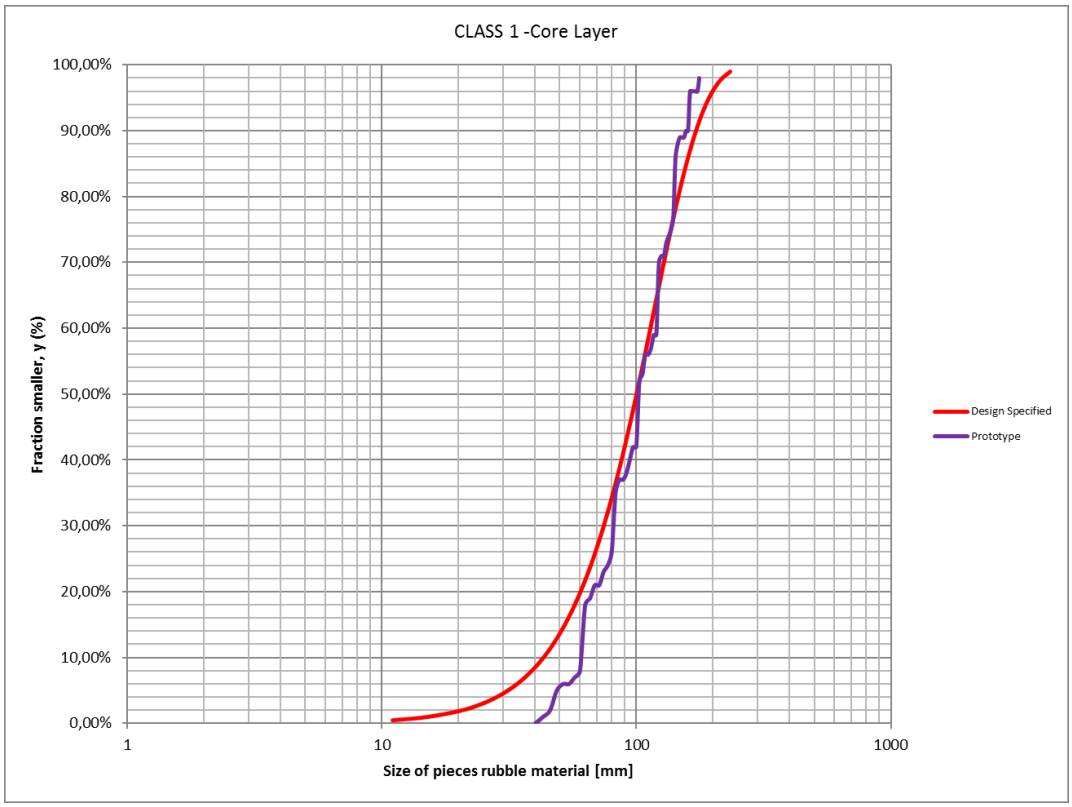

Figure A1: Grading curve of core layer

Figure A2: Grading curve of under layer

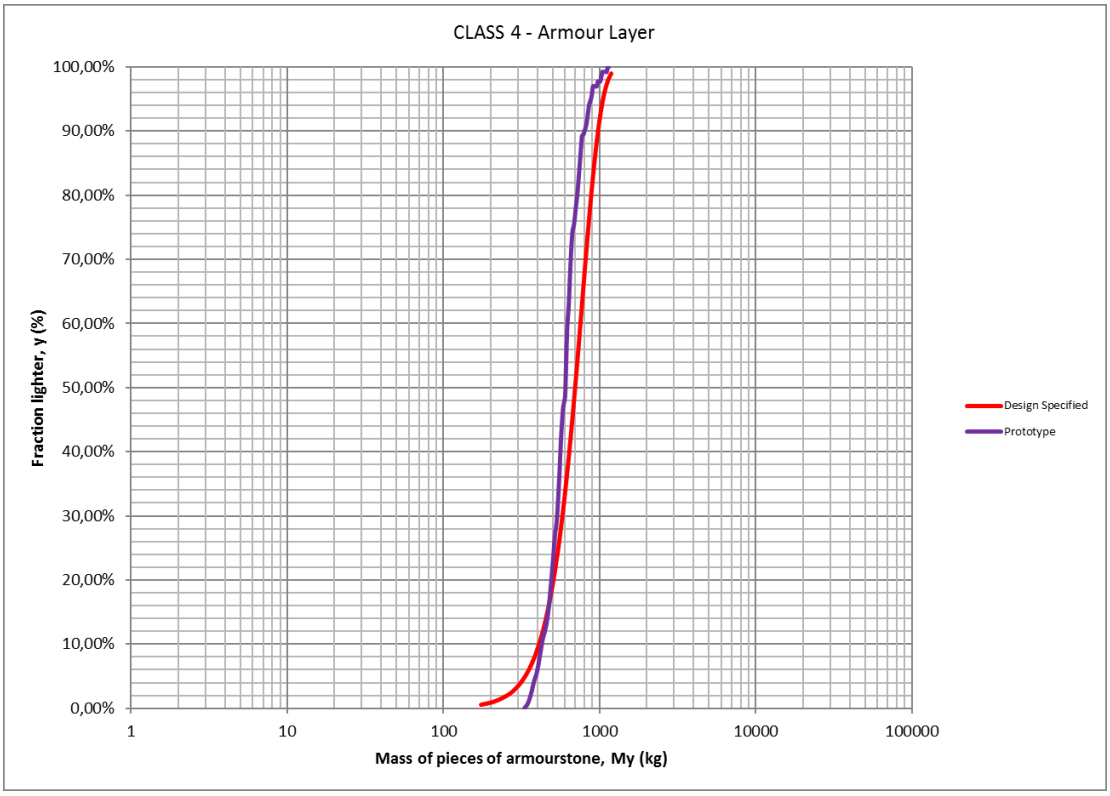

Figure A3: Grading curve of armour layer

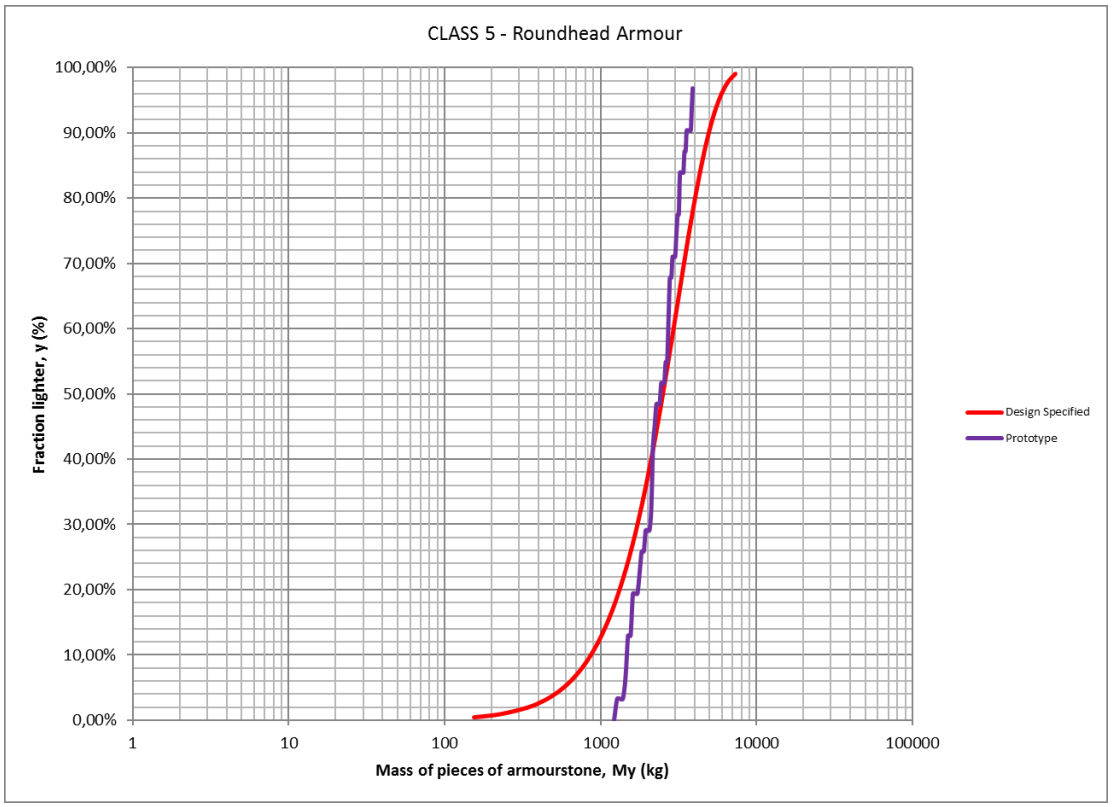

Figure A4: Grading curve of roundhead armour

Appendix B: Raw Data

Test A1																
Hs = 1,46m	cm	0	5	10	15	20	25	30	35	40	45	50	55	60	65	70	75
Tp = 8,101s	Small	10	9,5	5,7	5,1	3,5	3,2	3,1	3,9	3,5	3,6	3,9	7	8,5	9,3	8,5	5,3
	Large	8	5,6	4,3	3,3	2,7	2,3	2,1	3,2	2,7	2,9	2,9	5,3	5,2	7	5	3
	Average	9	7,55	5	4,2	3,1	2,75	2,6	3,55	3,1	3,25	3,4	6,15	6,85	8,15	6,75	4,15
Test A3																	
Hs = 1,522m	cm	0	5	10	15	20	25	30	35	40	45	50	55	60	65	70	75
Tp = 7,863s	Small	12,1	10,2	11,8	12,9	6,5	4,9	4,1	4,9	5,6	5,4	12,6	14,5	11,6	12,5	11,5	10,2
	Large	6,5	5,9	7,2	7,2	6	4,5	4	3,7	4,6	6,2	8,4	8	8,5	7,5	6,4	6,3
	Average	9,3	8,05	9,5	10,05	6,25	4,7	4,05	4,3	5,1	5,8	10,5	11,25	10,05	10	8,95	8,25
Test B1																	
Hs = 1,364m	cm	0	5	10	15	20	25	30	35	40	45	50	55	60	65	70	75
Tp = 8,069s	Small	12,4	12	14,1	11	13,1	11,6	14,7	15,5	13,5	12,6	13,5	11,8	11,4	10,8	9,4	8
	Large	4	5,5	5,5	7,5	6,7	6,7	8,5	9,1	8,2	8	9	8,1	7,6	8,1	5,7	2,9
	Average	8,2	8,75	9,8	9,25	9,9	9,15	11,6	12,3	10,85	10,3	11,25	9,95	9,5	9,45	7,55	5,45
Test B2																	
Hs = 1,505m	cm	0	5	10	15	20	25	30	35	40	45	50	55	60	65	70	75
Tp = 7,829s	Small	5,6	7,2	6,4	8	6,5	8,4	9,1	9,8	8	7	4,8	8	10,6	11	9,7	10
	Large	2,1	3,9	4,6	5,2	4,6	4,8	5,3	5,9	5,2	3,2	2,5	5,2	5,5	5,4	6	5,5
	Average	3,85	5,55	5,5	6,6	5,55	6,6	7,2	7,85	6,6	5,1	3,65	6,6	8,05	8,2	7,85	7,75
Test C1																	
Hs = 1,685m	cm	0	5	10	15	20	25	30	35	40	45	50	55	60	65	70	75
Tp = 7,806s	Small	8,5	7,8	5,7	4	3,5	4,1	5,1	4,5	4	3,8	7,5	7,1	9,4	9	6,9	5,6
	Large	4,2	4,5	3,7	3,2	2,6	3	2,9	2,5	2,9	3,4	5,9	5,5	3,2	5	4,6	3
	Average	6,35	6,15	4,7	3,6	3,05	3,55	4	3,5	3,45	3,6	6,7	6,3	6,3	7	5,75	4,3
Test C2																	
Hs = 1,703m	cm	0	5	10	15	20	25	30	35	40	45	50	55	60	65	70	75
Tp = 7,806s	Small	6,6	6,6	6,5	5	5,3	6,8	7,6	7,9	9,8	9,8	8,9	9,5	10	9,7	8,1	5,4
	Large	2,7	2,8	3,7	3,4	4,2	4,5	5,3	6,4	6,1	5,5	6,3	5,6	5,1	5,9	5	4,3
	Average	4,65	4,7	5,1	4,2	4,75	5,65	6,45	7,15	7,95	7,65	7,6	7,55	7,55	7,8	6,55	4,85
Test D1																	
Hs = 1,524m	cm	0	5	10	15	20	25	30	35	40	45	50	55	60	65	70	75
Tp = 7,831s	Small	5,2	5,7	3,8	4,4	4,3	5,5	6,4	6,2	6,6	8,1	10,4	6,5	7,2	9,4	7,3	7
	Large	1,8	2,3	2	2,9	3	3,2	3	3,1	4,3	7	4,6	4,4	4	5,5	5,9	4,9
	Average	3,5	4	2,9	3,65	3,65	4,35	4,7	4,65	5,45	7,55	7,5	5,45	5,6	7,45	6,6	5,95
Test D2																	
Hs = 1,413m	cm	0	5	10	15	20	25	30	35	40	45	50	55	60	65	70	75
Tp = 7,821s	Small	3,9	3,4	3,2	2,4	3	5,1	5,1	6,9	7,2	7,3	5	4,3	5,2	8,8	9,6	9,5
	Large	2,3	2,3	2,1	2	1,6	3	3,3	3,2	3,4	3,5	3,5	2,8	3	3,8	4,5	4,9
	Average	3,1	2,85	2,65	2,2	2,3	4,05	4,2	5,05	5,3	5,4	4,25	3,55	4,1	6,3	7,05	7,2

Test E1																	
Hs = 1,636m	cm	0	5	10	15	20	25	30	35	40	45	50	55	60	65	70	75
Tp = 7,831s	Small	8	9,8	7,5	6	5,6	6	6	6,3	5	4	4,5	4,5	4,2	4,9	7,1	5,8
	Large	2,5	4,3	4,1	3,8	4	3,4	3,5	3,6	3,4	2,5	2,8	2,1	2,4	3	4,7	2,5
	Average	5,25	7,05	5,8	4,9	4,8	4,7	4,75	4,95	4,2	3,25	3,65	3,3	3,3	3,95	5,9	4,15

Test F1																	
Hs = 1,43m	cm	0	5	10	15	20	25	30	35	40	45	50	55	60	65	70	75
Tp = 7,831s	Small	3	5,3	2,7	2,2	2	2,8	2,9	3	2,5	2,4	2,5	3	2,5	5	7,5	2,3
	Large	2,1	3	1,9	1,5	1,5	1,8	1,8	1,9	1,5	1,9	2	1,2	2,2	3,3	4,4	1,8
	Average	2,55	4,15	2,3	1,85	1,75	2,3	2,35	2,45	2	2,15	2,25	2,1	2,35	4,15	5,95	2,05

Rpt1																			
	cm	0	5	10	15	20	25	30	35	40	45	50	55	60	65	70	75	Hs	Tp
	1000 Waves	5,75	7,45	8,35	7,8	8,3	8,2	5	4,5	3,6	4,6	3,65	3,25	3,8	3,3	3,75	3,2	2,031m	7,968m
	2000 Waves	5,2	6,6	8,15	7,35	7,5	6,75	5,75	4,6	3,9	4,2	3,55	3,75	3,45	3,05	2,65	3,1	2,009m	7,968m
	3000 Waves	4,2	5,75	6,75	5,95	5,5	4,2	5,4	4,45	4,6	3,5	3,5	3,95	2,95	3,3	3,15	2,25	1,996m	7,753m
Rpt2																			
	cm	0	5	10	15	20	25	30	35	40	45	50	55	60	65	70	75	Hs	Tp
	1000 Waves	4,9	4,85	4,45	3,75	3,3	5,1	5,15	6,95	7,25	7,65	6,5	5,1	5,85	6,25	7	5,9	1,491m	7,976s
	2000 Waves	4,6	4,15	4,05	3,05	3,2	5	5,35	6,6	6,35	6,35	5,05	4,45	5,5	4,6	6,85	6,2	1,469m	7,976s
	3000 Waves	4,7	3,9	3,1	3,55	3,1	3,75	5,5	5,65	5,75	5,55	4,6	4,55	4,55	3,85	4,9	3,85	1,482m	7,976s

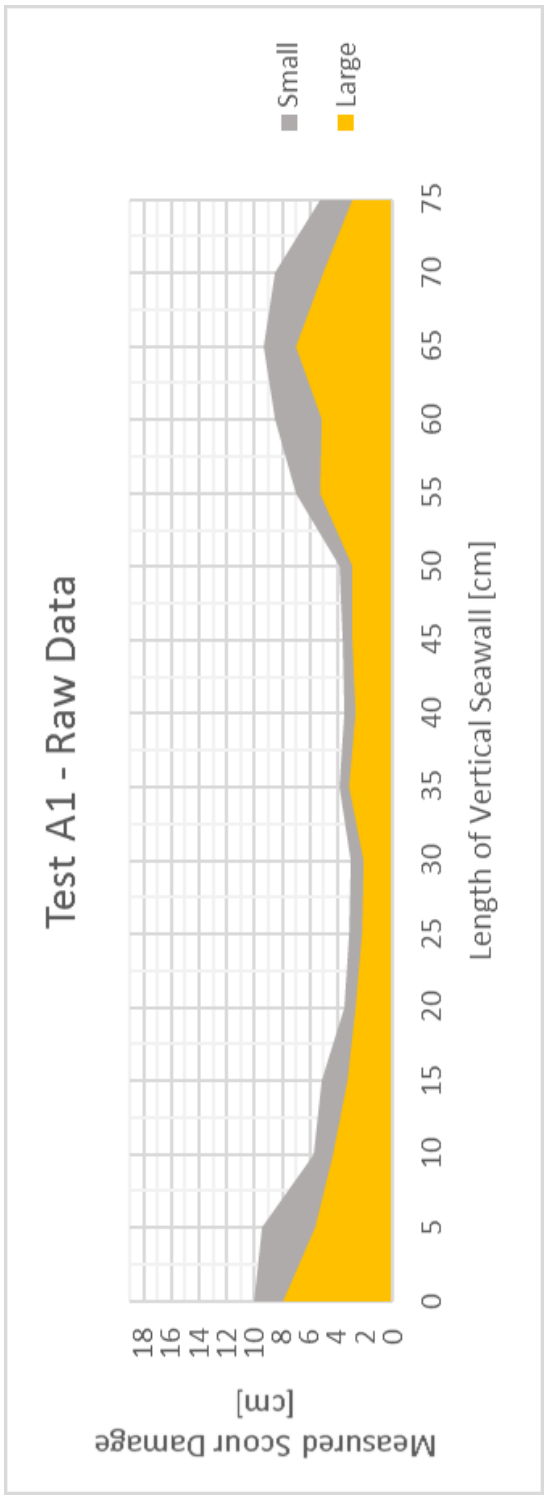

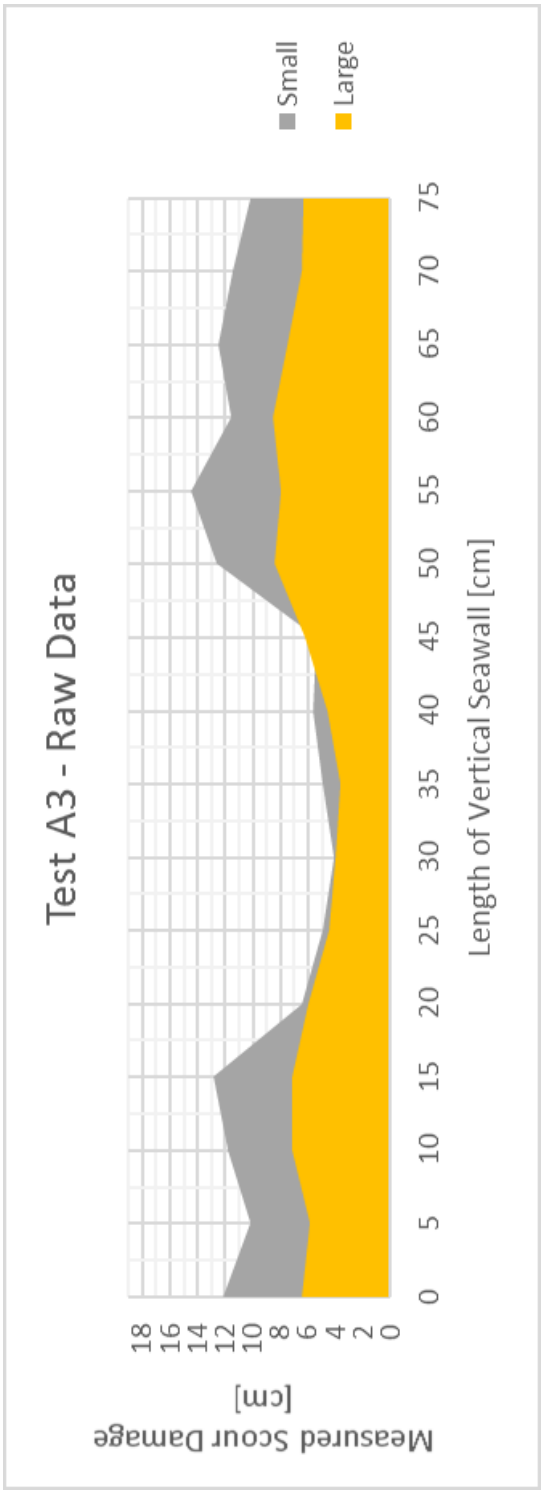

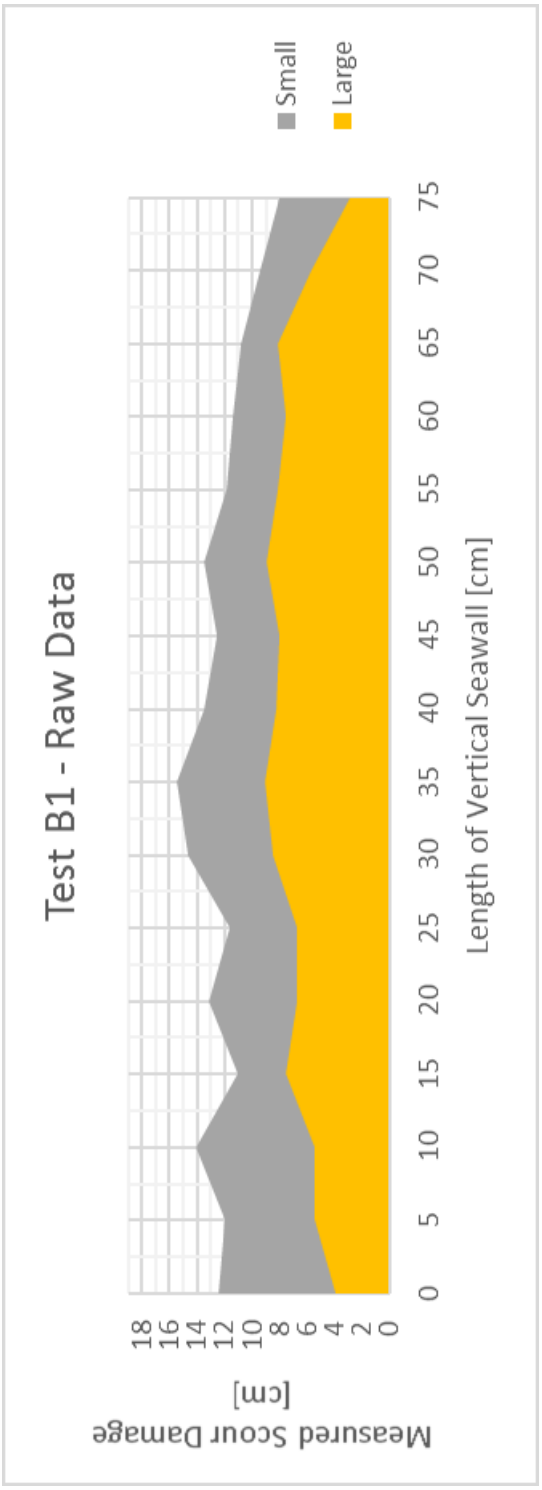

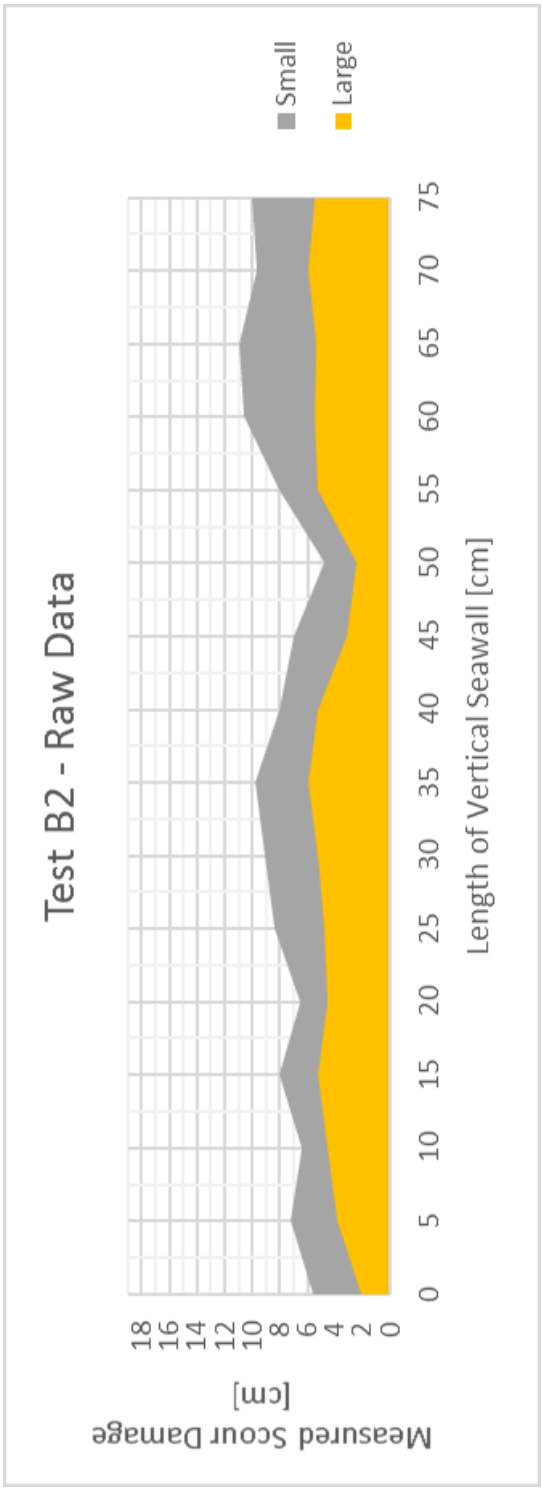

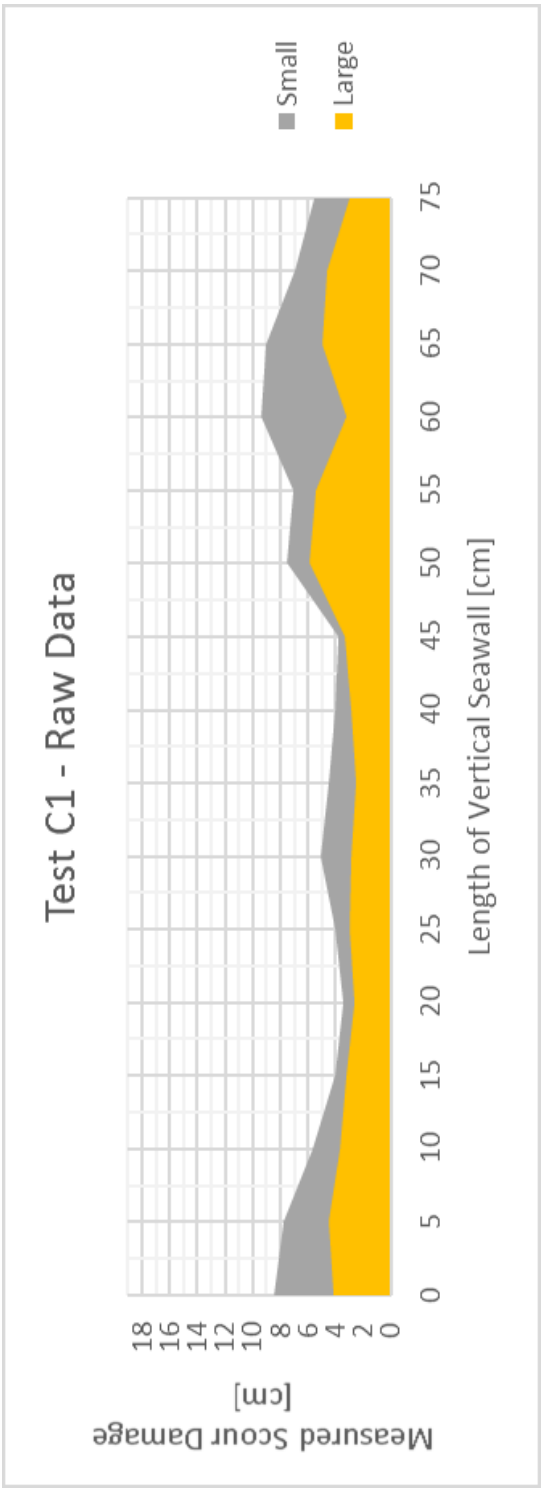

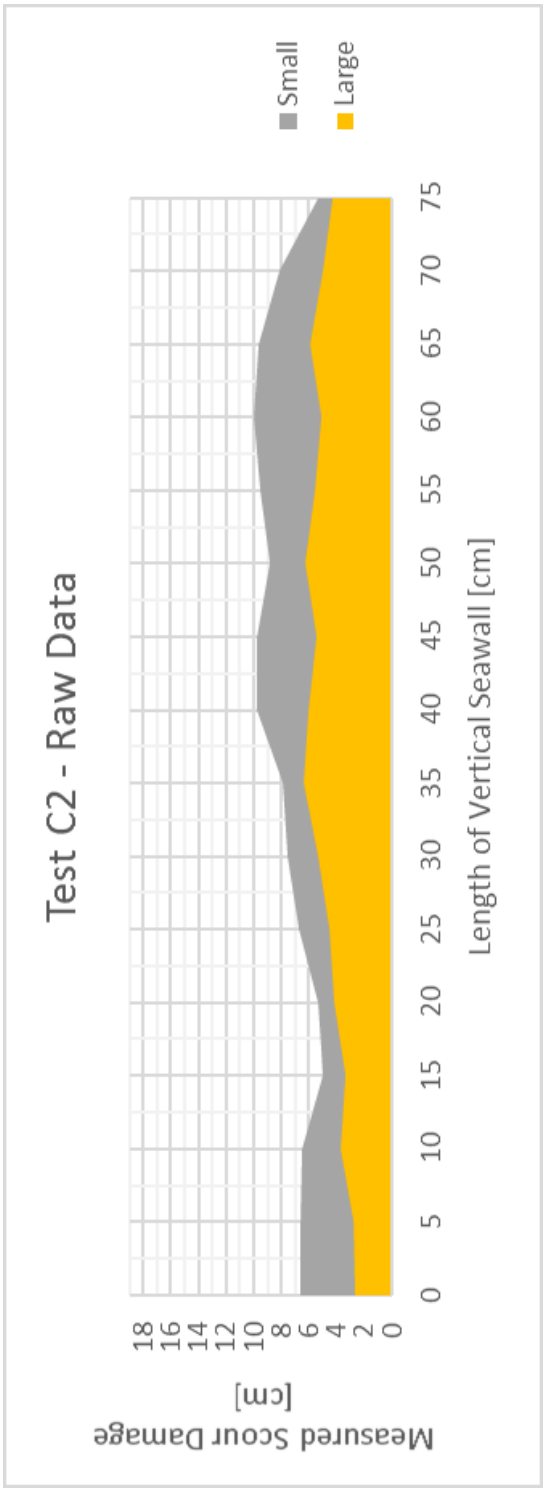

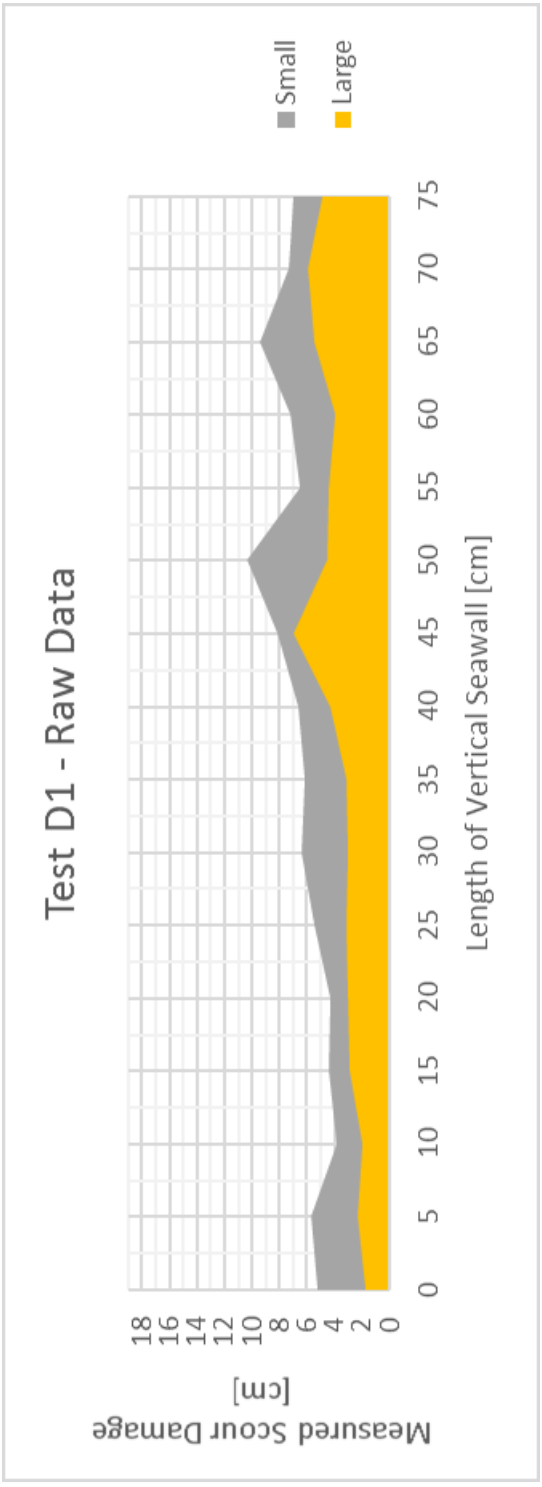

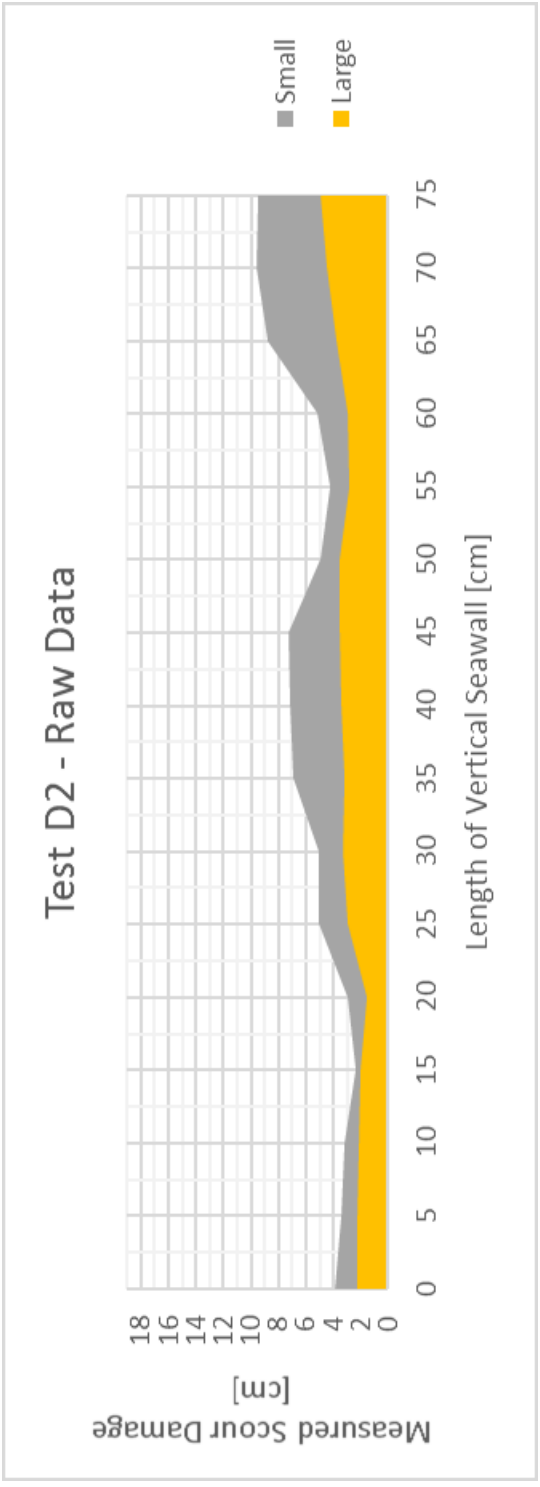

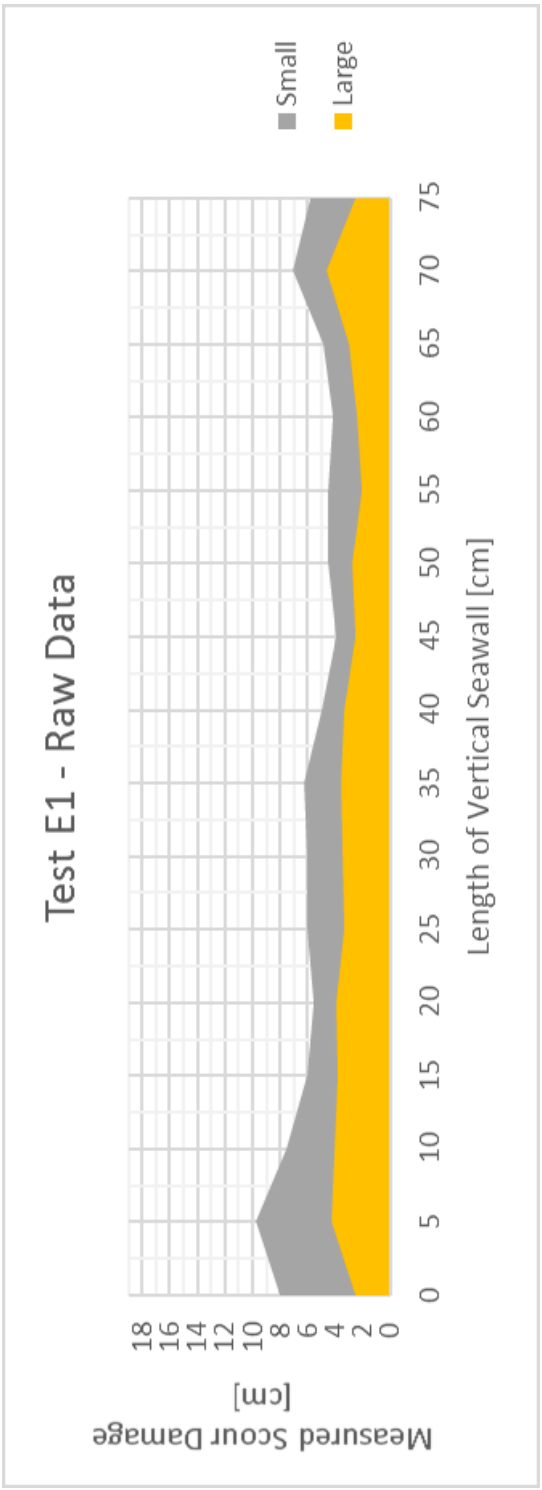

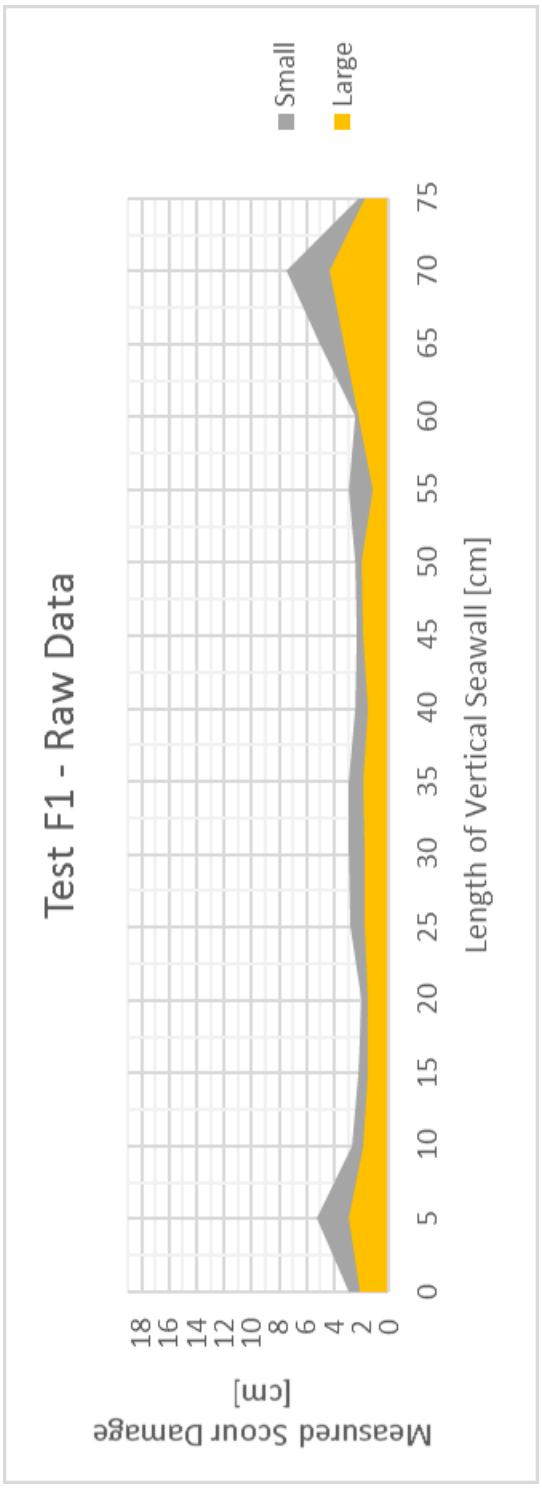

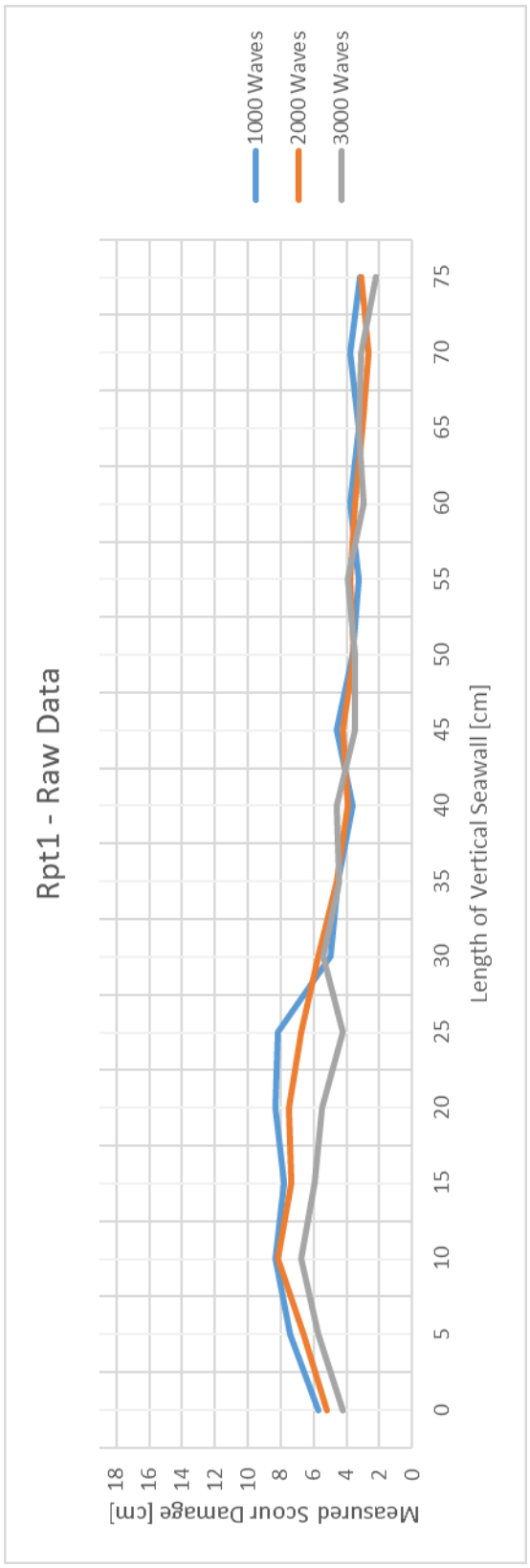

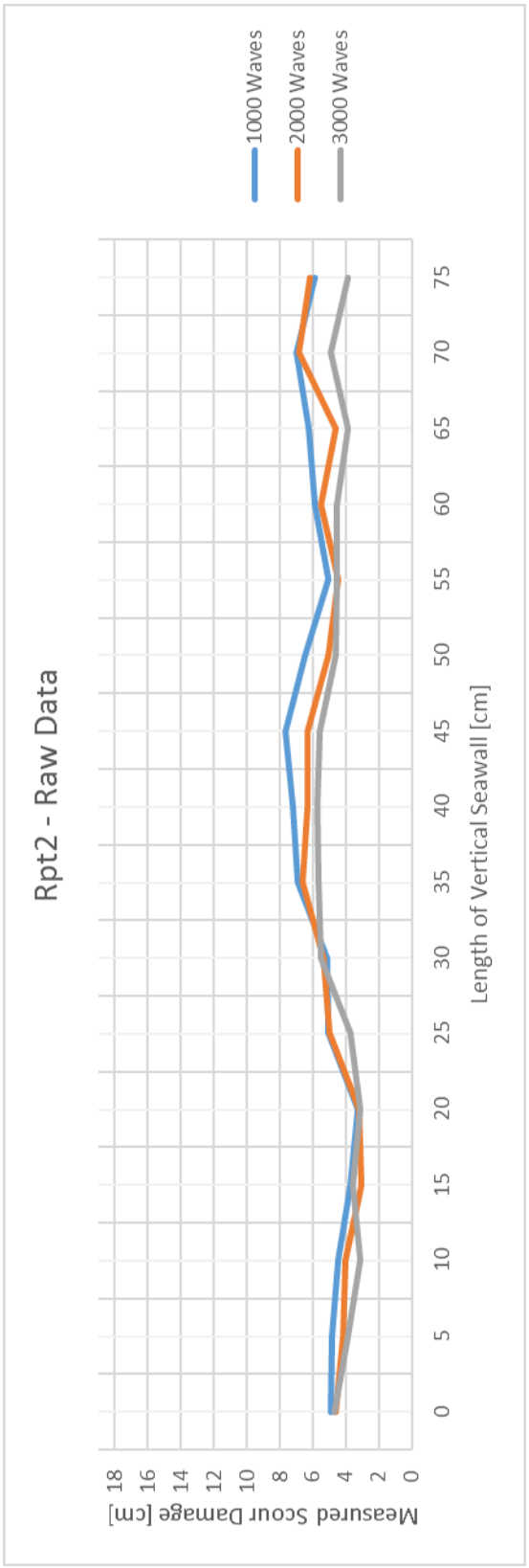

Appendix C: Construction Images

Figure C1: Levelling of core layer

Figure C2: Levelling of screed layer

Figure C3: Vertical seawall before armour layer

Figure C4: Placing of armour units

Figure C5: Complete cross-section

Figure C6: Plastic lining at back of structure

Appendix D: Testing Images

Figure D1: Test B2 before test - water level at design level

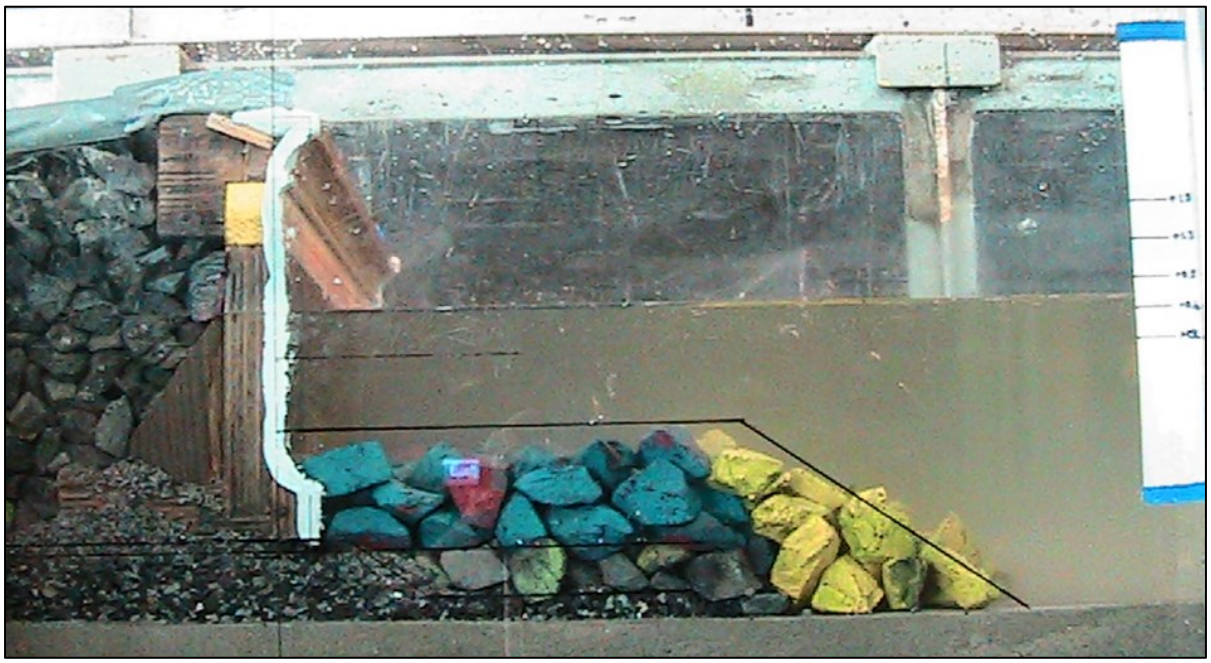

Figure D2: Test B2 after test - water level higher than design level

Figure D3: Test D2 after seawall had been removed - serrated base imprint

Figure D4: Test D1 (sand mixture) before and after

Figure D5: Test D2 (clay mixture) before and after

Appendix E: Scaling law to simulate wave transmission

Applying Froude scaling to prototype values yields model values given in Table E1. Note a different model value for kinematic viscosity is used.

Tabel E1: Scaled Parameters

Parameter	Prototype Vaues	Model Values
P	0.38	0.38
v	$1.0565\ (10)^{-6}\ m^2/s$	$1..007\ (10)^{-6}\ m^2/s$
Hi	$1.5\ m$	$0.075\ m$
h	$3.7\ m$	$1.185\ m$
T	$8\ s$	$1.789\ s$
L	$46.323\ m$	$2.316\ m$
D	$1.9\ cm$	$9.5\ (10)^{-4}\ cm$
ΔL	$0.1\ m$	$5(10)^{-3}\ m$

La Méhauté method:

Substitute parameters into Equation 33.

$$\frac{H_i}{\Delta L}\ D_p^3\ P_p^5 = \left(\frac{1.5}{0.1}\right)\ (1.9)^3(0.38)^5 = 0.815\ cm^3$$

Use La Méhauté's nomogram and extend an upwards line from the x-axis until it intersects with the y-axis value of Lp/Lm = 20.

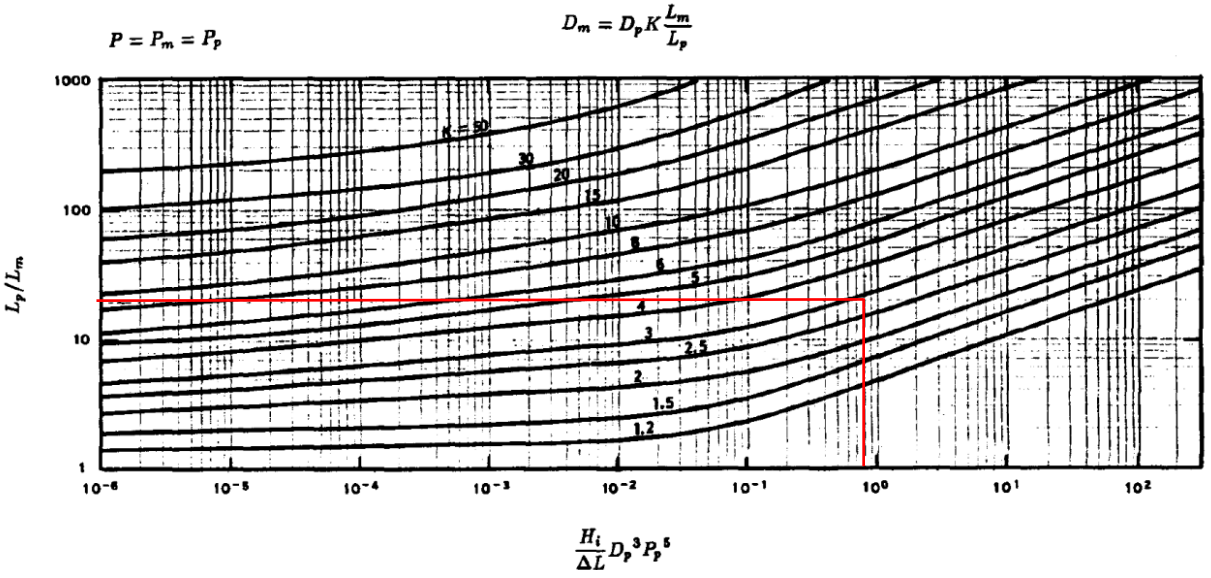

Figure E1: La Méhauté's nomogram with applied value

The intersecting point falls on $K = 2.8$

Keulegan method:

Calculate transmission wave for prototype. First use Equation 35.

$$\gamma_p = \frac{0.38^{-4}}{10.6}\left(\frac{46.323}{0.019}\right)\left((9.81m.s^{-2})(3.7m)\frac{(8)^2}{(46.323)^2}\right)^{4/3} = 12262$$

Then substitute in Equation 34

$$\left(\frac{H_i}{H_t}\right)_p = 1 + 12262\left(\frac{1.5m}{2(3.7m)}\right)\left(\frac{0.1}{46.323}\right) = 74.45$$

For similitude:

$$\left(\frac{H_i}{H_t}\right)_p = \left(\frac{H_i}{H_t}\right)_m \quad therefore \quad \left(\frac{H_i}{H_t}\right)_m = 74.45$$

Check Reynolds number by calculating Equation 38.

$$R_n = \frac{PH_iLD}{2vhT} = \frac{0.38(0.075m)(2.316m)(9.5(10)^{-6}\,m)}{2(1.007\,(10)^{-6}\;m^2/s)(0.185m)(1.789s)} = 0{,}941$$

Reynolds number is less than 2000. Solve D with Equation 36 and Equation 37.

$$(74.45)^{2/3} = 1 + \gamma_m\left(\frac{0.075m}{2(0.185m)}\right)^{2/3}\left(\frac{5(10)^{-3}\,m}{2.316m}\right)$$

$$\gamma_m = 22400$$

Substitute in Equation 37

$$22400 = \frac{(0.38)^{-4}}{1.52}\left(\frac{1.007\,(10)^{-6}\,m^2/s\,(1.789s)}{D(2.316m)}\right)^{1/3}\left(\frac{2.316m}{D}\right)\left((9.81m.s^{-2})(0.185m)\frac{(1.789s)^2}{(2.316m)^2}\right)^{4/3}$$

$$D_m = 0.439\,mm$$

By substituting the length scale together with prototype and model quarry run diameter into Equation 32, the K factor can be calculated.

$$20 = K\frac{19mm}{0.439mm}$$

$$K = 0.46$$

The final value for the K factor is calculated by taken the average of the K values of La Méhauté and Keulegan methods, which yields:

$$\underline{\boldsymbol{K = 1.63}}$$

By using Equation 32, the model stone diameter is calculated as:

$$20 = 1.63\frac{19mm}{D_m}$$

$$D_m = 1.55mm$$

Appendix F: Confidence Interval on mean

The equation for a confidence interval on a mean with the variance unknown is: (assuming the data to be normally distributed)

$$\bar{x} - t_{\alpha/2,n-1} \cdot s/\sqrt{n} \leq \mu \leq \bar{x} + t_{\alpha/2,n-1} \cdot s/\sqrt{n}$$

For Test A1:

$\bar{x} = 0.78m$

$s = 0.29m$

$t_{\alpha/2,n-1} = t_{0.05,9} = 1.833$

Thus

$$t_{\alpha/2,n-1} \cdot s/\sqrt{n} = 1.833 \cdot 0.29/\sqrt{10} = 0.168$$

This is the confidence interval for the function of the foundation condition. i.e. The variance in the measurements taken over the length of the seaward side of the seawall.

Now the confidence interval for the function of the exposed wave height must be added. As explained in Section 5.1.2 the variance for the function of the exposed wave height is 15% of the measured scour damage.

$$0.15 \times 0.78 = 0.117$$

The two confidence intervals can now be added together:

$$0.168 + 0.117 = 0.285$$

Finally, a 90% confidence interval can be stated as:

$$0.494 \leq \mu \leq 1.064$$

Table F1: t-distribution (Montgomery,2010)

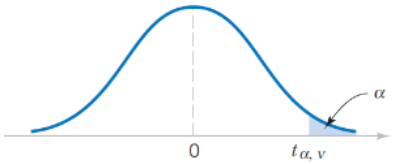

ν \ α	.40	.25	.10	.05	.025	.01	.005	.0025	.001	.0005
1	.325	1.000	3.078	6.314	12.706	31.821	63.657	127.32	318.31	636.62
2	.289	.816	1.886	2.920	4.303	6.965	9.925	14.089	23.326	31.598
3	.277	.765	1.638	2.353	3.182	4.541	5.841	7.453	10.213	12.924
4	.271	.741	1.533	2.132	2.776	3.747	4.604	5.598	7.173	8.610
5	.267	.727	1.476	2.015	2.571	3.365	4.032	4.773	5.893	6.869
6	.265	.718	1.440	1.943	2.447	3.143	3.707	4.317	5.208	5.959
7	.263	.711	1.415	1.895	2.365	2.998	3.499	4.029	4.785	5.408
8	.262	.706	1.397	1.860	2.306	2.896	3.355	3.833	4.501	5.041
9	.261	.703	1.383	1.833	2.262	2.821	3.250	3.690	4.297	4.781
10	.260	.700	1.372	1.812	2.228	2.764	3.169	3.581	4.144	4.587
11	.260	.697	1.363	1.796	2.201	2.718	3.106	3.497	4.025	4.437
12	.259	.695	1.356	1.782	2.179	2.681	3.055	3.428	3.930	4.318
13	.259	.694	1.350	1.771	2.160	2.650	3.012	3.372	3.852	4.221
14	.258	.692	1.345	1.761	2.145	2.624	2.977	3.326	3.787	4.140
15	.258	.691	1.341	1.753	2.131	2.602	2.947	3.286	3.733	4.073
16	.258	.690	1.337	1.746	2.120	2.583	2.921	3.252	3.686	4.015
17	.257	.689	1.333	1.740	2.110	2.567	2.898	3.222	3.646	3.965
18	.257	.688	1.330	1.734	2.101	2.552	2.878	3.197	3.610	3.922
19	.257	.688	1.328	1.729	2.093	2.539	2.861	3.174	3.579	3.883
20	.257	.687	1.325	1.725	2.086	2.528	2.845	3.153	3.552	3.850
21	.257	.686	1.323	1.721	2.080	2.518	2.831	3.135	3.527	3.819
22	.256	.686	1.321	1.717	2.074	2.508	2.819	3.119	3.505	3.792
23	.256	.685	1.319	1.714	2.069	2.500	2.807	3.104	3.485	3.767
24	.256	.685	1.318	1.711	2.064	2.492	2.797	3.091	3.467	3.745
25	.256	.684	1.316	1.708	2.060	2.485	2.787	3.078	3.450	3.725
26	.256	.684	1.315	1.706	2.056	2.479	2.779	3.067	3.435	3.707
27	.256	.684	1.314	1.703	2.052	2.473	2.771	3.057	3.421	3.690
28	.256	.683	1.313	1.701	2.048	2.467	2.763	3.047	3.408	3.674
29	.256	.683	1.311	1.699	2.045	2.462	2.756	3.038	3.396	3.659
30	.256	.683	1.310	1.697	2.042	2.457	2.750	3.030	3.385	3.646
40	.255	.681	1.303	1.684	2.021	2.423	2.704	2.971	3.307	3.551
60	.254	.679	1.296	1.671	2.000	2.390	2.660	2.915	3.232	3.460
120	.254	.677	1.289	1.658	1.980	2.358	2.617	2.860	3.160	3.373
∞	.253	.674	1.282	1.645	1.960	2.326	2.576	2.807	3.090	3.291

ν = degrees of freedom.

Appendix G: Probe Output

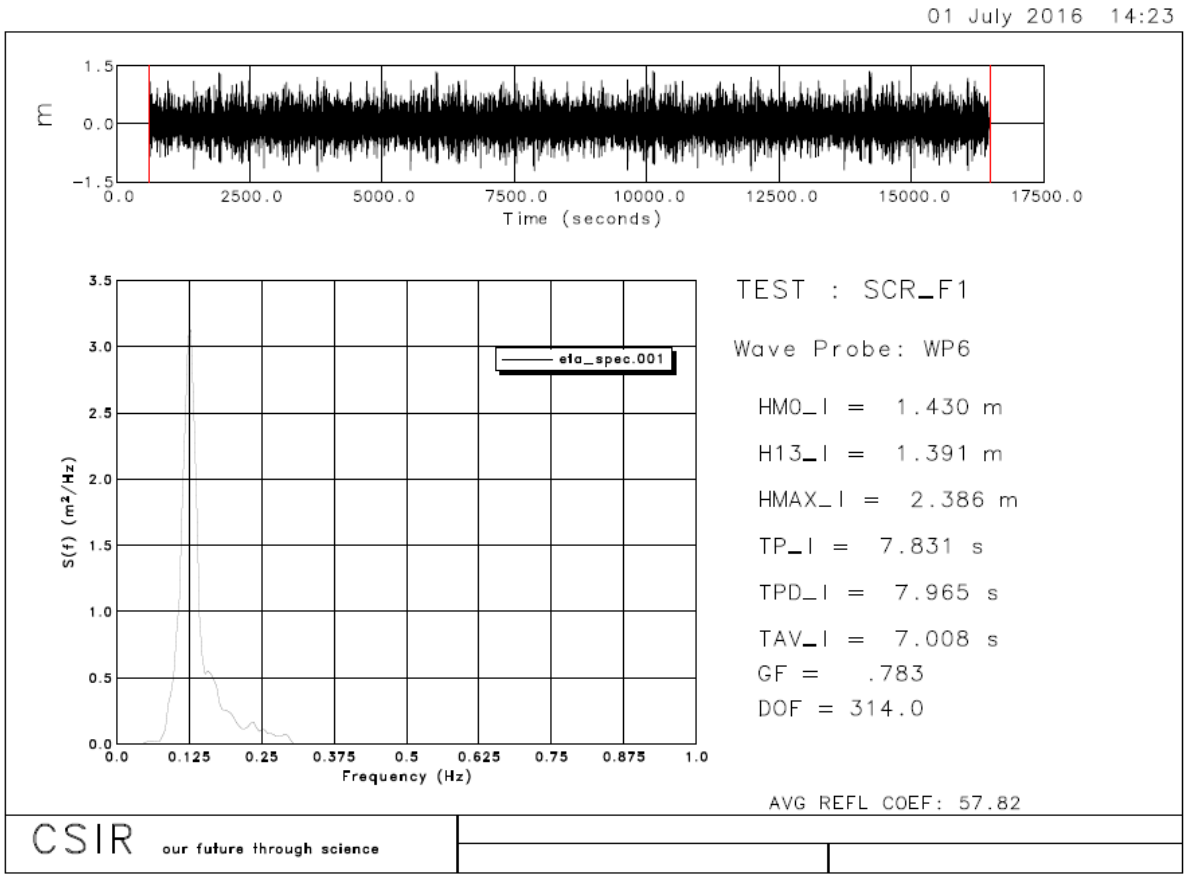

Figure G1: Probe output from test F1